

Syracuse University

SURFACE at Syracuse University

Dissertations - ALL

SURFACE at Syracuse University

5-14-2023

Pahoehoe Breakouts and Lava-Substrate Interactions: Insights from Large-Scale Experimental Lava Flows

Christopher Joseph Sant
Syracuse University

Follow this and additional works at: <https://surface.syr.edu/etd>

Recommended Citation

Sant, Christopher Joseph, "Pahoehoe Breakouts and Lava-Substrate Interactions: Insights from Large-Scale Experimental Lava Flows" (2023). *Dissertations - ALL*. 1675.
<https://surface.syr.edu/etd/1675>

This Dissertation is brought to you for free and open access by the SURFACE at Syracuse University at SURFACE at Syracuse University. It has been accepted for inclusion in Dissertations - ALL by an authorized administrator of SURFACE at Syracuse University. For more information, please contact surface@syr.edu.

General Abstract

Basaltic lava flows are one of the most visible geologic processes on Earth. Gaining a thorough knowledge of basaltic lava flow behavior is imperative to understanding Earth's formation processes and for the protection of humanity. Studies of basalt flow behavior have traditionally been completed on active natural basalt flows or in the laboratory using analog materials.

Studying active lava flows can be difficult due to unpredictable timing, remote locations, and dangerous conditions. However, the advent of meter-scale laboratory generated lava flows allows for safe and detailed study of active basalt flows. By using natural basaltic material at natural eruption temperatures, these experiments also act to bridge the gap between studies of active lavas and laboratory analog flows. This dissertation is a collection of studies performed on meter-scale basalt pāhoehoe flows to aid in the understanding of pāhoehoe flow dynamics.

Chapter one focuses on morphologic study and the details of formation of pāhoehoe sheets and breakouts. Chapter two describes newly observed lava behavior on various substrates, some of which contain abundant volatiles. Chapter three investigates chemical absorption of externally sourced volatiles into the lava and their effect on lava chemistry. These experiments provide the first steps toward more detailed study of pāhoehoe flows in the laboratory.

PĀHOEHOE BREAKOUTS AND LAVA-SUBSTRATE INTERACTIONS: INSIGHTS FROM LARGE-SCALE EXPERIMENTAL LAVA FLOWS

By

Christopher J. Sant

B.S., Brigham Young University - Idaho, 2009

M.S., Utah State University, 2012

DISSERTATION

Submitted in partial fulfillment of the requirements for the degree of

Doctor of Philosophy in Earth Sciences

Syracuse University

May 2023

Copyright © Christopher J. Sant 2023

All rights reserved

Acknowledgements

The completion of this dissertation could not be realized without the support of many involved behind the scenes. Special thanks to my primary advisors Jay Thomas and Jeff Karson for their continued faith and dedication in teaching me to reach greater heights to become the greatest scientist I can be. Thanks also to the remainder of my advisory committee for their counsel and guidance during my investigations of experimental basaltic lava flows. Additional gratitude and praise must be given to Robert Wysocki for his dedicated work to maintain the lava furnace for years of service. I must also thank the Department of Earth & Environmental Sciences, the Syracuse University Lava Project, and the Geological Society of America for their funding to make this work possible. Additional thanks to Holiday Ice Company for their kind helpfulness in assisting with providing ice substrates for our experiments. Thanks to the faculty mentors over the years that supported and encouraged me to follow my dreams. To my fellow students, colleagues, and friends, thank you for the lively scientific discussion and efforts to facilitate deeper scientific learning and growth. To my closest academic friends, thank you for the chats, lunches, softball games, and for your support, encouragement, and friendship.

Acknowledgements must also be given to my family. Without the unfailing love and support of family, this journey would have ended without the completion of this dissertation. Thanks to my children for enduring the many long hours I spent away from home, and for always being excited to see yet another lava flow. Most of all, a massive thank you to my wife Elizabeth. She has been by my side through every step of my entire academic journey. Her love and support cannot be overstated, and it will never be forgotten.

Table of Contents

General Abstract	i
Acknowledgements	iv
Table of Contents	v
List of Figures	vii
List of Tables	ix
Introduction.....	1
Chapter 1: Experimental constraints on pāhoehoe breakouts	5
Abstract	6
Introduction.....	6
Methods.....	9
Results.....	11
Observations	11
Metrics	13
Discussion.....	14
Morphology and Ψ	15
Transition to Breakouts.....	18
Comparison with Natural Flows	21
Conclusions.....	24
Tables	26
Figures.....	28
Chapter 2: Rapid slip of basaltic lava on volatile-bearing substrates	38
Abstract	39
Introduction.....	40
Methods.....	41
Results.....	43
General Description of Experiments.....	43

Definition of Lava ‘Slip’	44
Experimental Results by Substrate	46
Textural Observations	48
Discussion	50
Causes of Slip	50
Comparison with Natural Flows	52
Slip in Nature	53
Conclusions.....	55
Tables.....	57
Figures.....	59
Chapter 3: Incorporation of substrate-sourced water and carbon dioxide in large-scale basaltic experimental lava flows	69
Abstract	70
Introduction.....	70
Methods.....	72
Results.....	75
Observables	75
Raman analyses.....	75
FTIR analyses	76
Electron Microprobe	76
Discussion	77
Conclusions.....	81
Tables	82
Figures.....	86
Conclusion	93
References	94
Biographical Data	110

List of Figures

Chapter 1

Figure 1. Syracuse University Lava Project setup	28
Figure 2. Velocity measurement	29
Figure 3. Representative flow morphologies from lava experiments	29
Figure 4. Representative flow images.....	30
Figure 5. Histogram of flow morphology by slope angle.....	31
Figure 6. Ψ versus emplacement parameters	32
Figure 7. Four representative flows and associated Ψ values.....	33
Figure 8. Viscosity and effusion rate relative to Ψ	34
Figure 9. Ψ and slope.	35
Figure 10. Ψ and surface temperature at the end of each experiment	36
Figure 11. Single and dual breakout flows	37

Chapter 2

Figure 1. Basaltic lava flows being emplaced onto different substrates.....	59
Figure 2. Representative lava morphologies for lavas on each of the 5 different substrates.....	60
Figure 3. Morphological changes during lava slip.....	61
Figure 4. Velocity and acceleration for selected experiments on their respective substrates.....	63
Figure 5. Bubbles and related features.....	64
Figure 6. Vapor-inflated flow	65
Figure 7. Representative lava flow basal-crust textures	66
Figure 8. Lava behavior conceptual model.....	67
Figure 9. Slope map of volcano Villarrica.....	68

Chapter 3

Figure 1. Representative flows on various substrates used in experiments	86
Figure 2. Photomicrographs of lava samples	87
Figure 3. Representative spectra and transect data	88
Figure 4. Representative EMPA transects and secondary electron imagery from flows on wet sand and clay	89
Figure 5. Diffusion modeling results	90
Figure 6. Diffusion profile of Fe across the lava-substrate boundary.....	91
Figure 7. Modeled diffusion profiles of water and carbon dioxide	92

List of Tables

Chapter 1

Table 1. Experimental data.	26
Table 2. Measured maximum temperatures and other calculated values.	26
Table 3. Typical parameters of flows from PEG analog experiments, Sulp experiments, and natural Hawaiian pāhoehoe flow lobes.	27

Chapter 2

Table 1. Experimental data.	57
Table 2. Sliding angles.....	58

Chapter 3

Table 1. Volatile concentrations measured by spot analyses via FTIR spectroscopy.	82
Table 2. Compositions for glass and substrate particles measured via EMPA.....	83
Table 3. Lava-substrate diffusion distances.....	83
Table 4. Published, measured, and calculated values for diffusion equations.....	84

Introduction

Basaltic lava flows are abundant on the surface of Earth and other planetary bodies. Effusive volcanism is responsible for much of the repaving of Earth's surface and is a key component in the formation of tectonic plates. Basaltic lava flows have also been observed to overrun population centers across the globe. Additionally, the eruption of pāhoehoe sheet flows has been suggested as a major process in the formation of flood basalts, the largest volumetric outpourings of lava on Earth. Understanding the dynamics of basaltic lava flows has widespread application for understanding Earth's history and for managing volcanic hazards from lava.

Advance of basaltic lava across the landscape has been observed for centuries. Pāhoehoe lava flows advance across the landscape by three different methods: flowing in channels, through subsurface lava tubes, and slow lobe-by-lobe advancement. Study of actively flowing lavas is both difficult and dangerous due to eruptions occurring in remote locations and at unpredictable times. Another difficult aspect of studying active lava flows is that they must either be observed at a distance, or the observer must wear protective equipment to withstand the extreme heat of the lava. Due to the inherent danger and difficulty of studying active lava flows, other methods have been undertaken to understand basalt rheology and emplacement, including bench top experiments, as well as numerical and analog models. However, there is a large gap in scale between that of natural flows and small cm-scale analog flows.

The Syracuse University Lava Project laboratory is the first of its kind to produce meter-scale experimental lava flows. The lavas are generated at natural eruption temperatures ($\sim 1200^{\circ}\text{C}$) using basaltic material. The close-proximity and safety of these laboratory-generated flows provides the opportunity to perform detailed studies in a controlled environment and works to bridge the gap between small-scale analog flows and natural-scale investigations.

One of the themes of the research presented here is the relationship between lava flow morphology and emplacement conditions. Since most lavas on Earth solidified without being directly observed while active, the solidified deposits are the only product available for study. To understand the history of these lava flows, it is important to be able to connect morphology to eruption conditions. Studies of experimental lavas allow for control of eruption parameters, which can then be connected to observations of lava morphology formation in real-time. This will help to clarify connections between morphology and eruption conditions.

The first chapter of this dissertation focuses on one of the most commonly observed morphologic lava types, pāhoehoe flows, and the relationship between pāhoehoe morphology and emplacement conditions. These flows comprise inflated sheets behind a complex flow-front made up of many individual breakout lobes. Pāhoehoe flows form a variety of morphologies including tubes, channels, surficial folds, sheets, and breakout lobes. Analog studies using polyethylene glycol wax have focused on conditions that generate these morphologies.

Experiments in chapter one focus on comparing morphologic expression in the experimental lava flows to both natural lavas and wax flows. These flows are then compared to flow morphologies generated from laboratory analog experiments and natural flows. This has broad application to studies in locations such as the seafloor or other planetary bodies where lava properties and emplacement conditions are inferred from flow morphologies.

The second chapter of this dissertation focuses on the physical behavior and emplacement of lava over volatile-rich substrates. The interaction of lava on various substrates has received little attention, as it is often overlooked during active eruptions. Lava flows have been emplaced into or onto a wide variety of substrates including water, snow, ice, clay, sand, and saturated ground. Results from these experiments show that lavas create large bubbles, ejection of particles at flow

margins, and rapid downslope sliding of lava. The most significant finding is the short-lived sudden onset of rapid downslope acceleration of lava flows, termed ‘lava slip’. This has application to flows on Earth and other planetary bodies as well as natural hazard assessment.

The third and final chapter of this dissertation focuses on chemical modification of lava flowing over volatile-rich substrates. Both subaerial and submarine lavas contain dissolved volatiles (H_2O , CO_2 , SO_2 , H_2S , etc.), and understanding lava-volatile interactions is important because dangerous and explosive eruptions are driven by exsolution of dissolved volatiles. Recovered samples of natural lavas from various locations such as the seafloor, glaciovolcanoes, flood basalt provinces, and hotspots have been measured for their chemical makeup and dissolved volatile content. When assessing lava volatile content, it is assumed that dissolved volatile abundances reflect exsolution and degassing processes and that they are not influenced by external sources. Chapter three challenges that assumption. In this study, lava flows were emplaced onto different volatile-rich substrates to specifically look for evidence of externally sourced volatile chemical interaction. Glassy basalt samples were analyzed for water and carbon dioxide content via three different methods. Major element transport method and timing at the lava-substrate boundary is also discussed. This has application to lava-volatile interactions in many types of environments.

The works presented in this dissertation complement studies performed on remotely located lava flows, where morphology and chemistry are used to infer eruption conditions. Perhaps more importantly, the works discussed here highlight large-scale experimental flows as a tool that can be used to gain further insight and clarity into basaltic lava flow dynamics. The facilities used as part of this study offer the opportunity to perform detailed investigation of active flow processes in a safe and controlled environment. The potential for future studies using the meter-scale lava

flows as an investigate tool is immense, and it is anticipated that the desire to utilize this tool will only increase with time. The research presented here, coupled with previous studies, serve as a stepping-stone to additional possibilities and understanding of basaltic lava flow dynamics.

Chapter 1: Experimental constraints on pāhoehoe breakouts

In preparation for submission to:

Bulletin of Volcanology

Abstract

Basaltic pāhoehoe flows produce various types of flow morphologies, including meter-scale individual lobes to full-scale pāhoehoe flows. Connecting flow parameters of actively flowing lava to flow morphologies will improve the ability to estimate emplacement parameters in ancient lavas. As lavas advance downslope and progressively cool, their velocity decreases and their viscosity increases. As this occurs, the outer crust may rupture, releasing more fluid lava. Meter-scale, high-temperature basaltic lava flow experiments show that morphologic transition, particularly the segmentation of flows into smaller lobes, is related to lava viscosity. High-viscosity lavas produce breakouts of smaller lobes, while low-viscosity flows do not. Additionally, crustal thickness and surface temperature are related to two different observed modes of breakout. The dimensionless parameter Ψ is useful for quantitatively relating eruptive parameters to morphologies. High relative viscosity lavas developed into low- Ψ flows with breakouts. Compared to three recent basaltic eruptions, whole-flow effusion rate values greatly overestimate the Ψ value for breakouts developed at the flow front.

Introduction

Basaltic lava morphologies have been studied by volcanologists since at least the late 1800's (Dana 1890; Macdonald 1953; Swanson 1973; Peterson and Tilling 1980; Rowland and Walker 1990; Hon et al. 1994; Sehlke et al. 2014). Basaltic lava flows form similar morphologies in both subaerial and submarine environments, even though they have different names. The morphologies vary from individual bulbous extrusions to widespread lava sheets with a mostly flat upper surface (Ballard and Moore 1977). An understanding of basaltic lava emplacement and morphologic evolution is important for reconstructing the history of ancient lavas and for predicting lava hazards at modern volcanoes.

About 90% of all subaerial basaltic lava flows are classified into one of the two major basaltic morphologic groups, pāhoehoe and a'ā (Rowland and Walker 1990). Active pāhoehoe flows are typically 2-5 meters thick, have viscosities around 10-200 Pa s at 1200 °C and can cover large areas, up to tens of square kilometers (Walker 1973; Malin 1980; Hon et al. 1994). Hawaiian-style pāhoehoe flows have flat or billowy upper flow surfaces that, in places, may contain thin buckled crust, measuring centimeters in amplitude and wavelength, commonly referred to as pāhoehoe ropes (Fink and Fletcher 1978; Self et al. 1998). The basic flow types generated by submarine flows occur along a continuum from pillow lavas, to flows with breakouts, to pāhoehoe sheets, to massive pāhoehoe sheets. Pillows are bulbous molten lava extrusions typically tens of centimeters across, while typical pāhoehoe flows can be tens of meters wide and hundreds of meters in length (Kennish and Lutz 1998; Umino et al. 2000; McClinton and White 2015). An intermediate flow type between pillows and pāhoehoe sheets is flows with breakouts which form centimeter- to meter-scale extrusions that are larger and flatter than pillows with a smooth outer crust (Gregg and Chadwick 1996; Chadwick 2003). Pāhoehoe breakout morphologies are typically associated with ponded lavas or pāhoehoe flow lateral breakouts (Chadwick et al. 2013).

Foundational field observations of pāhoehoe flows have laid a solid groundwork for continued morphologic study (Nichols 1939; Macdonald 1953; Swanson 1973; Hon et al. 1994; Greeley et al. 1998). Key studies of tube formation (Swanson 1973), morphologic transitions (Peterson and Tilling 1980; Soule et al. 2004), inflation (Hon et al. 1994; Self et al. 1998), and breakouts (Hon et al. 1994; Gregg and Keszthelyi 2004) have greatly advanced our understanding of subaerial pāhoehoe flow emplacement and evolution. Field studies show that pāhoehoe flows commonly advance by tube-fed flow, channelized flow, and/or surficial flow (Swanson 1973; Malin 1980;

Peterson and Tilling 1980; Rowland and Walker 1990; Hon et al. 1994; Kauahikaua et al. 1998; Cashman et al. 2000; Gregg 2017; Dietterich et al. 2021). Two main mechanisms influence flow-front macroscopic behavior: inflation and breakouts. The process of inflation is driven by influx of new lava into the lava flow core, which causes vertical separation of the upper and lower crust, resulting in whole-flow thickening (Hon et al. 1994). The lava flow's upper crust comprises the upper surface and lateral flow margins, and the lower crust comprises the base of the flow that is in contact with the substrate (Hon et al. 1994). The upper and lower lava crusts insulate the molten core, thus allowing molten flow inside the crust (Self et al. 1997; Kauahikaua et al. 1998; Hoblitt et al. 2012). Breakouts are produced by extrusion through weak spots in the crust (Crown and Baloga 1999; Hamilton et al. 2013; Farrell 2019). Several different breakout mechanisms in natural basaltic lavas have been closely observed, and each can be explained by crustal weak spots or elevated internal pressure (Gregg and Keszthelyi 2004; Belousov and Belousova 2017).

Analog laboratory experiments have also been used to understand lava flow morphologies. Polyethylene glycol wax (PEG) has been a commonly used analog material because, like natural lava flows, rapidly following extrusion, the fluid wax it develops a thin flexible crust that later cools into a thick solid brittle crust. A notable set of studies, which used PEG wax as the lava analog, developed a dimensionless parameter Ψ , which is the ratio of diffusive heat transfer to advective heat transfer, and showed how Ψ was correlated to flow morphology (Fink and Griffiths 1990, 1992; Gregg and Fink 2000). Griffiths and Fink (1992a, b) then used Ψ to infer eruption conditions of natural flows in remote locations.

Here, the Syracuse University Lava Project (SULP) laboratory was used to further explore lava flow morphology by detailed investigation of the formation of pāhoehoe breakouts. We find that

morphology is closely related to viscosity, and that Ψ values for molten basalt and Sulp flows are higher than values for PEG flows, but that Sulp values match well with natural flows. We also find that the two distinct modes of breakout manifest in Sulp flows are related to surface temperature and crustal thickness.

Methods

The Sulp laboratory features a blast furnace inset with a silicon-carbide crucible capable of holding up to 40 liters of material and heating basalt to liquidus temperatures (Figure 1). The starting material used to create laboratory-generated lava flows is 1.2 Ga Keweenaw basalt (Wirth et al. 1997). The basalt was heated for approximately twelve hours until all material was fully melted. The molten basalt was then heated for several more hours, occasionally stirred to facilitate degassing and homogenization, and poured onto the experimental substrate to create a lava flow. Composition of the lava flows is near the defined chemical boundary of basalt and basaltic andesite, at 53 wt% SiO_2 .

All experiments were recorded using two high-definition video cameras at near-vertical and oblique angles. Infrared images of each flow were taken using a FLIR T300 camera at approximately 10-second intervals to record lava flow surface temperature. Two K-type thermocouples were placed on the substrate, at distances of thirty and sixty centimeters from the mouth of the delivery trough, to measure the basal temperature of the lava as it progressed downslope.

The plan-view area of each flow was calculated by outlining the flow margins using the browser-based irregular-area calculator, SketchandCalc (Dobbs 2013). Flow thickness was measured after solidification, along the central flow path fifty centimeters from the mouth of the delivery trough. Lava velocimetry was performed by extracting data from video recordings using a MATLAB-

based particle image velocimetry software, PIVlab (Thielicke and Stamhuis 2014). For each flow, velocimetry measurements were taken from a three-second duration video clip, starting thirty seconds after the flow contacted the substrate. For the three-second duration, extracted velocity vectors from each frame were averaged to produce one frame with many averaged velocity vectors (Figure 2). Velocity of each flow was measured across a transect located thirty centimeters downslope from the head of the flow. The reported velocity for each flow is the maximum velocity value from the transect. Due to the tilting mechanism of the furnace, the effusion rate could not be held completely steady during experiments, but care was exercised to maintain a nearly constant stream of lava throughout each experiment. The unsteady nature of lava effusion from the furnace required the effusion rate to be calculated as defined by Harris et al. (2007), using calculated total volume and pour duration, as time-averaged discharge. Effusion rates for all flows ranged from 44 to 345 cm³/sec. Reported lava temperature measurements are the maximum recorded temperature for each flow collected from infrared still imagery. Flow effective viscosity (η) was calculated via the commonly used field-based method, Jeffreys equation (Jeffreys 1925): $\eta = (\rho g h^2 \sin \theta) / 3v$ (equation 1) where ρ is density (kg/m³), g is gravitational acceleration (m/s²), h is thickness (m), θ is slope steepness (°), and v is velocity (m/s). The density used for all calculations was 2707 kg/m³ (Soldati et al. 2020). Calculated effective viscosities ranged from 15 to 165 Pa s, and these calculated viscosities are used as a flow-to-flow comparison.

The dimensionless Ψ parameter was also calculated for each flow. This incorporates multiple parameters into a single value that relates crustal growth rate to flow deformation. A single Ψ value was calculated for each flow using the simplified version of Fink and Griffiths' original equation (1990): $\Psi = \left(\frac{g\rho}{\eta}\right)^{3/4} Q^{1/4} t_s$ (equation 2), where g is gravitational acceleration (m/s²),

ρ is lava density (kg/m^3), η is viscosity (Pa s), Q is effusion rate (m^3/s), and t_s is solidification time (sec) of the lava crust. Viscosity and effusion rate values used for this calculation were determined by the methods described above. Determining the solidification time for the development of the outer crust for each flow was challenging because it is very difficult to measure a crust that cools and thickens with time on flowing basalt. Previous studies chose to use a constant value for t_s : < 1 second for submarine flows (Griffiths and Fink 1992a), and 10 seconds for subaerial Hawaiian flows (Gregg and Keszthelyi 2004). Solidification time in our experiments, based on incandescence and onset of surficial folding, was visually estimated to be between 3 and 8 seconds for each flow. Ultimately, for our experiments, a constant t_s value of five seconds was used as it is near the median of estimates for all flows.

The experimental set for this study consists of twenty-four lava flows emplaced at temperatures between 1000° and 1300° C on earthen slopes (1° to 30°) covered in one to two centimeters of dry quartz-rich sand. A variety of pāhoehoe lava morphologies were formed, producing flows of various shapes and sizes (Figure 3).

Results

Lava flows in this study generated two distinct morphologies. Flows were categorized either as a pāhoehoe or breakout flow, denoted by the absence or presence of a breakout. For the purposes of this study, flows without a breakout are referred to as pāhoehoe flows, and flows that contain at least one breakout are referred to as breakout flows. Here we discuss observations made during active flow, measurable parameters, and Ψ values for each flow.

Observations

Flows begin as a single pāhoehoe sheet that advances downslope. On shallow slopes ($< 5^\circ$) the lava initially advances as a several-centimeter-thick mostly circular sheet. On steep slopes ($\geq 5^\circ$)

the lava advances to become a thin (< 2 cm) oblong flow. As flows begin to cool, the slow-moving lateral margins chill to produce confining levees. Once lateral levees are established, the flow maintains a constant width and develops a centralized channel. As the flow cools and a thin viscoelastic crust is formed on the upper flow surface the advance rate at the flow-front slows. The flow lengthens as the newly extruded lava overruns the flow front. With influx of new lava, the flow rate at the head of the flow is greater than at the flow front, causing a pile-up of lava near the flow's leading edge resulting in buckling of the upper surface's viscoelastic crust. If lava supply is cutoff, or the flow rate significantly decreases, the crust becomes strong enough to resist advance or flow thickening, and the flow will solidify as a pāhoehoe flow devoid of breakouts. If lava supply continues as advance of the flow front stalls, the cooling and thickening lava crust acts as an insulating envelope to contain the influx of lava, resulting in flow-front inflation. Inflation can increase flow thickness by a factor of three and can lead to development of a lava breakout.

Flows that generate breakouts do so in two different styles: passive or active. Passive breakouts are generated as pliable crust rides atop the molten interior. As the crust is stretched and strained by downslope and lateral spreading, portions of the crust start to separate, tearing the crust and allowing the molten lava in the core to spill out. Active breakouts are generated as lava is injected beneath the upper crust from inflation, acting to increase flow thickness. Eventually, as new lava is injected into the flow core, the increased pressure from magmastatic head exceeds the strength of the outer crust, forcing a crustal rupture and resulting in a breakout. Flow evolution continues to follow the inflation-and-breakout pattern to produce the breakout flow morphology, analogous to pāhoehoe complex flow fronts.

Separate from passive and active style, breakouts were observed from both the upper and lower crust in our laboratory-generated flows, which we classify as type A or B. Breakouts most often rupture through the upper crust (Type A), but sometimes ruptures can occur through the lower crust (Type B). Type A breakouts can be produced from passive- or active-style breakouts.

Observations during active flow and through video analysis show that type A breakouts rupture through the upper crust and form at the flow front or at lateral flow margins. Type B breakouts are formed only from active-style breakouts. Type B breakouts rupture through the lower crust and form only at the flow front (Figure 4). Another distinctive difference between type A and type B breakouts is the presence of embedded sand grains in the crust. Breakouts that originate through lower crust are littered with embedded sand grains and are categorized as type B breakouts. Four of the seventeen breakout flows generated type B breakouts.

Most breakout flows solidified with either one or two main breakouts (Figure 3). The main difference between flows with one or two breakouts is the location of the breakout. Flows with a single lava extrusion develop a breakout at the leading edge of the flow and are termed single breakout flows. Flows with two main sources of lava are termed dual breakouts flows because both breakouts form simultaneously on opposite flow margins. Lava extrusions in dual breakout flows may also breakout near the toe of the flow, with each breakout occurring near a lateral flow margin (Figure 3). Sometimes one of the breakouts may develop fully out of a lateral flow margin. Seven of the seventeen breakout flows generated a dual breakout flow.

Metrics

Seventeen of twenty-four lava flows produced breakouts. Breakout flows are generated if any of the following conditions are satisfied: $\leq 10^\circ$ slope, $< 1100^\circ\text{C}$ maximum temperature, effective viscosity $> 50\text{ Pa s}$, or effusion rate $< 130\text{ cm}^3/\text{sec}$ (Table 1; Figure 5). Flows generated outside

of these conditions did not develop breakouts. In addition to the criteria mentioned above, there is a boundary around 40 Pa s where flows with viscosities lower than 40 Pa s predominately remained as pāhoehoe flows. Four of the seventeen breakout flows generated type B breakouts. Seven of the seventeen breakout flows developed more than one breakout.

Pāhoehoe flows are uniformly thin (2-3 cm thick), have an aspect ratio (length to width) of about three, possess a smooth centralized flow channel, and contain folds at the flow front (Figure 3). Breakout flows are thicker than pāhoehoe flows and have an aspect ratio of about two. Breakout flows also contain arcuate surface folding. However, folds in breakout flows may be asymmetrical, and the folded portion extends farther upslope than in pāhoehoe flows (Figure 3).

Generally, low-viscosity lavas produce pāhoehoe flows and higher viscosity lavas produce breakout flows. Even though pāhoehoe flows are not generated on slopes below ten degrees, slope steepness is not correlated to Ψ (Figures 5 and 6). Five of the seven pāhoehoe flows and six of the seventeen breakout flows were generated at effusion rates greater than 130 cm³/s (Table 1), suggesting that effusion rate is not closely correlated to Ψ . The strongest correlation to Ψ is viscosity. Only two of seventeen breakout flows have viscosities below 40 Pa s, while all seven pāhoehoe flows have effective viscosities below 40 Pa s. Table 1 shows that pāhoehoe flows are created at high Ψ values (avg Ψ : 109 ± 25 ; Figure 7) and breakout flows are created at low Ψ values (avg Ψ : 47 ± 23).

Discussion

The ultimate objective of morphologic study of lava flows using the Ψ parameter is to infer emplacement parameters of ancient flows based on a flow's final morphology. This study advances closer to that goal than ever before by exploring morphologic transition and flow evolution using molten basalt flows. Here we discuss active flow parameters that are related to

morphology. Additionally, we discuss the Ψ parameter, and the differences between type A and type B breakouts. We also discuss flow surface temperatures and crustal thicknesses at the time of breakout formation. Lastly, we compare our data against results from PEG wax flows and three recent basaltic eruptions.

Morphology and Ψ

The dimensionless parameter Ψ is calculated from lava density, gravitational acceleration, lava viscosity, effusion rate, and the time required for the flow surface to solidify. In the calculation of Ψ for our experiments (eq. 2), three of the five parameters were held constant: g , ρ , and t_s . For the purposes of understanding the parameter relationships to Ψ , grouping the constant parameters simplifies the equation to $\Psi \propto Q^{1/4}/\eta^{3/4}$ (equation 3). It is expected that η will have a greater influence on Ψ than Q because η is raised to a higher power than Q . A plot of Q vs η confirms this relationship (Figure 8). The data show no systematic variation of Ψ with change in effusion rate. However, a systematic relationship exists between viscosity and Ψ (Figure 8). Similarly, in the final morphologies of the lava flows, no systematic relationship of a flow's morphology is manifest with changes in effusion rate. Conversely, changes in viscosity show a clear trend: pāhoehoe flows are formed from lavas with relatively low viscosity and breakout flows are formed from lavas with higher viscosity. This suggests that, in morphologic expression, lava viscosity plays a more significant role than effusion rate.

Results from Ψ analysis of natural flows and PEG wax analog flows agree with the results from our investigation. Sulp flows, like Hawaiian lobes, display little morphologic variation.

Calculated Ψ values for Sulp flows ($\Psi = 21 - 144$) fall within ranges calculated for Hawaiian flow lobes ($\Psi = 2 - 334$) (Gregg and Keszthelyi 2004). While the raw Ψ values for PEG flows may not directly match Sulp values, PEG wax flows manifest the same general trend as Sulp

flows, with breakout flows being generated at low Ψ values and pāhoehoe flows at high Ψ values (Fink and Griffiths 1990; Gregg and Fink 2000). Calculated maximum Ψ values of PEG leveed and sheet flows are about four times lower than the maximum Ψ values of Sulp pāhoehoe flows (Figure 9).

One possible explanation for Sulp flows having higher Ψ values than PEG flows is that the tensile strength of molten basalt is two to three times lower than that of PEG (Soule and Cashman 2004). Lower tensile strength in Sulp flows allows for increased lateral spreading and development of breakouts under a wider range of conditions. When Ψ values of PEG are normalized to Sulp values, the morphologies of both flow materials fall within similar ranges (Figure 9). Pāhoehoe flows from our experiments plot in the highest established morphologic regime for PEG flows while breakout flows plot in the same regions as Gregg & Fink's (2000) 'folded' and 'rifted' flows.

Surface temperature of the lava is also related to morphologic expression. A cooling model was used to calculate the upper surface temperature of the lava at the 'end' of each experiment. For our purposes, the 'end' of the experiment is defined as the moment at which lava discharge from the furnace was terminated. For this analysis, the cooling model that we used was developed specifically for the initial cooling of pāhoehoe lobes (Keszthelyi and Denlinger 1996; equation 18): $t = \rho C_p H (T^{-3} - T_o^{-3}) / (3\epsilon\sigma)$, where t is time (s), ρ is density (kg/m^3), C_p is heat capacity ($5.67 \times 10^8 \text{ J/kgK}$), H is thickness (m), T is surface temperature ($^{\circ}\text{C}$) at time t , T_o is initial temperature ($^{\circ}\text{C}$), ϵ is emissivity of 0.95, and σ is the Stefan Boltzmann constant. We calculated the temperatures of the upper surface of each flow at the 'end' of each experiment and results ranged from 714 to 1098 $^{\circ}\text{C}$ (Figure 10; Table 2). The flows with the highest end-of-experiment temperatures generated pāhoehoe flows. Intermediate temperatures generated breakout flows

with type A breakouts, while the lowest temperatures generated breakout flows with type B breakouts. This pattern suggests that lava surface temperature is directly related to the morphology of each flow.

There is an apparent discrepancy between results from this investigation and PEG studies as to what parameter most closely controls morphology. Here, we find that morphology is strongly temperature dependent, whereas other studies found the strongest relationship to be with effusion rate (Fink and Griffiths 1990; Gregg and Fink 2000). Potential reasons for the discrepancy could be each material's cooling rate, effusion rates, or temperature differences between the experimental material and the environment. Our thin lava flows have higher cooling rates than PEG flows, which may allow for more rapid changes to the viscosity of the flow, thereby artificially increasing the rate of morphologic change. Another difference may be the measurement method of effusion rate. PEG flows measured instantaneous discharge, but effusion rate for our basalt flows was measured as a time-averaged discharge. Molten basalts have significantly higher temperatures than PEG wax extruded into solution, and each flow material contains different time scales required for crust development. Additionally, greater overall temperatures and higher cooling rates compound on each other, more clearly highlighting the lava's temperature dependence, which may outweigh the effects of effusion rate. While our results, which show that viscosity is the most closely related eruption parameter to morphology, differ from previous studies, we feel confident in our findings because our basalt flows more closely mimic natural systems compared to other analog materials.

Studies using analog experiments have strengths over studies of natural systems such as being performed safely in a controlled environment that is designed for detailed study. While analog experiments have greatly expanded our understanding of lava flows, they do not perfectly scale

up to natural systems (Lube et al. 2015). The most obvious characteristics that differ between wax analog flows, natural pāhoehoe flows, and Sulp flows are the physical dimensions of solidified flows (Table 3). Natural flows are the largest, PEG flows are the smallest, with Sulp flows in between. Other ways the three flow materials are different from one another - as discussed above - are viscosity, temperature, and effusion rate. These measurable parameters of Sulp basalt flows are more closely related to natural basalt flows than to PEG wax flows. While the physical dimensions of Sulp flows do not scale perfectly to natural systems, they are the most closely scaled analog experiments to date. Sulp values for Ψ are calculated using active molten basalt flows, so we expect calculated Ψ values from Sulp flows to represent a more accurate representation of Ψ for natural basalt flows than values from PEG flows.

Transition to Breakouts

Formation of a lava breakout is the clear moment marking the transition from a pāhoehoe flow to a breakout flow. It is the balance between crust formation and crustal disruption that controls the transition and the development of type A and type B breakouts. Heat loss promotes crust formation, and the flow of lava downslope promotes crustal disruption. In conditions with high effusion rate and low viscosity lava, the flow will advance downslope rapidly enough that it prevents crust formation allowing the lava to remain as a single thin sheet-like flow. However, if effusion rates are low and viscosities are high, then a crust will form rapidly enough to stall the advance of the lava. Accompanying lava flow stall, the flow may inflate and produce a type A or type B breakout, and hence, produce a breakout flow.

Field studies of active basalt flows show that a developing lobe can be broken down into three discrete layers. Starting from the inner-most portion of the flow, the upper crust layers are made up of the viscous core, the viscoelastic crust, and the brittle crust (Hon et al. 1994). Additionally,

based on observations from our experiments the life of a flow can be divided into three distinct flow stages: early, middle, and late. The presence or absence of the three flow layers characterizes each flow stage. The early flow stage can last from tens of seconds to minutes and is categorized by both the upper and lower viscoelastic crust enclosing the core. As such, the flow may accommodate an increase in core volume by stretching and thinning of the viscoelastic crust. The middle flow stage typically lasts several minutes and is marked by formation of a brittle crust on the upper flow surface, and the lower crust consisting of only the core and viscoelastic layer. This lower crust does not form a brittle crust at this stage. Empirical data from natural lavas show that the lower crust cools at approximately 70% the rate of the upper crust (Hon et al. 1994). During this middle flow stage, if lava influx continues to the flow front, the upper crust resists inflation due to the development of the outer brittle crust, forcing the lower crust to accommodate the volume increase via stretching of the viscoelastic crust until it also develops a brittle crust. A prominent characteristic of the middle flow stage is exposure of the lower crust via inflation, which is marked by rapid lobe thickening and the presence of sand grains embedded in the newly exposed lower crust. The late flow stage lasts through complete solidification of the flow, where both the upper and lower crusts consist of a brittle outer crust that no longer accommodates inflation by additional lava influx. Rather, the late stage is marked by either a breakout that occurs at crustal weak spots, or complete flow solidification.

The most striking and distinctive difference between type A and type B breakouts is the presence of sand grains on the outer lava crust surface of type B breakouts. The SULP flows were poured onto a sandy substrate because it is simple to sculpt to a planar surface, to remove any terrain-based substrate effects on morphology. During flow, sand grains from the substrate become adhered to the lava crust by two methods: welded to lower crust during flow or adhered to the

upper crust by particle-entrained steam jetting. First, as the lava advances downslope and cools, it becomes tacky. The weight and heat of the tacky lava welds the sand grains to the basal surface of the flow. As the base of the flow is exposed to the atmosphere via middle-flow-stage inflation, the sand grains are clearly visible (Figure 7). Second, over time, the lava flow heats the substrate via conductive heat transfer. Heating of the substrate volatilizes interstitial water causing steam jets at the margins of the flow. These steam jets sometimes entrain sand grains and produce airborne sand particles. Some airborne sand grains may land on the upper surface of flow, dotting the crust with light-colored sand grains. The sand grains welded to the lower crust during flow are continuous and densely spaced along the entire lower crust surface and are present on all newly exposed surfaces of the flow lobe, instead of being restricted to an area near a substrate volatile jet.

Over half (10 of 17) of the breakout flows produced single breakout flows. The remaining seven breakout flows produced dual breakouts. While no systematic relationship with maximum measured temperature, end temperature, or effusion rate was found, there is a recognizable relationship with viscosity (Figure 11). Single breakout flows have higher viscosity ($\text{avg} = 107 \pm 42$) than dual breakout flows ($\text{avg} = 66 \pm 38$). Type B breakouts were single breakout flows and had a low 'end' temperature and high viscosity. The most common method of generating a dual breakout flow is by crustal rollover. This occurs when the flow front develops a thin crust, decreases in velocity, but does not completely stall. The incoming upstream lava pushes the lava downslope with the upper crust riding atop the fluid inner core. This motion imparts a vertical velocity gradient with the slowest velocity at the flow base and the highest velocity at the upper surface of the flow. If the upper crust cools enough to cause the flow to stall, the lava in the core will rupture the hotter and thinner crust of the lateral margins. The resulting extrusions are

generated at the edges of the cool and rigid upper crust, producing the dual breakout morphology.

Lava crust forms as the lava cools to the glass transition temperature ($\sim 730^{\circ}\text{C}$). Therefore, the formation of a lava crust is controlled by heat loss. Additionally, a lava crust modifies lava behavior. If the early, middle, and late flow stages are controlled by heat loss and flow behavior, then a correlation between flow stages and type A and type B breakouts should also exist. To assess a potential correlation, we used an established empirical equation to estimate crustal thickness at the onset of breakout. The equation relates time since eruption to crustal thickness (Hon et al. 1994; equation 1). Based on travel time downslope of Sulp lavas, calculated crustal thicknesses for the upper crust on breakout flows range from 6.9 to 21.3 mm (Table 2). At breakout initiation, all type A breakouts had crustal thicknesses of 10.5 mm or less. The four type B breakouts had the four greatest crustal thicknesses at the time of breakout, at 10.9 mm or greater. This shows that type A breakouts have a thinner upper crust at the onset of breakout than type B breakouts. Crustal thickness estimates support the interpretation that type B breakouts are generated as the upper crust becomes too rigid to accommodate inflationary volume change. These findings show that crustal thickness is correlated to breakout type.

Comparison with Natural Flows

Finally, we compare natural pāhoehoe morphologies from three recent basaltic eruptions with pāhoehoe morphologies to morphologies of Sulp flows. The three eruptions to be compared to Sulp flows are: Tolbachik 2012-2013, Holuhraun 2014-2015, and Kilauea 2018. For each of these, the published values for density, viscosity, and effusion rate were used to calculate a local, or meter-scale, Ψ value. Based on results from our Sulp experiments, we expect Ψ values for

rounded bulbous breakouts to be $\Psi < 40$, extrusions containing surficial folding to be between Ψ of 40 and 80, and thin pāhoehoe breakouts to be $\Psi > 80$.

The 2012-2013 eruption of Tolbachik consisted of a months-long event extruding Hawaiian type lavas from a km-long fissure system (Gordeev et al. 2013; Belousov and Belousova 2017). As the eruption progressed, the emplacement style transitioned from a'ā to pāhoehoe (Belousov and Belousova 2017). The pāhoehoe flows were 1-5 m thick and contained toothpaste breakouts and lobes with folded crust (Gordeev et al. 2013). Raw calculated Ψ values for breakouts from this flow range from 33 to 316.

The 2014-2015 Holuhraun eruption was a fissure-fed eruption comprising pāhoehoe lobes, intermediate transitional types such as shelly, slabby, rubbly, and a'ā lavas (Pedersen et al. 2016). Field surveys indicate pāhoehoe flows were dominant proximally and at the active flow front where pāhoehoe breakouts were present (Pedersen et al. 2016; Voigt et al. 2021). Pāhoehoe breakouts from this eruption are described as having continuous coherent surfaces (Voigt et al. 2021), similar to what we describe in our experiments as a pāhoehoe flow. Raw calculated Ψ values for lava breakouts from this eruption range from 240 to 2719.

The 2018 Kilauea eruption was characterized by several phases that included explosive and effusive eruptions from the Kilauea crater and twenty-four individual fissures (Neal et al. 2019; Dietterich et al. 2021). The fissures fed numerous lava flows comprised mostly of channelized a'ā flows that eventually flowed into the sea (Gansecki et al. 2019; Soule et al. 2021). However, there were breakouts at active flow fronts, including toothpaste lava extrusions from fissure 17 (U.S. Geological Survey 2022). Toothpaste lava extrusions have been described as elongated pillows (Gansecki et al. 2019), so we expect Ψ values to be similar to that of pillow lavas. Raw calculated Ψ values range from 70 to 3525.

The Ψ values for breakouts from these eruptions are mismatched with Ψ values from experimental flows. This is likely due to the reported effusion rate values using the published values for each eruption, often measured at the vent, the Ψ values are unreasonably high compared to SULP Ψ values. For instance, we would expect the toothpaste lava extrusions from Kilauea 2018 to be a Ψ value of 40 or less. However, the minimum Ψ value from that eruption is 70, with the highest being over 3500. One reason for this may be that measurement of effusion rate (Q) is calculated from the main volcanic vent. Measurements at the vent are not an accurate representation of Q at the breakout site because published Q values represent the effusion rate for the entire flow. Pāhoehoe breakouts are commonly distributed at the flow front in a dendritic pattern, and thus represent only a fraction of the Q values measured at the vent. Therefore, for the purposes of lobe-scale Ψ studies, effusion rates measured at the vent provide a gross overestimate.

The study by Gregg and Keszthelyi (2004) highlights the disparity between published whole-flow effusion rates and local rates at the breakout site. They studied active Kilauean flows from 1996 which had a whole-flow effusion rate ranging from 3-5 m³/s. Yet, measured effusion rate values at the breakout site were three orders of magnitude lower than the reported whole-flow values. Re-calculated Ψ values for the 1996 Kilauea flow, using locally measured effusion rate, ranged from 2 to 129. Using whole-flow values for effusion rate, the Ψ values would instead range from 17 to 871. The difference in Ψ values from whole-flow effusion rate to local effusion rate highlights the need to measure effusion rate at the breakout site to reflect accurate Ψ values at the lobe-scale.

Applying an effusion rate scaling factor for the three eruptions described above can yield more applicable values for morphologic investigation. Similar to the 1996 Kilauea flow, using effusion

rate values that are three orders of magnitude less than Q values measured at the vent places the calculated Ψ values, based on their exhibited morphologies, more closely in the ranges exhibited in laboratory experiments. For the three eruptions discussed above, using whole-flow Q values divided by one thousand yields Ψ values as follows: Holuhraun ranged from 43 to 483, Tolbachik ranged from 6 to 56, and Kilauea 2018 ranged from 12 to 627. These values are much more in line with results from Sulp experiments. For example, Tolbachik contains pillow-like extrusions and breakouts with folded surfaces. Using Q values adjusted to the local-scale, the Tolbachik lobes have calculated values from 6 to 56, which is a reasonable range that is consistent with our observations for lobes with folded surfaces and pillow-like lobes (Figure 9). If values needed for the Ψ calculation are appropriately adjusted to the lobe scale, they may provide a good reflection of emplacement conditions.

Conclusions

Experimental lava flows were produced to investigate the development of pāhoehoe breakouts. Pāhoehoe flows transition to breakout flows as they simultaneously advance downslope, cool, and develop progressively thicker outer crusts. Breakouts occur via two distinct mechanisms: rupture of weak spots in exposed lower crust at the flow front, and rupture of thickened outer crust due to elevated internal pressure. Comparing flow morphology to emplacement parameters and the Ψ parameter shows that high-viscosity lavas develop into low- Ψ breakout flows, and low-viscosity flows solidify into high- Ψ pāhoehoe flows. Low- Ψ flows develop breakouts because crust forming processes impede crustal disruption processes. The transition of Sulp lavas from pāhoehoe flows to breakout flows occurs at much higher values of Ψ than PEG wax flows. Additionally, surface temperatures and crustal thicknesses are related to morphologic expression. Flows with high surface temperatures and low crustal thickness solidify as pāhoehoe

flows. Conversely, flows with low surface temperatures and thick outer crusts produce breakouts and solidify as breakout flows. Finally, Sulp flows were compared to natural pāhoehoe flows from recent eruptions of Tolbachik, Holuhraun, and Kilauea. Comparing Ψ values of Sulp flows to natural flows, it was determined that whole-flow effusion rates represent a major overestimate of local lobe-scale effusion rate. Scaling down whole-flow effusion rates by three orders of magnitude more appropriately places Ψ values for pāhoehoe lobes in the proper regime for exhibited by laboratory-generated lava flows.

Tables

Table 1. Experimental data. Horizontal line denotes separation between pāhoehoe flows and breakout flows. Pāhoehoe flows are flow numbers 1-7 and breakout flows are flow numbers 8-24.

Flow #	Experiment	Max Temp C	Slope °	Thickness cm	Velocity cm/s	Effective Viscosity Pa s	Effusion Rate cm ³ /s	Ψ -
1	160331-1	1104	15	2.5	5.8	25	138	101
2	160331-2	1120	15	1.7	3.6	18	141	128
3	160520-1	1200	25	2.3	4.7	41	265	81
4	160520-2	1140	24	2.2	5.1	34	196	87
5	160629-2	1183	11	2.1	4.9	15	132	144
6	161005-1	1118	17	2.4	6.8	22	345	140
7	180523-1	1172	13	2.5	3.7	34	176	85
8	151204-1	1156	20	3.0	3.9	70	56	37
9	160326-1	1015	25	3.0	2.0	165	213	27
10	160328-2	1123	25	3.7	3.3	153	139	26
11	160329-1	1111	20	3.0	2.0	134	44	21
12	160330-1	1089	20	3.4	4.3	79	84	37
13	160330-2	1134	17	3.1	4.8	52	172	61
14	160401-1	1129	12	3.1	2.7	66	144	49
15	160401-2	1070	10	3.0	4.4	31	232	97
16	160402-1	1154	5	5.0	2.0	86	155	41
17	160503-1	1059	5	3.6	2.3	43	135	66
18	160519-1	1142	7	3.8	1.0	151	112	25
19	160629-1	1206	11	3.0	4.9	30	202	97
20	160914-1	1083	8	3.4	3.4	42	106	64
21	170401-1	1001	12	5.0	2.9	159	101	23
22	170409-1	1178	13	2.5	1.2	101	57	28
23	180525-1	1243	23	3.0	4.1	76	345	55
24	180525-2	1297	22	2.4	2.0	97	305	44

Table 2. Measured maximum temperatures and other calculated values.

Flow #	Max Temp	Surface Temp, End	Travel Time	Crust Thickness	Breakout Type
	°C	°C	s	mm	-

8	1156	771	120	14.2	B
9	1015	900	28	6.9	A
10	1123	983	35	7.7	A
11	1111	901	32	7.3	A
12	1089	939	45	8.7	A
13	1134	939	52	9.4	A
14	1129	939	38	8.0	A
15	1070	890	67	10.6	A
16	1154	714	225	19.5	B
17	1059	949	47	8.9	A
18	1142	852	36	7.8	A
19	1206	1006	41	8.3	A
20	1083	828	65	10.5	A
21	1001	736	70	10.9	B
22	1178	823	269	21.3	B
23	1243	1098	47	8.9	A
24	1297	875	37	7.9	A

Table 3. Typical parameters of flows from PEG analog experiments, Sulp experiments, and natural Hawaiian pāhoehoe lobes.

	PEG Wax	Sulp	Hawaiian
Length (m)	0.2 - 0.5	1 - 3	0.5 - 5
Width (cm)	5 - 30	30 - 90	50 - 100
Thickness (cm)	1 - 4	2 - 5	15 - 30
Temperature (°C)	18 - 21	1000 - 1300	900 - 1200
Viscosity (Pa s)	1.5^{-4} - 2.1^{-4}	15 - 165	100 - 1000
Effusion Rate (m ³ /s)	4^{-6} - 10^{-6}	5^{-5} - 35^{-5}	5^{-4} - 2^{-3}
References	Fink and Griffiths, 1990; Gregg and Fink, 2000; Rader et al. 2017	This study	Crown and Baloga 1999; Gregg and Keszthelyi, 2004

Figures

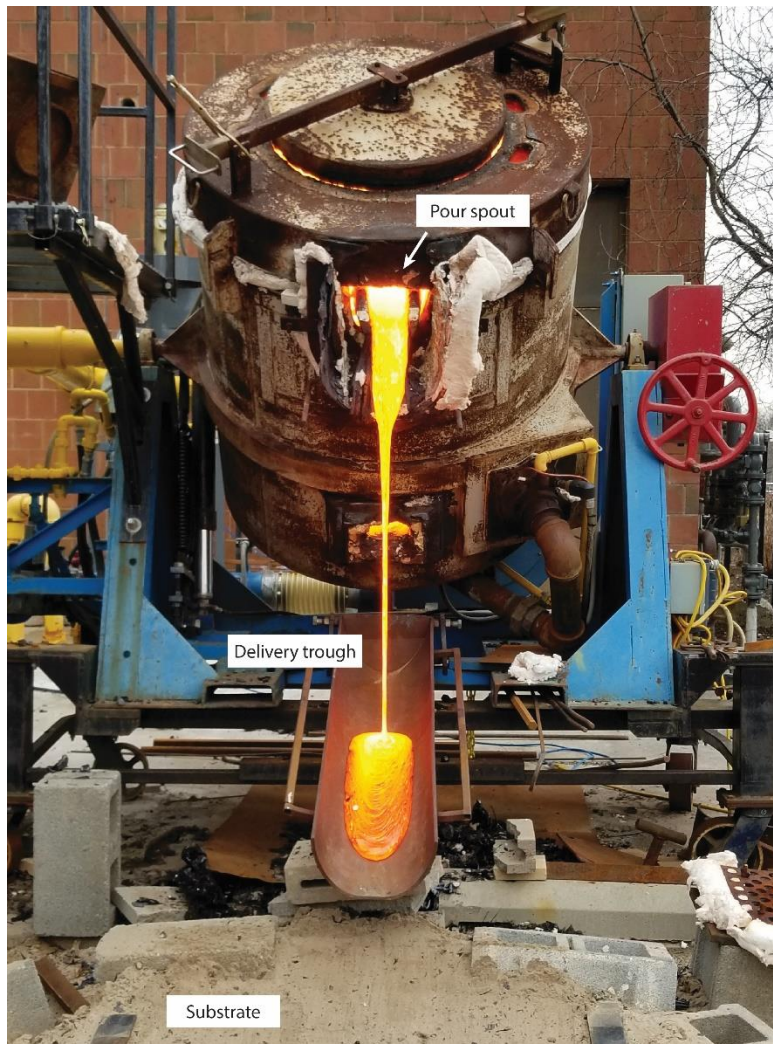


Figure 1. Syracuse University Lava Project setup, including the furnace, delivery trough, and experimental substrate.

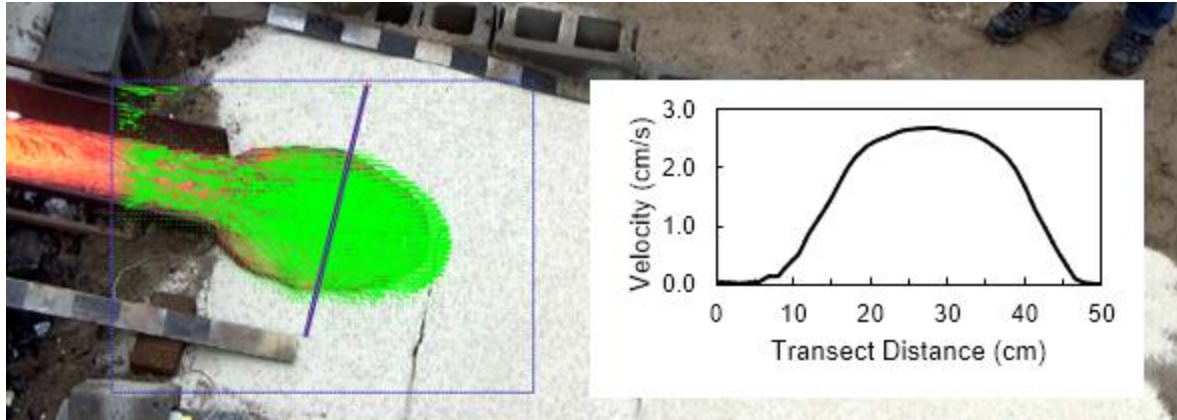


Figure 2. Velocity measurement. Flow velocity extracted from particle image velocimetry (PIVlab). Green overlay is a collection of velocity vectors averaged over a three-second duration. Velocity plot generated from transect across lava flow.



Figure 3. Representative flow morphologies from lava experiments, ranging from breakout flows (A-C) to pāhoehoe flows (D).

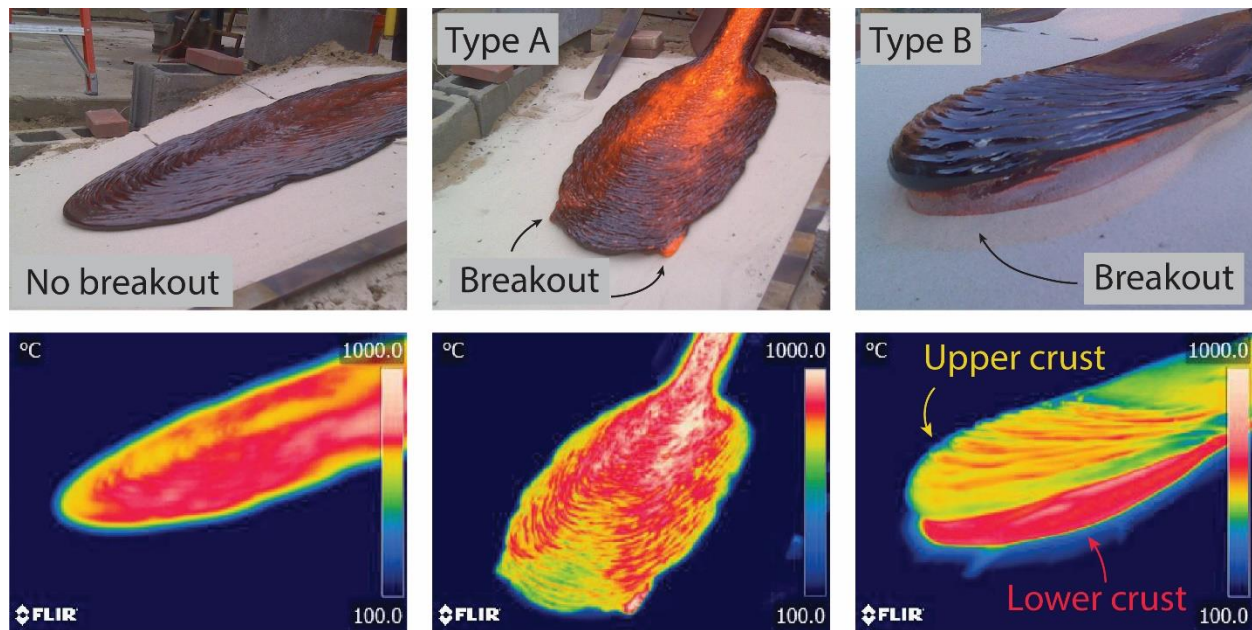


Figure 4. Representative flow images showing a pāhoehoe flow, a breakout flow with type A breakout, and a breakout flow with type B breakout along with their associated infrared images.

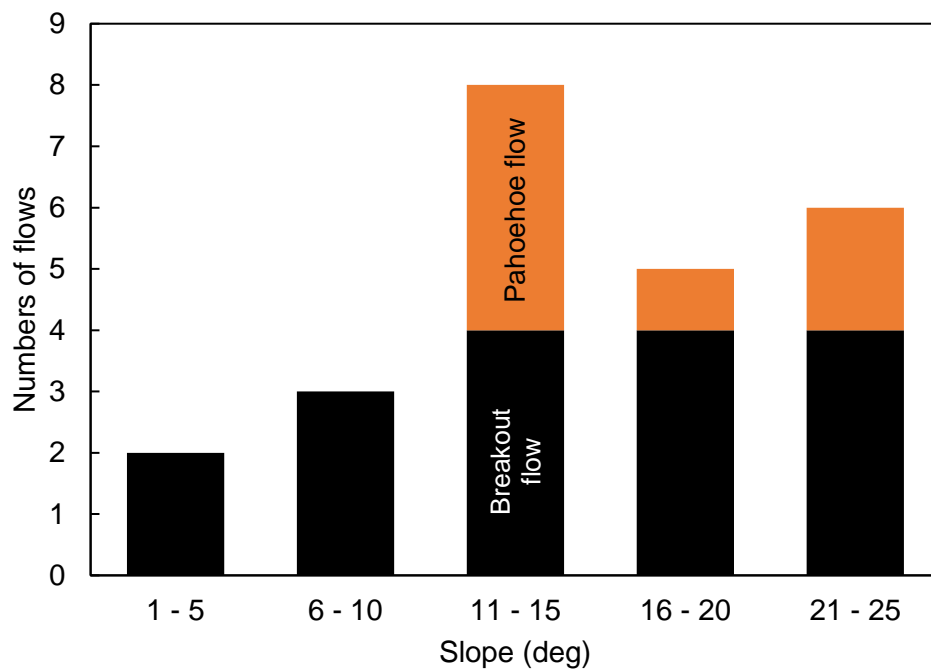


Figure 5. Histogram of flow morphology by slope angle.

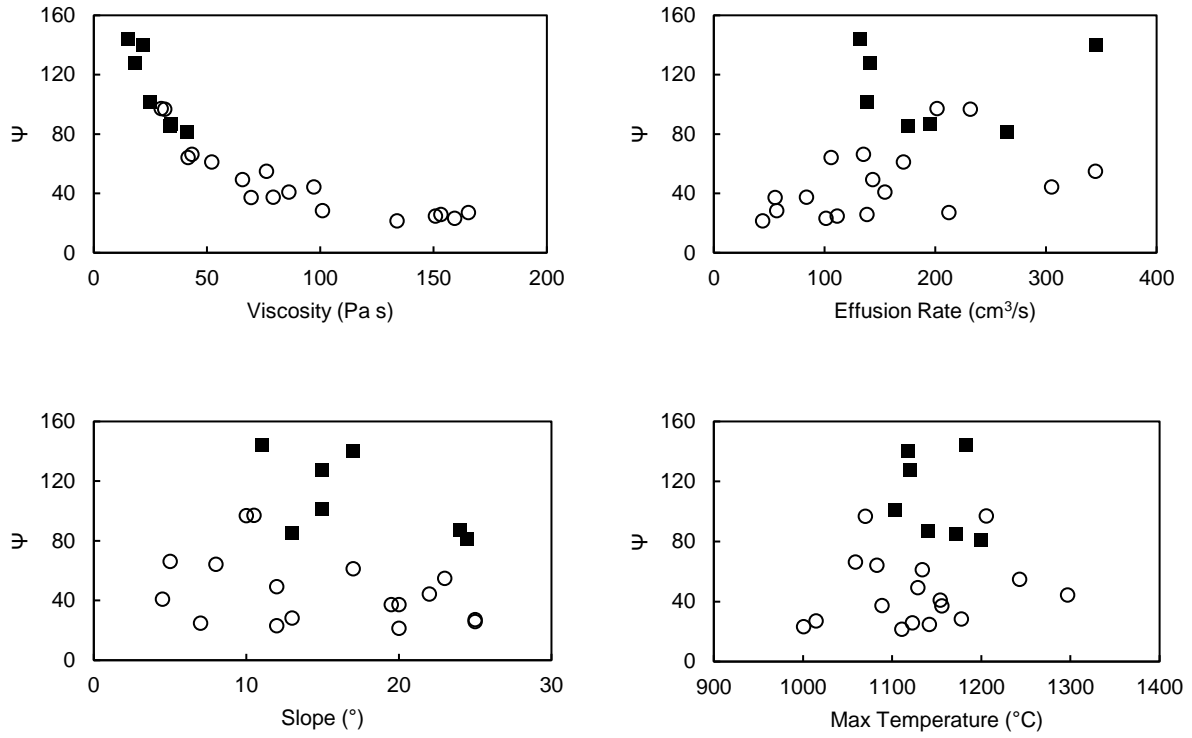


Figure 6. Ψ versus emplacement parameters: a) viscosity, b) effusion rate, c) slope, and d) maximum measured temperature. Squares are pāhoehoe flows and circles are breakout flows.

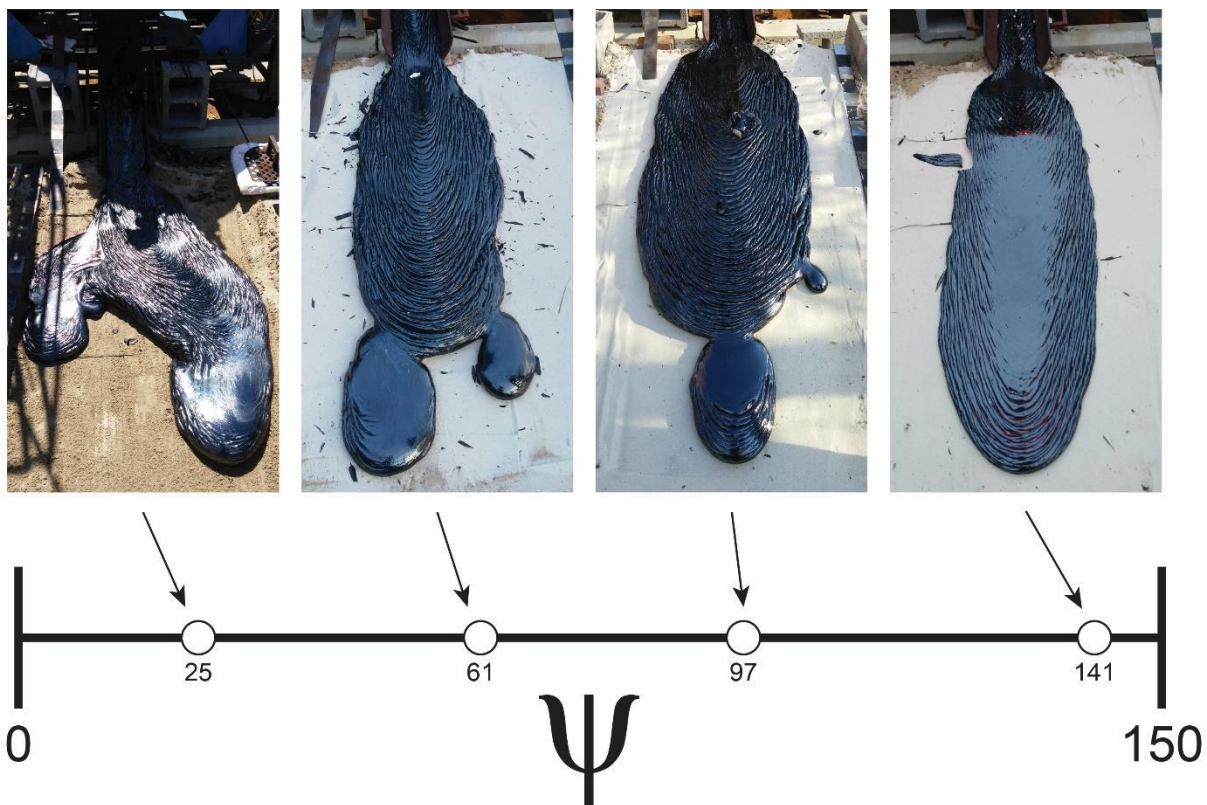


Figure 7. Four representative flows and associated Ψ values. These four lava flows highlight the spectrum of morphology, with breakout flows at low Ψ transitioning to pāhoehoe flows at high Ψ .

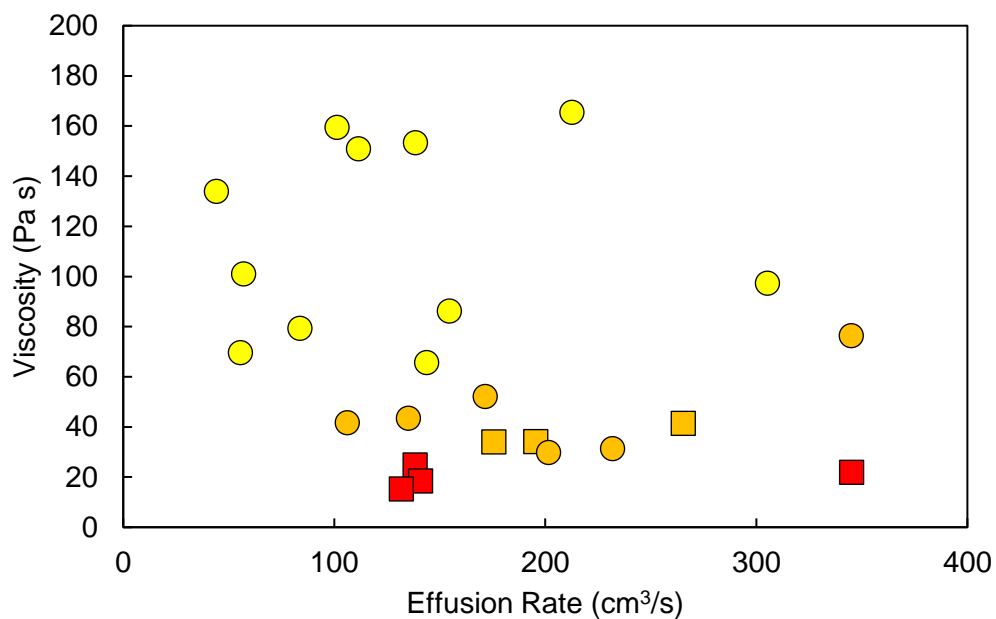


Figure 8. Viscosity and effusion rate relative to Ψ (colors). Squares represent pāhoehoe flows and circles represent breakout flows. Red, amber, and yellow represent high (100-150), medium (50-99), and low (0-49) Ψ values, respectively.

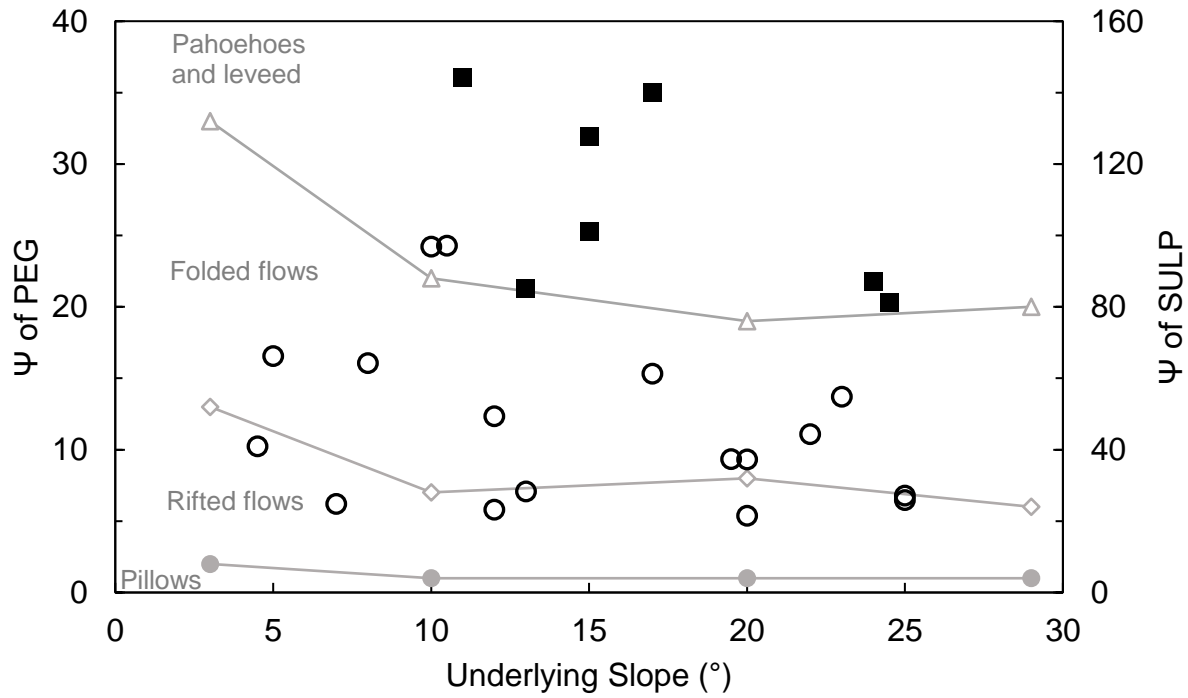


Figure 9. Ψ and slope. SULP data from this study is overlain on previously established Ψ regimes (grey lines and text) from Gregg & Fink (2000). SULP data is shown by black squares that represent pāhoehoe flows and black hollow circles that represent breakout flows.

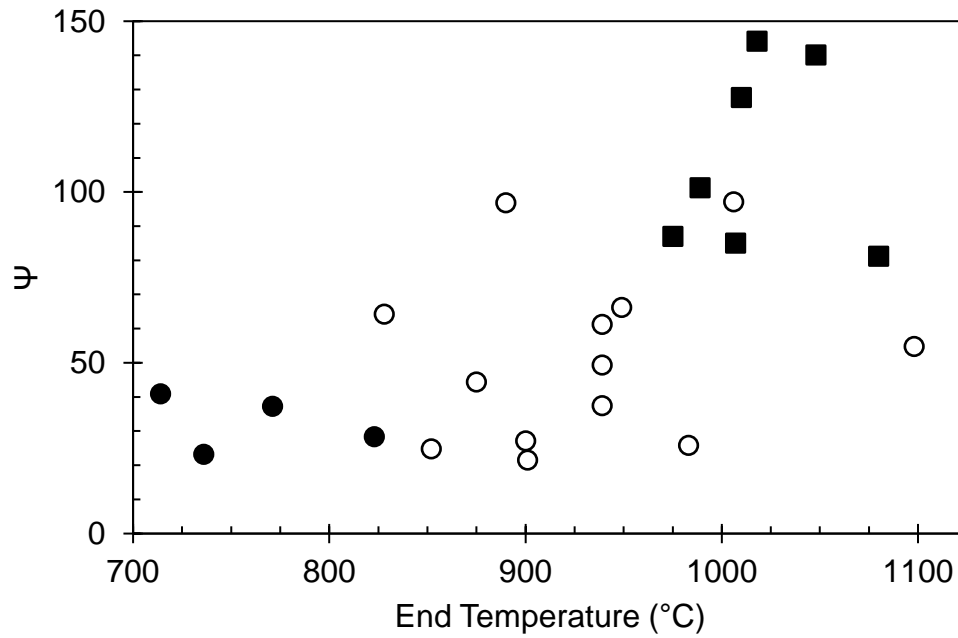


Figure 10. Ψ and surface temperature at the end of each experiment. Squares represent pāhoehoe flows, hollow circles represent breakout flows with type A breakouts, and filled circles represent breakout flow with type B breakouts.

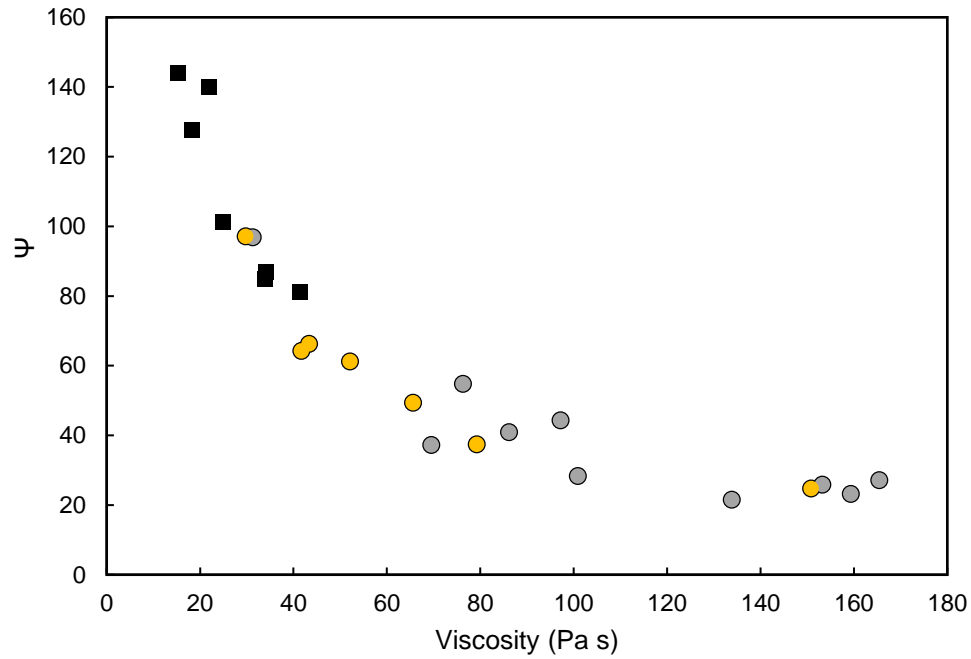


Figure 11. Single and dual breakout flows. Squares represent pāhoehoe flows that contain no breakout. Circles represent breakout flows. Grey circles represent single breakout flow. Yellow circles represent dual breakout flows.

Chapter 2: Rapid slip of basaltic lava on volatile-bearing substrates

In preparation for submission to:

Volcanica

Abstract

Re-melted basalt was used to study interactions between silicate flows and four different substrates (sand, clay, ice, dry ice) in large-scale, controlled experiments. The meter-scale flows were emplaced at natural eruption temperatures onto volatile-bearing substrates with slopes from 1° to 25°. Experiments were monitored for lava-substrate interactions and changes in flow morphology and velocity. Observations from experiments include steam jetting with particle entrainment, distinctive basal crust textures, flow necking, and short-lived rapid acceleration of flows (instantaneous velocities up to 1.2 m/s). The rapid accelerations are important as they are initiated by decoupling and displacement along the lava-substrate boundary, here termed 'lava slip'. We hypothesize that lava slip occurs due to confined and elevated pore pressure beneath the flow. Although lava slip apparently has not been recognized in nature, it may occur at steep-sided mafic glaciovolcanoes and should be considered as part of future hazard mapping at these and similar volcanoes.

Introduction

Understanding the processes associated with basaltic magmatism is a major goal of planetary volcanology because it is the dominant style of volcanism on Earth, Mars, and other planetary bodies of the Solar System (Basaltic Volcanism Study Project 1981). Basaltic eruptions occur in submarine, subaqueous, terrestrial and glaciovolcanic settings. Distinctive features of eruptions and lava flows in different environments permit preserved features in basaltic flows, such as Archean submarine pillow lavas, to be used to infer their eruption environments even billions of years after their emplacement (Furnes et al., 2004). As the dominant type of volcanism on Earth, understanding basaltic lava flows is also important for assessing hazards related to eruptions near population centers around the globe, including places like Kilauea volcano in Hawaii (Neal et al. 2019), Mount Etna in Sicily, and Nyiragongo in the Democratic Republic of the Congo (Zana et al., 2008).

Many important aspects of basaltic lava emplacement are relatively well understood (rheology, cooling and crystallization, formation of surface features) but one understudied aspect is the interactions between lava flows and their substrates. Apart from flowing onto previously erupted lavas, lavas on Earth can be emplaced over or into a wide range of materials including sediments (Jerram and Stollhofen 2002; Waichel et al. 2008), vegetation (Walker 1995), river and lake water (Tucker and Scott 2009; Pedersen et al. 2017), shallow and deep marine water (Moore et al. 1973; Perfit and Soule 2016), snow (Edwards et al., 2012; Edwards et al., 2015), and ice (Waythomas et al. 2014) (Figure 1). Part of the reason lava-substrate interactions have not been extensively investigated may be that active basaltic lava flows are hazardous and uncontrollable, or that they occur in remote locations that make observation limited or impossible (Macdonald 1953; Shaw et

al. 1968; Gregg and Keszthelyi 2004; Pedersen et al. 2016). In cases where active flows are not observed, lava-substrate interactions may be inferred from features preserved in inactive flows.

The advent of large-scale experimental facilities is dramatically improving our collective ability to conduct repeatable lava flow experiments, and is quickly expanding our ability to learn more about processes of basaltic lava emplacement (Lev et al. 2012; Edwards et al. 2013; Dietterich et al. 2015; Cordonnier et al. 2016; Rader et al. 2018; Rumpf et al. 2018; Tsang et al. 2019; Farrell 2020; Soldati et al. 2020). Experimental volcanology is a growing field and several institutions now have laboratories for large-scale experiments where lava flows can be studied in detail; in particular, facilities at Syracuse University have the capability to produce meter-long basalt flows at natural eruption temperatures, and this facility was used to produce experiments that examine lava-substrate interactions in detail.

Here we focus on detailed examination of analog sheet flows at natural eruption temperatures to investigate interactions between basaltic lava flows and five different volatile-producing substrates. Though many of these flows share similar features, our results show that some characteristics are unique to flows over specific substrates. One of the new and most important observations from this study is documentation of lava lobes undergoing high-velocity downslope movement, here termed ‘lava slip’. These types of events, although as yet undocumented in nature, yield insight into a possibly common, but generally unrecognized mechanism of emplacement that has potentially important implications for lava flow hazard assessment and for understanding the emplacement of basaltic lava flows over volatile-rich substrates in a wide variety of environments.

Methods

Experimental basaltic lava flows at the Syracuse University Lava Project laboratory (<http://lavaproject.syr.edu/>) were created at natural eruption temperatures, providing the

opportunity to study lava flow behavior under controlled conditions. The facilities featured a tilt-furnace that can melt over 50 liters (0.05 m^3) of basaltic material at one time, reach temperatures of $1300 \text{ }^\circ\text{C}$, and expel material at a rate in excess of $600 \text{ cm}^3/\text{s}$. Starting material for these experiments used 1.2 Ga Keweenaw basalt (Wirth et al. 1997), which was heated for several hours and stirred occasionally to promote homogeneity and facilitate degassing. The volume-limited basaltic lava flows were poured out of the furnace and flowed to the slope via a steel chute approximately one meter in length. Within minutes the flows quenched into a crystal-free glass with vesicles ranging from 2 to 24 vol% (Soldati et al. 2020).

The lava flows created at the lava laboratory generated morphologies with ropey textures, toey breakouts, inflated lobes, lava channels, and lava tubes. Typical viscous flows on dry sand had velocities between 3 and 6 cm/s (mean = 0.5, median = 0.46 cm/s, $n = 17$) and have flowed up to 18 cm/s.

Forty-eight experiments were performed on beds of dry sand, wet sand, clay, ice, and dry ice over local soils at various slopes ranging from 1° to 25° . Dry and wet sand experiments used beds composed of 1 cm-thick medium grain-size quartz sand. Experiments performed on clay ($< 1 \text{ mm}$) flowed onto a 1 cm-thick bed of powdered unpacked, montmorillonite. Ice experiments were performed on slabs of water ice $1 \text{ m} \times 0.5 \text{ m} \times 6 \text{ cm}$ thick, or on a bed of shaved ice approximately $2 \text{ m} \times 1 \text{ m} \times 6 \text{ cm}$ thick. Experiments performed on dry ice consisted of 2.5 cm thick slabs, laid out in a $1.2 \text{ m} \times 0.7 \text{ m}$ abutted grid.

Each flow was recorded using two stationary Sony HD (720p) digital video cameras. Temperatures at the base of the flows were recorded using 6.32 mm diameter Type-K thermocouples. Lava surface temperatures were collected using a FLIR T300 infrared camera. Standard error for Type

K thermocouples is reported as ± 2.2 °C or 0.75% (Omega Engineering 2003). Uncertainty for the FLIR T300 is reported as $\pm 2\%$ (The Zen Cart Team and others 2020).

Infrared images were used to collect surface temperatures at various locations and times during flows. Visible light images were captured during active flow to document shapes. Measurements of plan-view surface area were made using the web-based app SketchAndCalc (Dobbs 2013). The open-source tracking software, Kinovea, was used to track flow particles frame-by-frame at 30 fps, by tracing markers at three closely spaced locations down the center-axis of flow to calculate distance and average velocity with time. Particle-tracking of full-slip events began within 2 seconds after the initial lava-substrate contact began and lasted from 2 to 4 seconds. In three cases, Kinovea was unable to track particles properly; velocities for these flows were measured manually (Table 1). Effusion rate was measured as time-averaged discharge. The well-established equation of Jeffreys (1925) was used to estimate apparent viscosity, which integrates several factors controlling downslope movement of lava including crust formation and the concentrations of bubbles and crystals. Calculated apparent viscosities in this study were used for comparison purposes among flows.

The potential for lava slip was initially investigated on slopes of 1° to 25°, at increments of 5°. Slopes close to the minimum slip angle were reevaluated in 1° increments to accurately determine the minimum angle of slip.

Results

General Description of Experiments

Experiments producing meter-scale flows, on both volatile-poor and volatile-rich substrates, had smooth or ropy surfaces. Flows dimensions averaged about one meter long, half a meter wide, and two to four centimeters in thickness. Lava flows developed a crust within tens of seconds and

quenched to a crystal-free glass. Vesicularity in all lava flows ranged from 2 to 24% (Soldati et al. 2020). Apparent viscosities for all flows were below 200 Pa s.

A total of forty-eight experiments were performed (Table 1): seventeen on volatile-poor substrates (dry sand) and thirty-one on volatile-bearing substrates (wet sand, clay, ice, dry ice). The flows on the volatile-poor substrates (dry sand) served as a representative suite for comparison with flows over volatile-rich substrates. Hundreds of flows have been generated on dry sand at the Syracuse University Lava Project laboratory which show similar results to the dry sand flows in this study. The substrates used for the other thirty-one experiments in this study were volatile-rich and show several features not seen in dry sand experiments, including jetting, bubbling, necking, and rapid slip downslope. For our suite of experiments, flow thicknesses varied from 1.5 to 5 cm (average 2.8 cm), effusion rate varied ranged from 108 to 776 cm³ per second (average 394 cm³/s), apparent viscosity estimated using Jeffreys equation varied from 0 to 164 Pa seconds (average 28 Pa s), maximum measured temperature varied from 1115 to 1481 °C (average 1286 °C), pre-slip velocity varied from 1 to 25 cm per second (average 9 cm/s), and syn-slip velocity varied from 9 to 122 cm/s (average 49 cm/s). Flows slipped downslope on slopes as low as 1° (Table 2), some with high velocities (up to 123 cm/s) (Figure 2).

Definition of Lava ‘Slip’

The laboratory-generated lavas initially flowed with a steady velocity and then slowed with time as the flow cooled. However, some flows in this suite displayed a dramatic and newly observed phenomenon, lava ‘slip’. We are not aware of this lava emplacement mechanism being described before, but because it is a critical part of our experimental descriptions, we define it here before discussing the other results in detail. Lava slip is defined as the decoupling of viscously flowing lava from the substrate accompanied by a sudden onset of rapid velocity as the lava moves

downslope. The slip process and the morphological changes to the lava can be seen in still images (Figure 3), although it is best viewed via video (see supplemental files). Prior to slip, flows are comparatively wide, and may initially have convex flow fronts. Viscous flows exhibited no signs of slippage along the substrate. As slip began, the flow front increased in velocity and stretched downslope, causing the flow neck to narrow. Partial-slip and full-slip were both observed. Partial-slip occurred when only a fraction ($< 50\%$) of the flow exhibited slip along the substrate. Full-slip was characterized by the entire lava mass slipping along the lava-substrate boundary. Centimeter-scale behaviors observed during lava flow experiments included steam jetting, particle-entrained jetting, and bubble formation. Steam jetting from flow margins was inferred as water vapor condensed on the exposed steel sheet adjacent to the lava flow. Jetting with particle entrainment was observed as sand blows at flow margins, and clouds of substrate particles were blown from flow margins and through burst bubbles.

Some of the lava flows on volatile-rich substrates exhibited behaviors in addition to lava slip. In several flows that exhibited slip the lava neck increased in length and decreased in width as the lobe slid downslope (Figure 3). In a few cases, the thinned lava neck then acted as a single marginal levee for incoming lava to slide against.

Additionally, as the flow front cooled, slipping lava pushed the initial lobe out of the way. This created a convex lobe front that was wider than the original flow width (Figure 3). In the most extreme cases, the lava slipped downslope with a great enough velocity that the lobe completely detached from the lava supply. In flows that experienced slip, key characteristics include narrow necks, wide flow fronts, and in some cases, detached flow lobes.

Velocity of each flow was tracked for viscous flow, partial-slip, and full-slip for each flow (Figure 4). Flows that did not slip showed, as expected, relatively low velocity and deceleration during

flow. Conversely, flows that exhibited partial-slip and full-slip showed an increase in velocity throughout the duration of the flow. The onset of slip events corresponds to marked changes in velocity and acceleration (Figure 4).

Experimental Results by Substrate

Dry sand substrate

The sand substrate comprised medium-sized quartz grains and contained minimal interstitial water that evaporated upon exposure to high heat; this ‘dry’ substrate is used as a control for comparison with ‘wet’ substrates. Lava flows on dry sand were performed on slopes of 4.5° to 25° and advanced downslope by viscous flow, creating ropy sheet flows (Table 1; Figure 2). None of the flows on dry sand slipped. All flows on dry sand decelerated during flow, with a range of maximum flow velocities of 4 to 25 cm/s, with a mean of 10.3 cm/s and standard deviation of 5.4 cm/s (Table 1; Figure 4).

Wet sand substrate

A set of twelve experiments were performed on wet sand slopes of 3° to 20° with the minimum angle of slip on wet sand determined to be 7°. Wet sand flows were not tested below 3° because no slip was observed on 3° or 5° slopes. Seven of twelve flows on wet sand exhibited some degree of slip (Table 1; Figure 4). All twelve flows on wet sand had a pre-slip maximum flow velocity range from 4.4 to 24 cm/s, with a mean of 10.8 cm/s and standard deviation of 5.7 cm/s. Syn-slip flow average velocities were more than three times higher (35.1 cm/s) than pre-slip velocities. Four flows exhibited full-slip and had slip velocities ranging from 9.3 to 65 cm/s, and three flows experienced partial-slip with a similar range of velocities (10.9 to 54 cm/s; Figure 4). Particle tracking of full-slip events began between 1 and 4 seconds after the initial lava-substrate contact began and lasted from 7 to 10 seconds.

Clay substrate

A set of five experiments were performed on clay from 1° to 20° with the minimum angle of slip determined to be $< 1^\circ$, as flows slipped on all tested slopes down to 1° (Tables 1 and 2). One flow exhibited partial-slip, and four flows exhibited full-slip. The four full-slip flows had slip velocities ranging from 12.2 to 54.5 cm/s. Presumably the clay released molecularly-bound water via dehydration. All five flows on clay had a range of pre-slip maximum flow velocities of 2.1 to 6.1 cm/s, with a mean of 4.1 cm/s and standard deviation of 1.3 cm/s. Syn-slip average flow velocities were more than six times higher (27.7 cm/s) than pre-slip velocities. Four flows exhibited full-slip and had slip velocities ranging from 12.2 to 54.5 cm/s, and one flow experienced partial-slip with a velocity of 25.5 cm/s (Figure 4).

Ice substrate

A set of nine experiments were performed on water ice from 5° to 20° with the minimum angle of slip determined to be 10° as none of the flows on slopes below 10° slipped downslope (Table 2). All flows on a solid ice slab above 10° exhibited slip. No flows were tested below 5° . Three of the nine flows on ice slipped, with a slip velocity range of 85.2 to 122.9 cm/s. All flows began to bubble immediately upon contact with the ice (Figure 2). However, the two flows on shave-ice did not slip at even double the angle of 20° . Ice slabs composed of entirely frozen water melted or sublimated when exposed to the extreme heat of the lava. All nine flows on ice had a range of pre-slip maximum flow velocities of 6.3 to 14.1 cm/s, with a mean of 10 cm/s and standard deviation of 2.4 cm/s. Syn-slip average flow velocities were more than ten times higher (100.7 cm/s) than pre-slip velocities. Three flows exhibited full-slip and had slip velocities ranging from 85.2 to 122.9 cm/s; and no flows experienced partial-slip (Figure 4). Particle-tracking of full-slip

events began within 2 seconds after the initial lava-substrate contact began and lasted from 3 to 5 seconds.

Dry ice substrate

A set of five experiments were performed on dry ice from 1° to 20° with the minimum angle of slip determined to be 1° (Tables 1 and 2; supplementary video 1). One flow exhibited partial-slip and four flows exhibited full-slip. The four full-slip flows on dry ice had a slip velocity range from 23.3 to 107.3 cm/s. The flow on the steepest angle (20°) slipped with high velocity (107 cm/s), and exhibited complete lobe detachment from the lava supply, sending several small individual lobes (< 30 cm in length) of lava sliding downslope one after another. The small sliding lobes became airborne for a fraction of a second when they met a raised dry ice tile junction and later piled up and coalesced into one main lobe. Solid dry ice tiles sublimated carbon dioxide. All five flows on dry ice had a range of pre-slip maximum flow velocities of 0.7 to 10.8 cm/s, with a mean of 6.2 cm/s and standard deviation of 3.7 cm/s. Syn-slip average flow velocities were more than nine times higher (59.2 cm/s) than pre-slip velocities. Four flows exhibited full-slip and had slip velocities ranging from 23.3 to 107.3 cm/s, and one flow experienced partial-slip with a similar velocity of 58.6 cm/s (Figure 4). Particle-tracking of full-slip events began within 1 second after the initial lava-substrate contact began, and lasted from 3 to 6 seconds.

Textural Observations

Textures formed during lava-substrate interactions include distinctive features in the lava as well as distinctive features in the substrate. One of the most apparent features in the lavas are bubbles. Here we use the term ‘bubbles’ instead of ‘vesicles’ because the latter are generally inferred to be the result of gases exsolved from a parent magma due to a decrease in solubility as pressure and or temperature decrease. While all flows contained some vesicles, only flows on volatile-rich

substrates contained surficial bubbles. As discussed below, we think the observed bubbles resulted from devolatilization of the substrate, so they are sourced externally from the lava. Bubbles were observed forming on the surface of flows on all the volatile-rich substrates, varying in diameter up to 30 cm. Some bubbles are entirely contained within the lava, as is typical of ‘normal’ lava vesicles, but other bubbles are ‘rootless’ (Figure 5). The rootless bubbles do not have a lava floor but formed through the entire thickness of the lava. In a few cases rootless bubbles became breached, and gas and substrate particles were ejected through a hole in the uppermost portion of the bubble, leaving a permanent aperture in the bubble (Figure 5).

The most extreme example of bubbling was observed in a flow performed on a damp sand substrate. The two-meter-long flow was emplaced on a low angle ($\sim 5^\circ$), was about three centimeters thick, and was comprised of a main lobe and a breakout, roughly equal in size. Near the end of the experiment, after viscous downslope flow advance had nearly ceased, a large (20-30 cm) bubble grew near the head of the flow. After the bubble’s formation, the flow continued to thicken for several minutes. Upon dissection, the entire flow was hollow and contained one small 2-3 cm diameter hole in the flow base (Figure 6). Rather than many ephemeral bubbles, this flow contained a single sustained bubble that inflated the flow with substrate-derived vapor.

Other distinctive textural features were observed on lavas and some substrates, including lava basal crust textures (Figure 7) and substrate scoring. The basal crust texture of flows on wet sand is similar to the basal crust of dry sand flows, smooth and dimpled with sand grains embedded in the crust (Figure 7A); in several flows as the lava contacted the slope, it incorporated lithic fragments into the basal crust and dragged them along the lava-substrate boundary during slippage (Figure 5). The most easily recognizable basal crust texture was from flow over ice, and is characterized by a glassy botryoidal texture, with individual globules measuring about one centimeter in

diameter (Figure 7B). The basal crust textures of flows over clay are characterized by millimeter-sized pits filled with clay, plus small (< 1 mm) globular balls of clay on the crust surface (Figure 7C). Basal crust textures of flows on dry ice are characterized by a smooth surface with a mirror-like finish containing no embedded particles (Figure 7D).

Discussion

Part of the lava slip definition is a sudden onset of rapid velocity. A key measurable characteristic of a slip event was the increase in velocity during flow duration. When comparing pre-flow velocity and syn-slip velocity, the flows that exhibited slip all showed an increase in flow velocity (Table 1; Figure 4). Cooled lava on the various substrates used in this study did not slip on slopes lower than 20°. Yet, the minimum slip angle for all volatile-rich substrates was 10° or less. The remainder of this manuscript will discuss why flows slip on low slopes, the factors that contribute to slip, as well as observations and documentation of jetting, bubbling and slip in natural settings.

Causes of Slip

The presence of volatile vapor beneath our experimental flows was evidenced by ejection of particles and bubbling. In addition to these behaviors, the hollowed flow (Figure 6) suggests inflation due to vapor. This striking example showed that substrate-derived volatiles are present with enough pressure to lift the lava crust. Edwards et al. (2013) showed in their large-scale experiments that basaltic melts emplaced onto ice immediately developed bubbles, and they speculated that anomalously large ‘vesicles’ in some natural lava flows might have a component of externally derived substrate vapor. Other researchers have also hypothesized that heat transfer from lava to the substrate creates a buildup of steam beneath a lava flow (Maicher and White 2001; Waichel et al. 2008; Belousov et al. 2011; Moore 2019). Observations of steam emanating from the edges of lavas emplaced on snow during the 2010 Eyjafjallajökull eruptions and the 2012-13

Tolbachik eruption confirm that steam production occurs beneath advancing lava flows (Edwards et al., 2012; 2015). Our hypothesis is that heat transfer from the lava releases substrate volatiles to create elevated vapor pressure beneath the flow, resulting in jetting, bubbling, and slip (Figure 8).

The classic work of Hubbert and Rubey (1959) showed that massive thrust sheets can be transported tens of kilometers on low-angle slopes due to elevated pore pressure. When pore pressure is introduced into the system the effective normal stress can be modified to promote sliding (Hubbert and Rubey 1959). When the component of shear stress can overcome the other stresses in the system, the mass may slide downslope. The same principle applies to our experimental lavas. Heat transfer from the lava released volatiles that became pressurized beneath the flow and acted to reduce the effective normal stresses in the system. This counteracted the weight of the lava to enable slip to occur. The source of substrate volatiles used in our experiments include interstitial water between sand grains, molecularly-bound water in clay, solid water-ice, and solid carbon dioxide slabs. Heat from the lava released the volatiles as gas or melt-water causing the observed behaviors in our experiments. Interstitial water evaporated, clay sheets underwent dehydration reactions to release molecularly-bound water, ice slabs melted, and dry ice rapidly sublimated.

Volatile escape varies by the size of the reservoir and permeability of the substrate material. Higher permeabilities allow for higher rates of evaporation. Larger quantities of substrate material allow for larger volumes and greater durations of volatile release. Available interstitial water in our experiments was limited by a thin sand layer. Locations with abundant sand, such as beaches, could produce nearly limitless quantities of interstitial water. Molecularly-bound water stores in clay are limited by the thickness of clay deposits, as well as the permeability of the clay layers. Dry ice deposits and water ice deposits are limited by the thickness of the accumulated ice. The

ice substrates used in this study had a limited volume of volatiles due to the thickness of the ice slab as compared to thick ice deposits on glaciovolcanoes.

The observed behaviors of jetting, bubbling, and slip are influenced by the ‘strength’ of the lava itself. As soon as the lava was exposed it began to cool and develop a crust. Early in the flow bubbling was abundant. As time progressed, bubbling gave way to jetting and slip. The behavioral transition was caused by crust development. Within tens of seconds the lava formed a basal crust which became impervious to vapor, effectively trapping the volatiles beneath flow. It is the combination of substrate vapor release, permeability of the substrate, volatile source volume, and volatile containment by lava crust formation that work together to produce lava slip.

Comparison with Natural Flows

The various behaviors observed in our experimental lava flows including mainly jetting and bubbling have also been observed in natural basalt flows. Steam and jetting observed in our experiments are analogous to steam jets, water jets, and tephra jets observed in active natural lava flows. At Hawaii, shallow submarine lava channels created centimeter-scale steam jets and high-temperature water jets (Tribble 1991). Meter-scale tephra jets have been also documented in zones of lava-surf interactions in Kilauea’s littoral zones (Mattox and Mangan 1997). Surface lava bubble formation has been observed in natural submarine flows, centimeters in diameter, rapidly growing and bursting during Hawaiian submarine eruptions (Tribble 1991; Maicher and White 2001). Lava bubble bursts may also occur on a meter-scale. Steam creation produced overpressure such that a dome-shaped bubble was observed, meters in diameter, in a subaerial lava channel and suddenly burst releasing trapped steam (Mattox and Mangan 1997). Lava and seawater interaction in mid-ocean ridge settings contain lava drip features on lava pillars and cavities suggesting the presence of vapor during active flow (Chadwick 2003; Perfit et al. 2003; Soule et al. 2006).

Slip in Nature

Many examples of geologic materials moving downslope have been documented in the literature. Experiments using water-saturated sand beds below atmospheric pressure showed boiling water causing wet sand pellets to levitate on a cushion of vapor down a slope (Raack et al. 2017). Submarine water tank debris flows were observed hydroplaning along the tank floor caused by forced injection of water beneath the leading edge of the flow (Mohrig et al. 1998). The Blackhawk landslide in California was shown to travel at extreme speeds due to trapped air beneath the landslide (Shreve 1968). The largest subaerial landslide on Earth, Heart Mountain landslide, Wyoming, was shown to slide a distance greater than 45 km on a 2° slope caused by carbonate decompression releasing CO₂ gas that produced a cushion of pressurized air which allowed for sliding (Mitchell et al. 2015). It has been documented that basaltic submarine landslides have travelled tens of kilometers on very low slopes, and it has been suggested that this may occur due to a combination of fine grain-size material and increased pore pressure (Masson et al. 2006; Soule et al. 2021). It has also been proposed that a persistent vapor layer beneath submarine lava crusts can increase flow rates up to three-times faster than typical flow rates (Soule et al. 2006). Air-particle experimental flows, as an analog for pyroclastic flows, were shown to have an over-pressurized flow base due to high pore pressure (Roche et al. 2010). Finally, a recent study showed large-scale laboratory pyroclastic density currents with high basal shear that generated a basal gas layer that enabled long distance sliding on shallow angles (Lube et al. 2019).

Villarrica volcano, a snow- and ice-covered stratovolcano on the Chilean regional borders of Araucania and Los Rios, is one type of volcano at which lava slip might be expected to occur. The volcano erupts basalt to basaltic-andesite lava flows and has had a significant eruption as recently as 2015 (Van Daele et al. 2014; Romero et al. 2018). While the lower slopes of Villarrica range

from 5° to 10°, the upper slopes of the edifice are greater than 20° (Figure 9). Based on our experiments, the minimum angle of slip for lavas on ice is 10°, so we would predict that lava flows coming down the steep upper slopes of Villarrica would be at risk for slip events. Llaima volcano, ~50 km north of Villarrica, is another steep-sided, snow- and ice-covered mafic edifice where slip events might be expected. In North America, many of the ice-covered volcanoes in the Cascade Range have slope characteristics favorable for slip events, but at present most of the Cascade volcanoes produce either explosive eruptions or much more viscous lavas (andesite-dacite). Thus, due to eruption of higher viscosity lavas, we cannot predict locations of possible slip events in the Cascades. But, several volcanoes in the Aleutian Arc and the Kamchatka Arc do effuse more fluid lavas onto steep, snow- and ice-covered slopes. For example, during the 2013 eruption at Pavlof volcano, which periodically produces lava fountaining onto its snow/ice covered slopes; distant observations from the Cold Bay web-camera showed ‘...several light colored plumes rising off the north flank well below the summit, indicating flowage of hot debris over ice and snow lower on the flank’ (Waythomas et al. 2014). Waythomas et al. (2014) proposed that some of these flows might be the result of lava-fed spatter deposits collapsing down steep, glacier-covered slopes. Lavas on the snow- and ice-covered cone Klyuchevskoy have produced low-viscosity lava flows that explosively disintegrated into pyroclastic flows, and it was hypothesized that the observed flows underwent gravitational sliding before breakup (Belousov et al. 2011).

Because of the hazardous nature of lavas emplaced onto volatile-producing substrates, it is not surprising that these very rapid short-lived events have not yet been directly observed in nature. However, other documented observations of lava flows in nature have similar styles of volatile interaction or morphology, and may hint at slip events. Subaerial and shallow submarine flows at Hawaii have been observed to produce steam jets and abundant bubbling (Tribble 1991; Maicher

and White 2001). Dune complexes in Brazil and Namibia were buried by pāhoehoe flows. Striations in dune sands, parallel to flow direction, on the dune's stoss side have been documented as well as thin, narrow lava necks on the leeward side of the dune (Jerram and Stollhofen 2002; Holz et al. 2008; Waichel et al. 2008), hinting at lava slip events. Areas of water-saturated ground in Iceland have produced long lava flows with thousands of rootless cones, suggesting explosive interaction with environmental water (Fagents and Thordarson 2007; Boreham et al. 2018). We suspect that with increasingly better remote surveillance during eruptions at steep-sided volcanoes, and increasing recognition of the textures and processes we have described, observation of lava slip events in nature, and/or the resulting deposits, will happen in the near future.

Conclusions

Meter-scale basaltic lava experiments at natural eruption temperatures were performed on volatile-rich substrates to investigate lava behavior in relation to the release of substrate volatiles. Viscous flows on volatile-poor substrates rarely show evidence of volatile interaction and none slid downslope. Behaviors on volatile-rich substrates include gas jetting, surface bubble formation, and whole-lobe downslope sliding termed 'lava slip'. Gas jetting occurred at flow margins and through surface bubbles, some of which were entrained with substrate particles. Bubbles form on the surface of the lava flow, and rootless bubbles form through the entire thickness of the flow, sometimes venting gas and substrate particles. The most dramatic and important observation is lava slip on angles as low as 1°. Distinctive basalt crust textures correspond to specific substrates investigated. Flows that slip downslope commonly stretch into a narrow neck, while viscous flows form a parallel-sided elongated oval shape. Lava behaviors observed in this study (jetting, bubbling, slip) are interpreted as the result of entrapment of vaporized substrate volatiles creating

elevated vapor pressure beneath the flow, allowing for the reduction of the normal stress and the downslope sliding of lava lobes.

Tables

Table 1. Experimental data. Data organized by substrate and slope. † = shaved ice substrate. * = slip on wet sand after lava flowed off toe-end of ice slab. ** = velocity measured manually.

	Experiment	Slope (°)	Thickness (cm)	Effusion (cm ³ /s)	Apparent Viscosity (Pa s)	Max Temp (°C)	Pre-slip Velocity (cm/s)	Syn-Slip Velocity (cm/s)	Slip Event?
Dry Sand	160402-1	4.5	5	161	30.9	1177	5.6	-	no
	160503-1	5	3.6	230	19.9	1222	5.0	-	no
	160519-1	7	3.8	110	23.2	1254	6.7	-	no
	160401-2	10	3	415	10.8	1266	12.8	-	no
	160629-1	10.5	3	376	19.3	1245	7.5	-	no
	160629-2	11	2.1	139	8.0	1283	9.3	-	no
	160401-1	12	3.1	694	16.2	1194	10.9	-	no
	160331-1	15	2.5	180	5.6	1203	25.6	-	no
	160331-2	15	1.7	214	5.0	1333	13.3	-	no
	160330-2	17	3.1	341	30.3	1238	8.2	-	no
	160330-1	19.5	3.4	254	48.7	1234	7.0	-	no
	160329-1	20	3	77	129.8	1172	-	-	no
	160520-2	24	2.2	228	11.7	1272	14.8	-	no
	160521-1	24	3.5	269	41.1	1222	10.7	-	no
	160520-1	24.5	2.3	313	11.1	1244	17.5	-	no
	160328-1	25	4.5	264	164.3	1132	4.6	-	no
	160328-2	25	3.7	143	94.6	1222	5.4	-	no
Wet Sand	170707-1	3	4	463	16.4	1279	4.5	10.9	partial
	170701-1	5	4	345	17.6	1256	7.0	-	no
	170701-2	5	1.5	602	1.0	1369	17.9	22.6	partial
	180522-1	6	3.5	205	16.9	1115	6.7	-	no
	170712-1 *	7	3	300	10.4	1481	9.3	9.3	yes
	170630-1	10	2	373	13.9	1256	4.4	28.5	yes
	170707-2	10	2.2	919	3.1	1481	24.0	54.0	partial
	170629-1 **	15	2	195	13.2	1200	6.9	-	no
	170708-1	15	1.5	776	5.4	1369	9.5	65.0	yes
	170520-1	20	2.3	472	11.2	1273	14.2	-	no

	170521-1	20	2.5	541	12.4	1324	15.2	-	no
	170708-2	20	1	532	3.1	1425	9.8	55.5	yes
Clay	170704-1	1	4	676	6.7	1143	3.7	13.2	yes
	170705-1	2	3	570	4.5	1324	6.1	54.5	yes
	170702-1 **	5	3	384	16.5	1267	4.2	12.2	yes
	170522-2	15	3.5	323	133.3	1234	2.1	25.5	partial
	170518-1	20	3	535	60.4	1295	4.5	33.0	yes
Dry Ice	170706-2	1	1.5	652	0.3	1425	10.8	60.7	yes
	170703-1 **	5	3	400	7.1	1312	9.8	23.3	yes
	170630-2	10	2.8	408	29.3	1211	4.1	46.1	yes
	170523-1	15	2	138	130.6	1273	0.7	58.6	partial
	170519-1	20	2.3	108	28.0	1256	5.7	107.3	yes
Ice	170706-1	5	3.8	500	17.6	1290	6.3	-	no
	170712-1	7	3	300	10.4	1481	9.3	-	no
	180717-1	9	5	282	48.0	1290	7.2	-	no
	180717-2	9	2.5	281	8.5	1397	10.1	-	no
	170711-1	10	1.5	755	2.8	1402	12.2	85.2	yes
	170710-1	15	1	489	1.9	1425	12.2	122.9	yes
	170710-2	20	2	544	12.8	1295	9.4	93.9	yes
	170519-2 †	20	2.5	456	21.0	1335	9.0	-	no
	170522-1 †	20	2.7	983	15.6	1369	14.1	-	no

Table 2. Sliding angles of molten lava on volatile-rich substrates.

Substrate	Minimum angle of slip	Number of experiments
Clay	1	5
Dry Ice	1	5
Ice	10	7
Wet Sand	7	10

Figures



Figure 1. Basaltic lava flows being emplaced onto different substrates. (A) Pāhoehoe toes encroaching on vegetated soil (courtesy of HVO). (B) Lavas flowing into Champagne Pond, Hawaii (courtesy of U.S.G.S.). Width of photo is approximately one-half kilometer. (C) Lava flowing onto snowpack, Tolbachik, Russia (B. Edwards). Thickness of lava is approximately 0.5 m.



Figure 2. Representative lava morphologies for lavas on each of the 5 different substrates. Lava flow experiments on their respective substrates on angles of 5° and 20°. Scale bars have 0.1 m graduations.

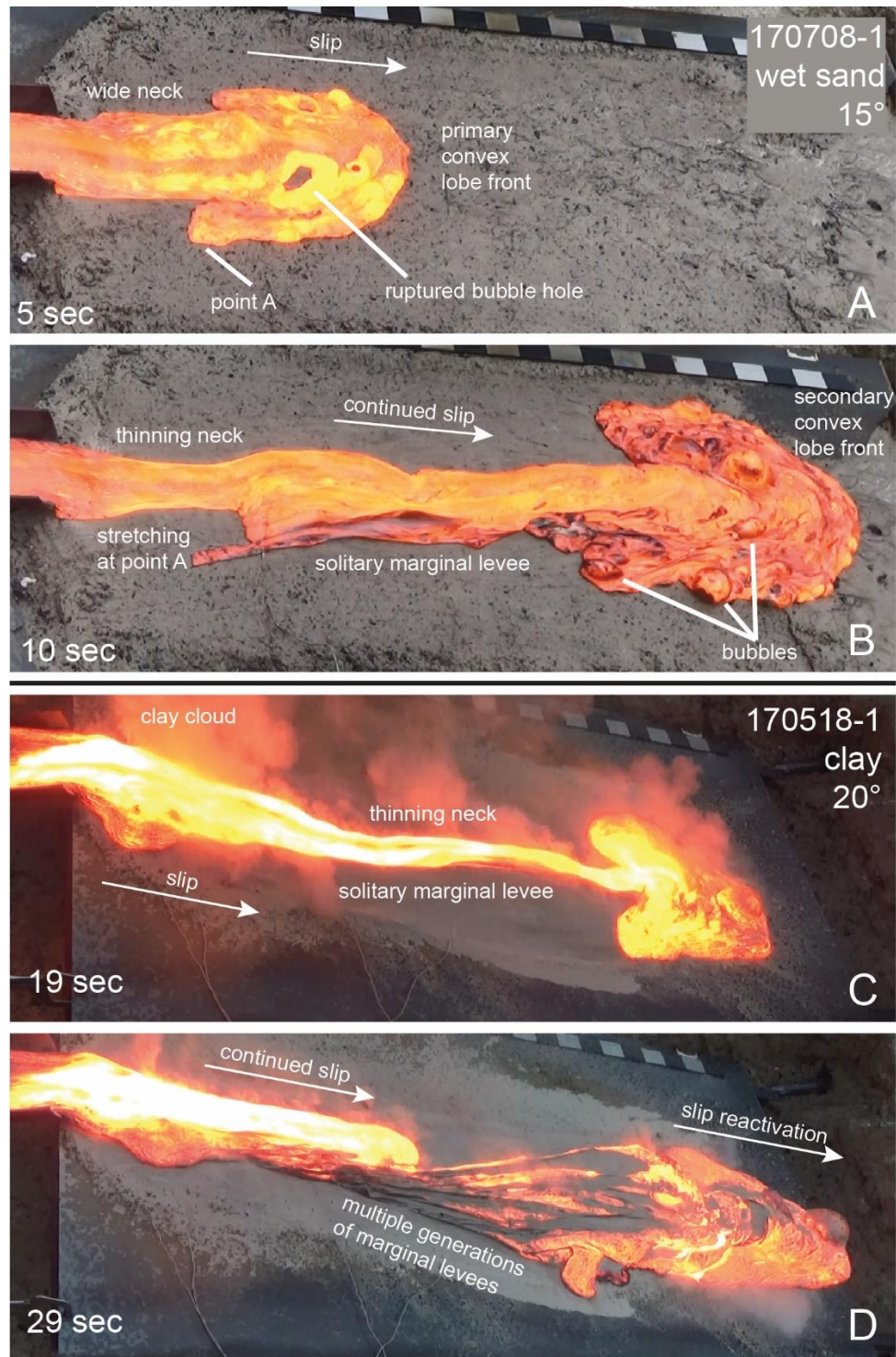


Figure 3. Morphological changes during lava slip. (A) Lava flow at the onset of slip, five seconds after contacting substrate, showing a wide flow neck and convex lobe shape. (B) Flow five seconds into slip events showing a thinned neck and stretching from point A allowing

formation of a marginal levee. (C) Flow in the process of slip showing dramatic necking and a marginal levee. (D) Ten seconds after photo c showing the formation of multiple marginal levees.

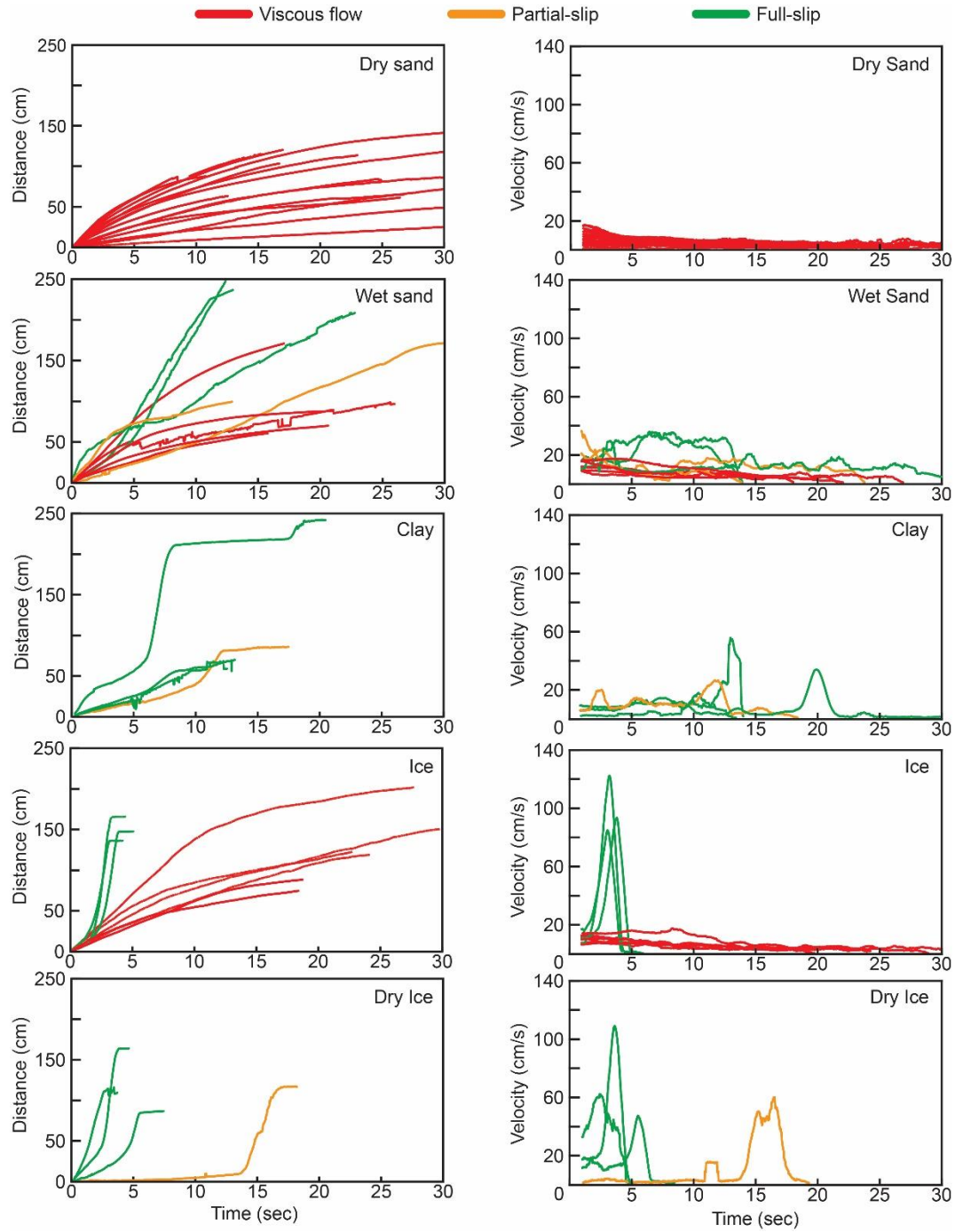


Figure 4. Velocity (left column) and acceleration (right column) for selected experiments on their respective substrates. Red, amber, and green lines indicate flows that recorded no-slip, partial-slip, and full-slip, respectively.

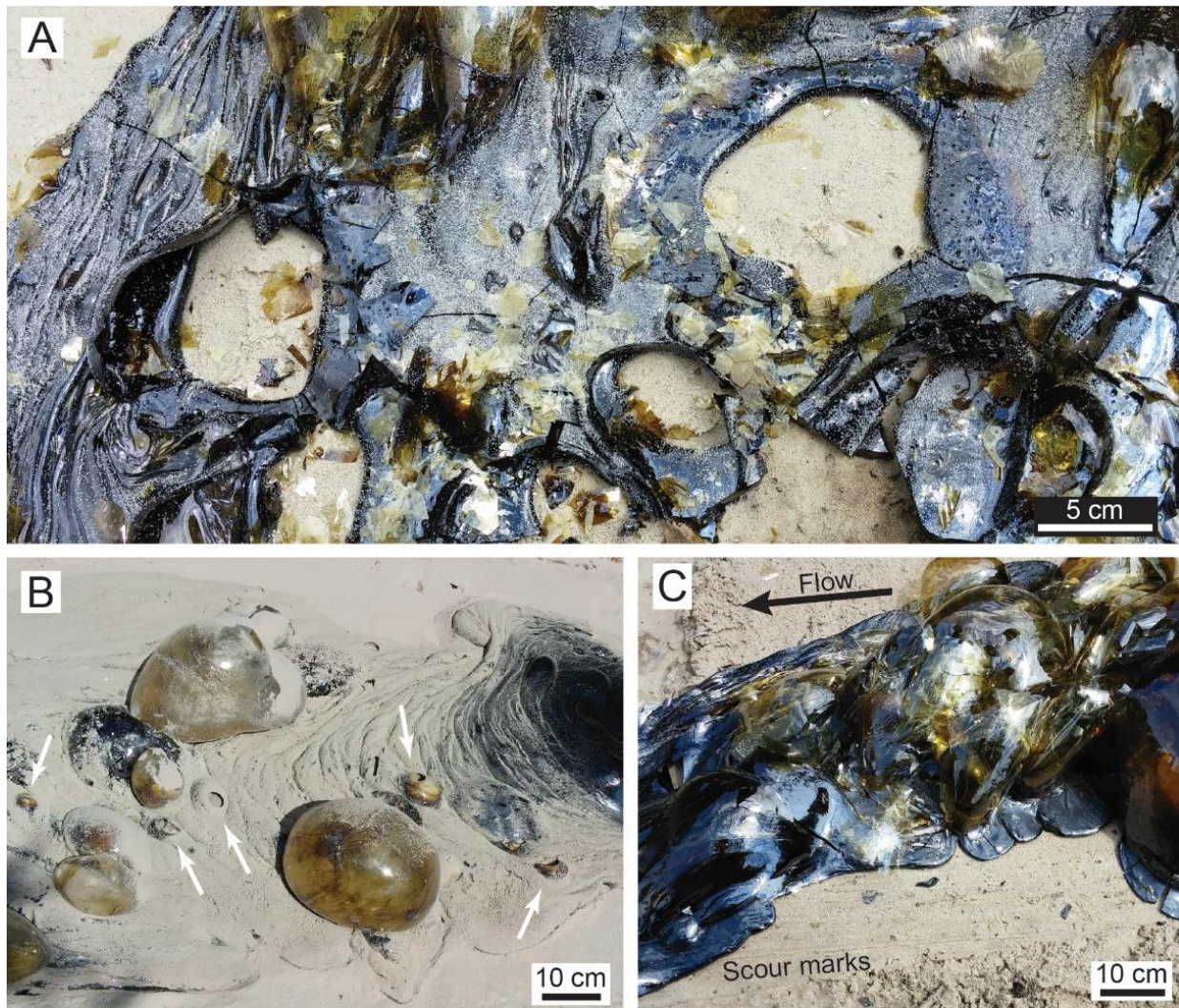


Figure 5. Bubbles and related features. (A) Solidified flow over wet sand with shattered bubble fragments scattered over the surface of the flow. Holes in lava flow where sand substrate is visible are rootless bubbles, with the largest being about 9 cm in diameter. (B) Breached bubbles at arrow tips. (C) Embedded lithic fragments in basal crust left scour marks in the sand as the flow slid downslope from right to left.



Figure 6. Vapor-inflated flow. (A) Large bubble formed during cooling. Flow is approximately 2 meters long. (B) Profile view of flow inflation. (C) Hole in flow-base where vapor entered the interior of the flow. (D) Dissection revealed a single bubble that filled the flow interior. White square marks the location of hole in flow base shown in image C.

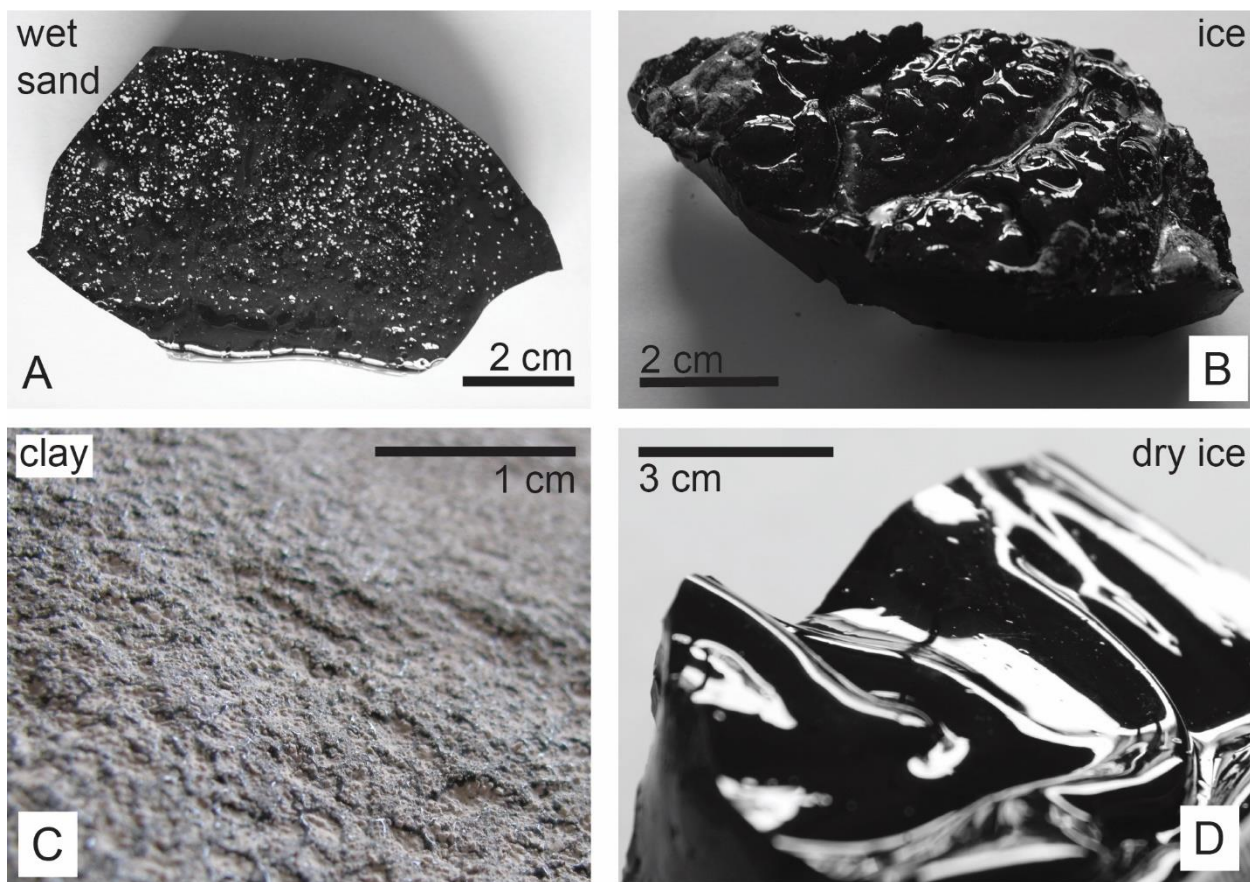


Figure 7. Representative lava flow basal-crust textures. (A) Flows over sand have a dimpled base with embedded sand grains. (B) Flows over ice are characterized by glassy botryoidal texture with individual glass beads up to 1 cm in diameter. (C) Flows on clay contain clay-filled pits and are coated with clay globules. (D) Flows over dry ice substrates have a smooth glassy base with no embedded particles.

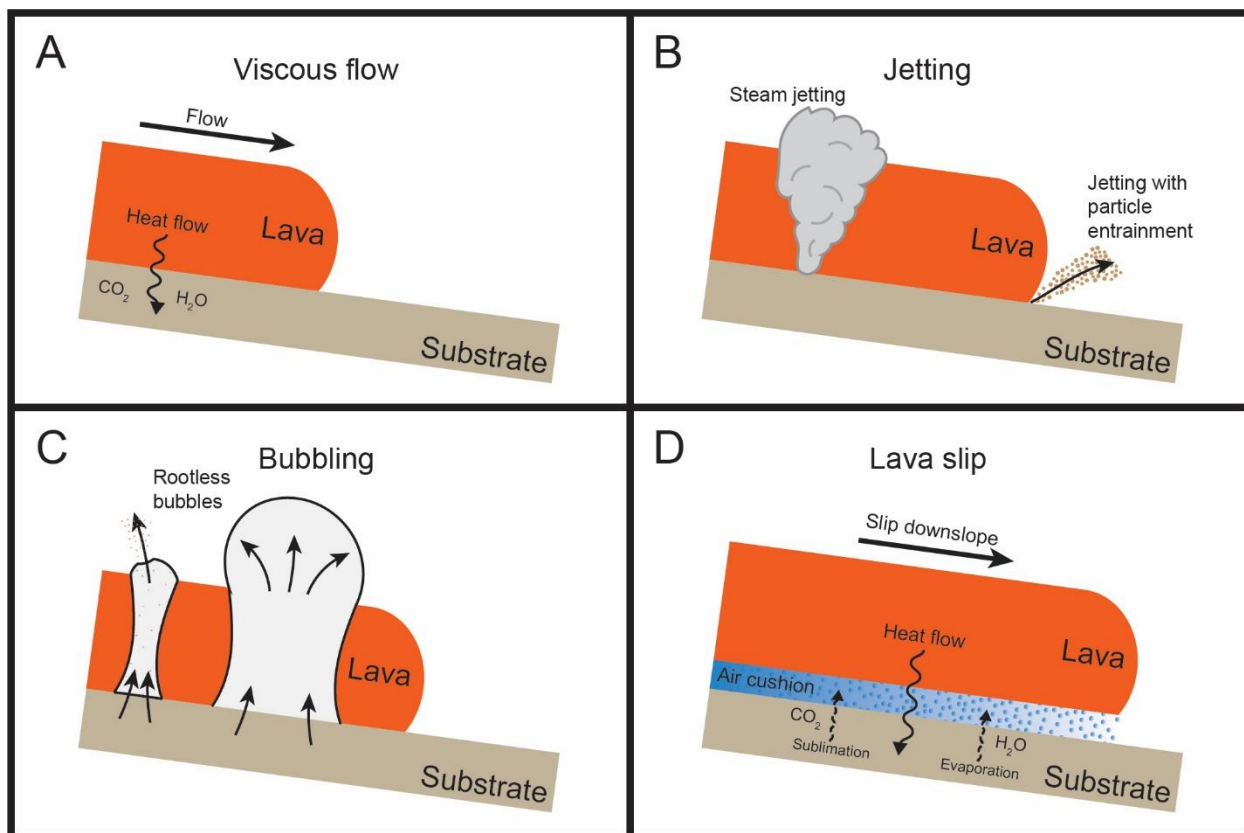


Figure 8. Lava behavior conceptual model. (A) normal flow behavior with no venting, bubbling, or sliding. Substrate volatiles heated during this phase. (B) as substrate volatiles are heated, vaporization occurs creating steam and particle-entrained jetting. (C) high conductive heating creates rapid vaporization resulting in vapor escaping through the thickness of the lava flow, creating breached and rootless bubbles. See text for full description. (D) lava cooling generates an impermeable crust thereby increasing pressure build-up under the flow, which may create a vapor barrier promoting slippage downslope.

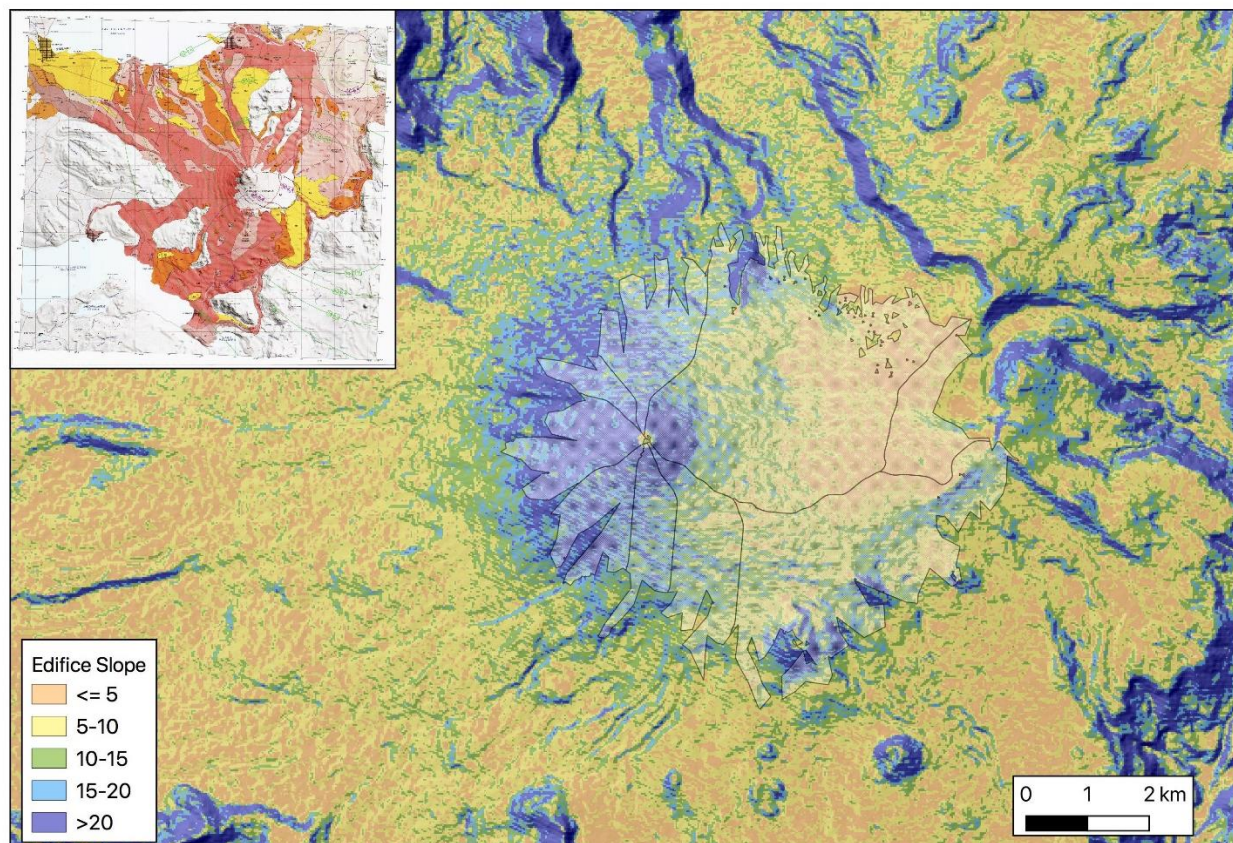


Figure 9. Slope map of volcano Villarrica. Slopes above the minimum slip angle on ice of ten degrees are indicated as green, blue, and purple, and may indicate locations of potential lava slip. Irregularly shaped polygon overlaid onto volcano indicates snow-covered slopes. Inset map is lahar hazard map of Villarrica.

Chapter 3: Incorporation of substrate-sourced water and carbon dioxide in large-scale basaltic experimental lava flows

In preparation for submission to:

Geology

Abstract

It is assumed that volatile content of basaltic glass and melt inclusions have not been affected by external influences such as the substrate upon which lavas flow. We investigated chemical absorption of water and carbon dioxide into basalt by allowing meter-scale experimental lavas to flow over volatile-bearing substrates (wet sand, clay, ice, dry ice). Substrate-derived volatiles interacted physically with lava flows to produce jetting with entrained particles and surface bubbling. The glassy lava samples were analyzed for water and carbon dioxide concentrations using Fourier Transform Infrared and Raman spectroscopy. CO₂-bearing bubbles were identified in samples from flows on dry ice. Water and carbon dioxide concentrations in lava glasses from all substrates were very low (< 200 ppm H₂O, < 50 ppm CO₂). Volatile concentrations in samples from flows over volatile-poor substrates (dry sand, steel) were higher than volatile concentrations for flows over volatile-rich substrates. Dissolved water concentrations were below model-predicted values of 900 ppm H₂O. Dissolved volatile content levels away from bubble walls were constant within uncertainty. Additionally, we investigated major element transport across the lava-substrate boundary via electron microprobe analyses. Diffusion profiles were fit to the measured concentration gradients. Characteristic diffusion lengths and times for major element transport were 1.2 μm and 0.5 seconds, respectively. These results suggest that dissolved volatile species present in silicate melts were not a product of external volatile absorption and the substrate volatile interaction with the lava was limited to physical interaction.

Introduction

Volatile concentrations in volcanic glasses or melt inclusions are commonly used to explore volcanic eruption history, degassing processes, volatile budgets, and magma explosivity (Wilson 1980; Metrich and Wallace 2008). Volatiles are present in silicate melts in a variety of

components including H₂O, CO₂, H, S, C, F, and Cl with water concentrations having the highest abundances by orders of magnitude (Fine and Stolper 1986; Newman et al. 2000; Baker et al. 2005). As the melt travels toward the surface, temperature and pressure decrease causing volatile exsolution (Lavallée et al. 2015). Solubility studies show that very little water or carbon dioxide (< 1000 ppm) will remain dissolved in basaltic melts at surface conditions (Dixon et al. 1995; Newman and Lowenstern 2002).

Dissolved water and carbon dioxide have been measured in silicate glasses using Fourier Transform Infrared (FTIR) and Raman spectroscopy (Stolper 1982; Dixon et al. 1995). Subaerial and submarine basaltic lavas from around the world have water contents that range from 0.06 to 5 wt % (most < 1 wt %), and CO₂ contents ranging between 4 and 1700 ppm (0.17 wt %) (Dixon et al. 1988; Shaw et al. 2008; Métrich et al. 2009; Stefano et al. 2011; Moore et al. 2015; Wallace et al. 2015; Aster et al. 2016). Studies of natural basaltic glass make a basic assumption that the volatiles in the lava are from the original melt and not incorporated from external sources.

Volatiles contained in bubbles originate from one of two sources, exsolution from within the melt or external reservoirs that become entrapped in the melt. Exsolved volatiles either become trapped as bubbles within the melt or escape the melt altogether (Hon et al. 1994; Moore et al. 2015). Physical interaction of external volatiles with lava flows has been documented, including bubbling on the surface of a flow in littoral zones, subaqueous steam jets, and localized explosions after lava lake-drain events (Tribble 1991; Maicher and White 2001; Edwards et al. 2013; Neal et al. 2019). Apart from physical interaction, external volatiles may be incorporated by the lava and modify its chemical composition. The degree to which such external substrate volatiles are incorporated by the lava has received little attention to date.

Chemical alteration of lavas may occur by incorporation of foreign material into the lava (xenoliths) or by diffusion at material boundaries (Brady 1995; Zhang et al. 2010). Most volatile analyses are made on glassy submarine basalt rinds, glassy melt inclusions, or synthetic glasses. However, obtainment of natural samples can be difficult. In this study, we used natural basaltic material under easily sampled conditions by using re-melted ancient basalts that are poured-out to generate meter-scale basalt flows.

Laboratory-generated lava flows are ideal for studying lava-volatile interactions because they mimic subaerial eruption conditions. In the laboratory, parameters such as composition, effusion rate, slope, and substrate volatile content can be carefully controlled. Here we analyze dissolved volatiles, trapped volatiles, and inferred major element transport by FTIR, Raman spectroscopy, and electron microprobe analyses (EMPA), respectively, to better understand the influence of the externally sourced volatiles on lava chemistry.

Methods

Twelve lava flow experiments performed at the Syracuse University Lava Project laboratory were created using a gas-fired tilt furnace (Karson and Wysocki 2012). The 1.2 Ga Keweenawan basalt (Wirth et al. 1997) was heated to ~1300 °C for several hours and manually stirred to facilitate degassing, convection, and homogenization. Hundreds of flows have been generated at the laboratory, most of which are ropy pāhoehoe sheet flows. Most flows lasted minutes in duration and were about one meter long, half a meter wide, and two to four centimeters in thickness (Figure 1). Lava flows developed a crust within tens of seconds and quenched to a crystal-free glass (Figure 2). Lavas typically contain 2 to 24% vesicles by volume (Soldati et al. 2020). Apparent viscosities for all flows were below 200 Pa s, as calculated using the Jeffreys

equation (Jeffreys 1925). Chemical analyses show that flows range from basalt to basaltic andesite in composition (Farrell et al. 2018; Farrell 2020; Soldati et al. 2020).

Meter-scale lava flows were produced by pouring molten basalt from the furnace into a 80-cm long steel trough which directs the lava onto the experimental flow surface. Volatile-bearing substrates comprised wet sand, powdered montmorillonite clay, ice slabs, dry ice, as well as a basin of freshwater. Flows on dry sand served as the volatile-poor control (Figure 1).

Doubly polished basaltic glass wafers (60-400 μm thick) were analyzed via Fourier-Transform Infrared Spectroscopy (FTIR) spectroscopy. Water and CO_2 concentrations in the glass were measured with a Bruker Vertex 70-Hyperion FTIR microscope instrument in transmission mode using 128 scans at 4 cm^{-1} resolution. Spectra were collected in the 350 cm^{-1} to 7000 cm^{-1} range using an open-air stage with a 30x IR objective. Infrared absorption bands in the 3570 cm^{-1} and 2350 cm^{-1} regions were used to determine H_2O and CO_2 concentrations, respectively. Nine total measurements were collected on each sample at three locations with three repeat measurements at each spot, taking care to avoid bubbles. Transects at two different resolutions were measured orthogonally away from bubbles and into the glassy matrix. Coarse resolution transects were measured using 5 spots with a $350\text{ }\mu\text{m}$ spacing, also with three repeat measurements at each spot (Figure 2). Fine-scale resolution transects were measured using 10 spots with a $20\text{ }\mu\text{m}$ spacing. H_2O and CO_2 concentrations were determined using background-corrected peak height and the Beer-Lambert Law:

$$c = \frac{wA}{d\rho\varepsilon} \quad (1)$$

where c is concentration ($c \cdot 10^6 = \text{ppm}$), w is the molecular weight of the compound, A is absorbance, d is thickness in cm, ρ is glass density in g/L, and ε is molar absorptivity. Molar

absorption coefficients used in this study for the 3570 cm^{-1} total H_2O and 2350 cm^{-1} CO_2 bands were 63 and 945, respectively (Fine and Stolper 1985; Dixon et al. 1995). FTIR uncertainty was determined by measuring nine spots with ten repeat measurements at each spot across three samples, resulting in a standard error of 0.34 ppm.

Samples were also analyzed for CO_2 concentration via Raman spectroscopy. The presence of carbon dioxide was detected by analyzing vapor in bubbles using a Renishaw inVia Raman confocal microscope. The 532 nm laser was focused on bubble centers contained in the basaltic glass through a 20x objective, using 1800 grooves/mm grating, and resulting in a spectral resolution of $\sim 0.5\text{ cm}^{-1}$. The spectrometer was calibrated using neon and silicon standards, and the position of the 520.5 cm^{-1} silicon peak was checked at the start of each analytical session. Raman spectra were acquired at 25°C and 1 atm. Intact bubbles about $200\text{ }\mu\text{m}$ in diameter from lavas that flowed over dry ice were analyzed for the presence of CO_2 vapor. For bubbles containing evidence of CO_2 vapor, we obtained the best results by performing measurements for 45 seconds at 50% laser power and averaging 10 accumulations which produced the highest and sharpest Fermi diad peaks at 1388.2 cm^{-1} and 1285.4 cm^{-1} (Lamadrid et al. 2017). Raman uncertainty was determined using ten analyses with identical parameters on the same sample location. Peak positions for the 1388 cm^{-1} and 1285 cm^{-1} peaks were identical.

Electron microprobe analyses (EMPA) were used to measure major element concentrations across the lava-substrate boundary. Analyses and secondary electron images were carried out using a Cameca SXFive microprobe at Syracuse University, with operating conditions of 15 kV acceleration voltage and 20 nA beam current. Transects spanned from substrate particles into the basaltic glass and consisted of 40 spots along a transect length of $80\text{ }\mu\text{m}$ with a $1\text{ }\mu\text{m}$ -diameter spot size. Adjacent spot concentrations were compared to neighboring spots to explore major

element transport across the lava-substrate boundary. Element transport distances were determined by examining spot-to-spot variation. The total transport distance was defined as the length of consecutive adjacent spots with greater than 15% variation in concentration.

Results

Observables

Several behaviors were observed as lava flowed onto the substrates, including jetting, bubbling, and sliding. Gaseous jets of heated substrate volatiles (jetting) occurred at flow margins and through surface bubbles. On materials of sand and clay some jets contained substrate particles that threw sand and clay up to 10 cm away from the margins of the flow. During early flow stages, vigorous bubbling occurred, with some growing up to 20 cm in diameter. The solidified surface area of some flows was covered with over 50% of lava bubbles greater than 5 cm in diameter (Figure 1). Here we use the term ‘bubbles’ as opposed to vesicles because the gas filled cavities in our samples may have been filled with volatiles liberated from the substrate as opposed to volatiles exsolved from the melt. The most distinctive and exotic behavior observed was whole-lobe downslope sliding in six of the twelve flows used in this study.

Raman analyses

The objective of Raman analyses was to determine if substrate-derived volatiles may become trapped in the lava as bubbles. Only samples from lavas emplaced on dry ice were analyzed because of the easily identifiable nature of CO₂-filled bubbles. Eight bubbles across three samples from flows on dry ice were analyzed via Raman spectroscopy for determination of bubble content. The characteristic CO₂ peak splitting is easily identifiable in the Raman spectra (Moore et al. 2015). Raman analyses revealed that three of the eight analyzed bubbles contained

the characteristic spectral carbon dioxide Fermi diad peak splitting at 1285 and 1388 cm^{-1} (Figure 3a), confirming the presence of CO_2 trapped in bubbles.

FTIR analyses

Twenty-three samples were analyzed for dissolved water and carbon dioxide using FTIR. The broad water peak in the uncorrected spectrum indicates low concentrations of dissolved water (Figure 3b). Measured water concentrations range between 42 to 188 ppm (Table 1). Within uncertainty, flows on wet sand and dry sand have the same water concentrations. Carbon dioxide concentrations for all samples contain $\ll 1$ wt % and fall within a narrow range from 9 to 18 ppm. All CO_2 measurements were very near or below the detection limit of 50 ppm.

Six transects were measured away from bubble walls in samples from flows on dry sand, wet sand, and in fresh water. Flows on ice were not examined because no suitable sample was obtained due to the lava glass being fragile and crumbling on contact. Dissolved water contents ranged from 20 – 174 ppm. Five of the six transects away from bubbles show no observable trends of increasing or decreasing volatile content with distance from the bubble (Figure 3c), and the sixth shows an increase in water concentration away from the bubble.

Electron Microprobe

We used electron microprobe analyses to examine the extent of major element transport at the lava-substrate boundary. For flow samples that contained substrate particles (sand and clay) embedded or adhered to the base of the lava, we examined major element distributions along transects across substrate-glass interface (Table 2; Figure 4). Eleven total transects from flows on dry sand, wet sand, and clay contained concentration gradients that ranged from 4 - 10 μm (Table 3). The shortest concentration gradient distance is on dry sand, and the longest on clay.

Discussion

Experiments on volatile-poor substrates compared to volatile-rich substrates have many similar characteristics but are significantly different with respect to the interaction of released volatiles with the lava flows. Flows on volatile-poor dry sand form into sheet flows with no surficial bubbles. Flows on volatile-rich substrates also form thin flows with surficial bubbles, sometimes over 50% of the surface is covered with large surface bubbles. Physical interaction of substrate volatiles with active flows creates particle-entrained jetting and formation of large (>20 cm diameter) surface bubbles (Edwards et al. 2013). Raman analyses from lava flows on dry ice show that substrate-derived volatiles are preserved inside small vesicles (< 300 μm). Surface bubble formation and identification of CO_2 trapped in bubbles confirms that substrate-derived volatiles physically interact with the lava and modify its behavior.

The extent of external volatile chemical influence can be evaluated using a solubility model. The VolatileCalc solubility model (Newman and Lowenstern 2002) predicts water saturation of basalt at 1200°C and 1 atm to be 900 ppm. Spot measurements and transects near bubbles as well as bubble-free areas in our glassy lavas show that in all cases dissolved water contents are below 200 ppm. This is well below the model-predicted 900 ppm saturation level and indicates that our experimental lava flows are undersaturated and could incorporate additional dissolved water. Fine-resolution scans via FTIR reveal that orthogonal transects away from bubbles show no concentration gradient with one exception. This sample shows a concentration increase in water content *away* from the bubble. In other words, the dissolved water concentration near the bubble is depleted, a trend opposite of what is expected if external volatiles are being readily incorporated into the lava. Our results suggest that substrate-derived water is not being incorporated through bubbles because all dissolved water concentrations near bubbles are lower

than expected. One possible reason for this may be that the lavas are extensively degassed in the furnace as the lava is heated and stirred, thereby removing exsolved volatiles. Another explanation may be that the solubility model may not accurately predict water content at atmospheric pressure. Finally, the solubility model may not be tuned for the specific composition of basalts used in these experiments, therefore outputting a value inconsistent with composition of SLP basalt flows.

To determine the method of transport, major element concentration gradients were modeled as a one-dimensional diffusion system with a reservoir of constant concentration. Measured concentration gradients were matched to diffusion model curves to determine element transport distance.

Measured concentrations from the sample with the shallowest gradient were input into the model. The best fit was achieved using a common solution in Crank (1975):

$$C = \frac{C_S + C_L}{2} + \frac{C_L - C_S}{2} \operatorname{erf} \frac{x}{\sqrt{4Dt}} \quad (2)$$

where x is distance (m), t is time (s), and D is diffusivity (m^2/s). C is concentration (wt %), and C_S and C_L represent measured concentrations of the substrate and lava, respectively. For basaltic melt at 1200 °C and 1 atm (0.1 MPa), diffusivity values ($\times 10^{-11}$) used in our model are: Si = 0.3, Ca = 1.58, and Fe = 0.32 (Leshner et al. 1996; Zhang 2010), with additional values listed in Table 4. Closely fitted curves to measured concentration gradients show that major element transport across the boundary is likely caused by diffusion.

Solving for t in equation 2 can provide an estimate for duration of major element diffusion across the lava-substrate boundary. Duration estimates for each element are 0.1 or 0.5 seconds (Figure

5). Using D for Si, Ca, and Fe, and the times from curve fitting, characteristic length of diffusion ranges from 1.22 to 1.26 μm . Published diffusivity values for aluminum (D_{Al}) in basalt at 1200 $^{\circ}\text{C}$ were only found for pressure above 1 atm (Brady 1995; Zhang et al. 2010). However, a combination of the measured concentration gradient, time estimates from curve fitting, and the narrow range for characteristic length of diffusion can constrain D_{Al} at 1 atm. A D_{Al} of $1.5\text{E-}11$ fits the Crank (1975) curve extremely well (Figure 5), and produces a characteristic diffusion length of 1.22, nearly matching characteristic diffusion lengths for Si, Ca, and Fe. Temperature values for D_{Al} are likely near 1200 $^{\circ}\text{C}$, but a simple method outlined by Watson and Cherniak (2015) can also be used to estimate initial temperature of elemental diffusion and thereby constrain the temperature for D_{Al} at 1 atm. By measuring the slope (S_0) of a concentration curve the initial temperature (T_i) can be calculated using:

$$\log S_0 = 2.504 - \frac{1}{2} \log D_0 - \log T_i + \frac{1}{2} \log E_a + \frac{1}{2} \log \dot{T} + \left(26.11 \frac{E_a}{T_i} \right)$$

where S_0 is the slope in %/m, D_0 and E_a are the preexponential factor and the activation energy of the element of interest, respectively, T_i is the initial temperature (K), and \dot{T} is cooling rate ($^{\circ}\text{C/s}$). Measuring S_0 is simple; it requires measuring the slope of a normalized concentration curve at its midpoint (0.5 normalized concentration, Figure 6). S_0 is equal to the distance between where the linear slope line contacts 0 and 1.0 on the vertical axis (Figure 6) and is reported as % per meter (in Figure 6, $100\% / 4.4 \mu\text{m}$). Using published D_0 and E_a values at 1200 $^{\circ}\text{C}$ and 1 atm for Fe and Ca, as well as measured \dot{T} at the lava-substrate boundary, solving for T_i (Eq. 3) estimates initial temperatures of 1053 (Ca) and 1212 (Fe) $^{\circ}\text{C}$. Finally, using the median calculated initial temperature of $1132 \pm 80 \text{ }^{\circ}\text{C}$, and fitting the diffusion model curve (Eq. 2) to the diffusion profile, we determine D_{Al} to be $1.5\text{E-}11 \text{ (m}^2\text{/s)}$ at 1132 $^{\circ}\text{C}$.

Diffusive distance of water and carbon dioxide into the lava glass can also be modeled using Equation 2. The longest time scale of diffusion (0.5 sec) modeled curves for Si, Fe, and Ca, listed above, was input into the model to determine the farthest distance that water and carbon dioxide could diffuse into the lava during our experiments. The characteristic diffusive length scales for water and carbon dioxide were calculated as 11.18 and 1.94 μm , respectively. These modeled distances suggest that diffusively incorporated water will only travel tens of micrometers (< 0.1 mm) into the flow at the time scales presented here.

Diffusion of O has been observed in previous Sulp lava flow experiments. Lava flow experiments performed on ice by Edwards et al (2013) developed abundant surficial bubbles produced by melting and evaporation of sub-flow ice. Glassy lava surface bubbles were analyzed for interactions between meltwater and the lava via O and H isotopes. A slight decrease in $\delta^{18}\text{O}$ was reported from the starting material to the glassy bubble walls. Observed trapping of CO_2 in bubbles, combined with the slight shift in $\delta^{18}\text{O}$ values implies that external volatiles can affect lava rheology and may affect lava chemistry. Results from Edwards et al (2013) and this study serve as initial steps into investigating lava chemical modification via external volatiles.

Conductive cooling equations derived by Carslaw and Jaeger (1959) describe the progression of solidification temperature, or crustal growth, from the flow base into the core:

$$d = \lambda\sqrt{4\kappa t} \quad (4)$$

where d is crustal thickness (m), dimensionless λ is a value determined by field measurements (Carslaw and Jaeger 1959, p. 288), κ is thermal diffusivity of $5.454\text{E-}7$ (m^2/s) (Hon et al., 1994, Table 3), and t is time (hr). Field measurements for the melt (1142°C) and solidification (1070°C) temperatures for basaltic sheet flows and lobes were used to determine λ at the flow base to

be 0.611 (Hon et al., 1994, Table 3). Inputting values from Hawaiian basalt flow measurements (Hon et al. 1994) and estimated diffusive time scales from above, we find that at 0.1 seconds the crust is 4.7 μm thick, and at 0.5 seconds the crustal thickness is 10.6 μm . Diffusion models presented above predict that measured diffusion distances ranging from 2 and 10 μm occurred in durations between 0.1 and 0.5 seconds, consistent with crustal thickness progression calculated from Equation 4. This suggests that diffusion in our lavas occurred on the micro-scale during the melt phase. We also propose that during very early stages of flow equation 4 can be used as a proxy for diffusive distance.

Based on our observations of experimental flows used in this study and the modeling presented above we conclude that volatile concentration measurements are not artificially high due to substrate volatile influences. Rather, they represent concentrations that are inherent to the melt itself. It is recommended that caution is used when volatile concentrations in basaltic glass samples are measured near the lava-substrate boundary to ensure that measurements do not contain any external volatile influence.

Conclusions

Volatiles released from volatile-bearing substrates physically interacted with large-scale experimental lava flows, producing jetting and large surface bubbles. The extent of chemical interaction was investigated by measuring basaltic glass samples via FTIR and Raman spectroscopy, as well as EMPA. Chemical analyses show low concentrations (< 200 ppm) of dissolved water and CO_2 in the basaltic glass samples, and entrapment of CO_2 in bubbles. Diffusion models fit to concentration gradients across the lava-substrate boundary suggest diffusive times below 0.5 seconds. Our results show that volatiles derived from volatile-rich substrates are not significantly dissolved in the lava, despite obvious macroscopic interactions.

Tables

Table 1. Volatile concentrations measured by spot analyses via FTIR spectroscopy. Some flows flowed on both dry and wet sand, indicated by ‘wet/dry’ in the Substrate column. The bold text represents which substrate the sample was taken from.

Experiment	Substrate & Sample Position	Thickness (μm)	H ₂ O Conc. (ppm)	CO ₂ Conc. (ppm)
180523-1	dry sand	190	54	13
190912-1TB	wet/ dry sand, tube, base	350	188	10
190912-1TT	wet/ dry sand, tube, top	350	186	11
190912-1C	wet/ dry sand, center	410	100	11
190912-1AT	wet/ dry sand, above trough	440	113	9
190912-1T	wet/ dry sand, trough	410	171	11
190912-1TEL	wet /dry sand, toe end lobe	320	96	9
190912-1B	wet /dry sand, bubble	60	174	18
190912-1BB	wet /dry sand, breakout in bubble	240	97	10
170708-1 toe	wet sand	300	53	11
170701-1	wet sand, high ves	270	71	14
170630-1	wet sand	270	43	10
170630-1 T	wet sand, trough	300	95	9
191024-1	subaqueous	330	78	17
170710-2	ice	240	44	16
170706-1	ice	150	77	12
170702-1	clay	200	42	10
170702-1 hv	clay, high ves	230	83	11
190924-1T	dry ice, trough	330	131	14
190924-1B	dry ice, bubble	330	133	13
190924-1BW	dry ice, bubble wall	320	132	12
170630-2	dry ice	120	88	14
170706-2	dry ice	190	56	9

Table 2. Compositions for glass and substrate particles measured via EMPA. All values listed in wt %.

<i>BASALT GLASS</i>											
Sample	SiO2	Al2O3	Na2O	MgO	P2O5	K2O	CaO	TiO2	FeO	MnO	Total
160329-1 ds 1_4	54.66	15.76	2.26	6.02	0.16	0.79	8.49	1.82	9.31	0.17	101.30
160329-1 ds 2_1	54.72	15.82	2.15	5.97	0.17	0.79	8.44	1.83	9.23	0.17	99.30
160329-1 ds 3_1	54.72	15.82	2.15	5.97	0.17	0.79	8.44	1.83	9.23	0.17	99.30
160329-1 ds 5_1	54.66	15.89	2.14	6.01	0.17	0.78	8.40	1.83	9.21	0.18	99.27
170701-2 ws base 2_1	53.28	15.68	2.73	6.30	0.15	0.74	8.52	1.86	9.97	0.19	99.42
170701-2 ws base 3_1	54.72	15.82	2.15	5.97	0.17	0.79	8.44	1.83	9.23	0.17	99.30
170701-2 ws base 5_1	53.35	16.07	2.62	6.28	0.15	0.74	8.55	1.88	10.00	0.19	99.83
170701-2 ws tube 1_1	53.26	15.88	2.64	6.27	0.16	0.74	8.55	1.86	9.98	0.18	99.53
170701-2 ws tube 2_1	53.18	15.91	2.60	6.28	0.16	0.74	8.54	1.88	10.00	0.19	99.48
170702-1 clay 1_4	53.66	15.75	3.01	6.07	0.18	0.79	8.33	1.89	9.20	0.18	99.06
170702-1 clay 4_1	53.38	15.96	2.46	6.28	0.19	0.75	8.50	1.87	9.77	0.20	99.34
<i>SUBSTRATE PARTICLE</i>											
Sample	SiO2	Al2O3	Na2O	MgO	P2O5	K2O	CaO	TiO2	FeO	MnO	Total
160329-1 ds 1_4	100.87	0.01	0.04	0.05	0.02	0.01	0.07	0.02	0.23	-0.01	99.44
160329-1 ds 2_1	96.62	0.34	0.01	0.05	-0.02	0.01	0.12	0.03	0.22	-0.01	97.36
160329-1 ds 3_1	94.13	1.06	0.18	0.66	-0.01	0.12	0.70	0.12	1.06	0.00	98.00
160329-1 ds 5_1	99.16	0.00	-0.02	0.01	-0.01	0.00	0.04	0.02	0.14	0.01	99.36
170701-2 ws base 2_1	98.49	0.00	0.01	0.02	0.02	0.01	0.05	0.01	0.14	-0.02	98.73
170701-2 ws base 3_1	98.76	0.02	0.00	-0.01	0.04	0.02	0.03	0.00	0.13	-0.04	98.94
170701-2 ws base 5_1	98.10	0.04	-0.03	0.02	-0.02	0.00	0.02	0.00	0.20	0.01	98.35
170701-2 ws tube 1_1	99.84	0.08	-0.03	-0.02	0.02	0.01	0.02	0.03	0.14	0.01	100.12
170701-2 ws tube 2_1	99.34	0.12	0.05	-0.01	-0.02	0.00	0.04	0.01	0.20	0.02	99.75
170702-1 clay 1_4	51.50	41.37	0.51	0.34	0.04	0.50	0.34	1.50	1.26	-0.03	97.33
170702-1 clay 4_1	43.24	40.29	2.63	1.89	0.03	1.52	3.84	0.37	2.55	0.03	96.40

Table 3. Lava-substrate diffusion distances. Diffusion distance for each measured sample and element. All distances are listed in micrometers.

Lava-Substrate Diffusion Distance (μm)
--

	Sample	Si	Al	Ca	Fe	Na	Mg	Ti	K
Dry sand	160329-1 dry sand 1_4	2	2	2	4	6	2	2	4
	160329-1 dry sand 2_1	2	4	4	6	4	6	6	6
	160329-1 dry sand 3_1	2	4	6	6	2	4	2	6
	160329-1 dry sand 5_1	2	4	4	6	4	2	4	4
	Maximum	2	4	6	6	6	6	6	6
Wet sand	170701-2 wet sand flow base 2_1	2	4	2	2	2	2	2	2
	170701-2 wet sand flow base 3_1	4	4	6	4	4	6	2	6
	170701-2 wet sand flow base 5_1	2	4	2	4	2	2	2	2
	170701-2 wet sand lava tube 1_1	2	4	4	6	6	4	4	4
	170701-2 wet sand lava tube 2_1	2	6	4	4	4	4	4	2
	Maximum	4	6	6	6	6	6	4	6
Clay	170702-1 clay 1_4	0	4	6	6	8	6	4	8
	170702-1 clay 4_1	2	10	8	6	4	6	4	8
	Maximum	2	10	8	6	8	6	4	8

Table 4. Published, measured, and calculated values for diffusion equations. D values are listed as $D = x \cdot 10^{-11}$. References indicated by superscript in header are as follows: ¹ Chen & Zhang, 2008, ² Hofmann & Magaritz, 1977, ³ Lowry et al., 1982, ⁴ Moore et al., 2015, ⁵ Sigurdsson et al., 2000, ⁶ Zhang & Stolper, 1991.

	Si ^{1,5}	Fe ³	Ca ²	Al	H ₂ O ⁶	CO ₂ ⁴
<i>Published</i>						
D (m ² /s)	0.30	0.32	1.58	-	25.0	0.75
log D ₀	-5.52	-2.2	-4.272	-		
E _a (kJ/mol)	262.6	264	184.1	-		
<i>Measured</i>						
\dot{T} (°/s)	1.7	1.7	1.7	1.7		
T _i (K)	1473	1473	1473	1473		
S ₀ dist (μm)	4	4.4	4.1	4.5		
S ₀ (%/m)	2.50E+06	2.22E+06	2.27E+06	2.44E+06		
log S ₀	6.40	6.36	6.39	6.35		
<i>Calculated</i>						
T _i (K)	-	1485	1326	-		

D (m ² /s)	-	-	-	1.50
Dt ^{-1/2}	1.22	1.26	1.26	1.22

Figures



Figure 1. Representative flows on various substrates used in experiments. Substrate type and slope are listed above or below each photo. Top middle photo is on a substrate with dry sand at the head and wet sand at the toe of the flow.

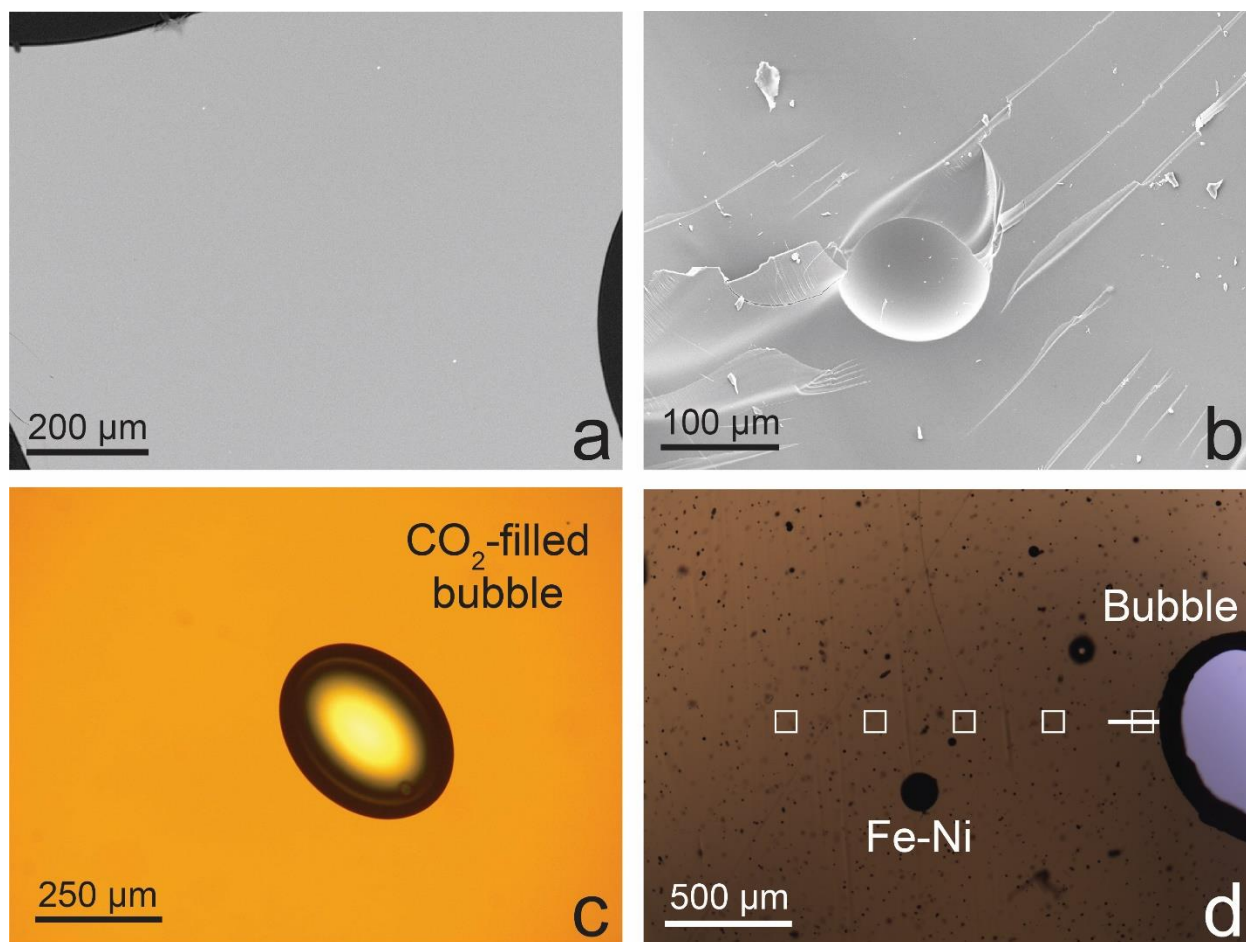


Figure 2. Photomicrographs of lava samples. (a) BSE image of polished basaltic glass sample showing the crystal-free nature of the glass. (b) SE image of unpolished glass sample showing the crystal-free nature of the glass. (c) Sample of a flow emplaced on dry ice. Raman analyses indicate CO₂ in bubble. (d) Sample of a flow emplaced on wet sand. White squares represent analytical points of a FTIR transect (right to left) away from the visible bubble in the far right of the image. Horizontal white line represents the fine scale transect location, measured from right to left.

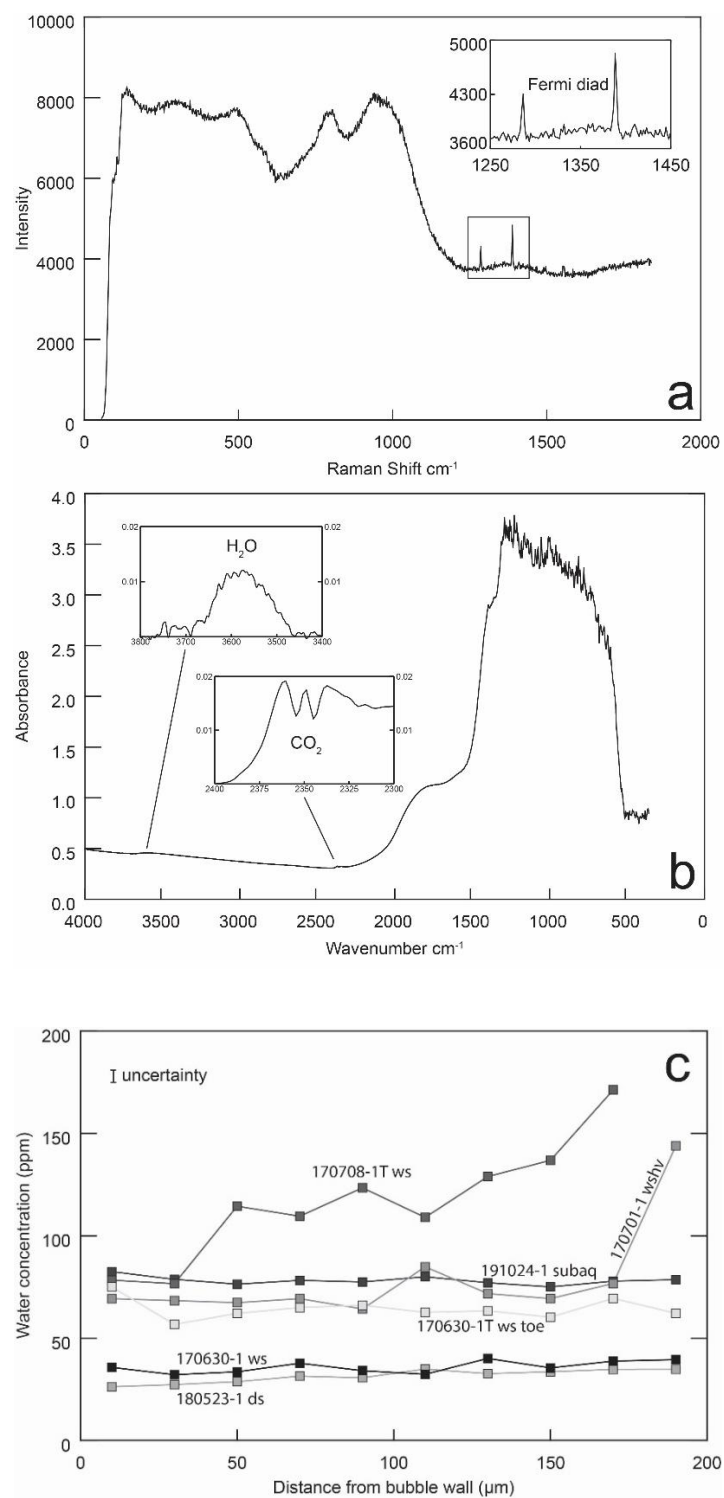


Figure 3. Representative spectra and transect data. (a) Representative Raman spectrum from experiment 190924-1, bubble C, showing the Fermi diad peaks (inset in upper right) indicating

the presence of CO₂ vapor in the bubble. (b) Uncorrected FTIR spectrum from experiment 170630-1 showing analysis range from 500 to 4000 cm⁻¹. Insets are background-corrected spectra zoomed into the total-water and CO₂ regions of the IR spectrum. (c) Water concentrations of transects near bubbles.

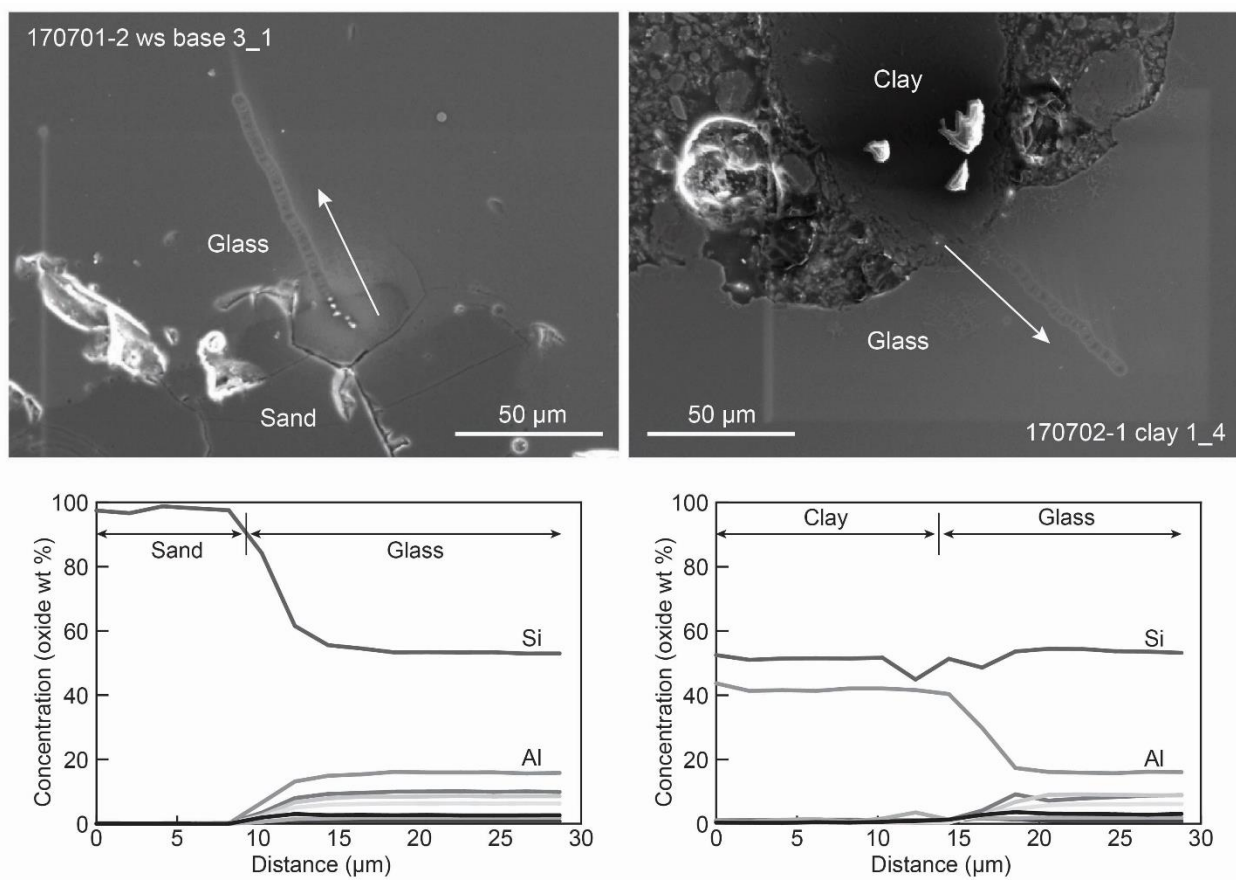


Figure 4. Representative EMPA transects and secondary electron imagery from flows on wet sand and clay. Arrows indicate direction of transect measurement progression. Glass and substrate particles are marked on each image and in their corresponding plot. For ease of viewing, each plot only shows the beginning 30 μm of the 80 μm transect.

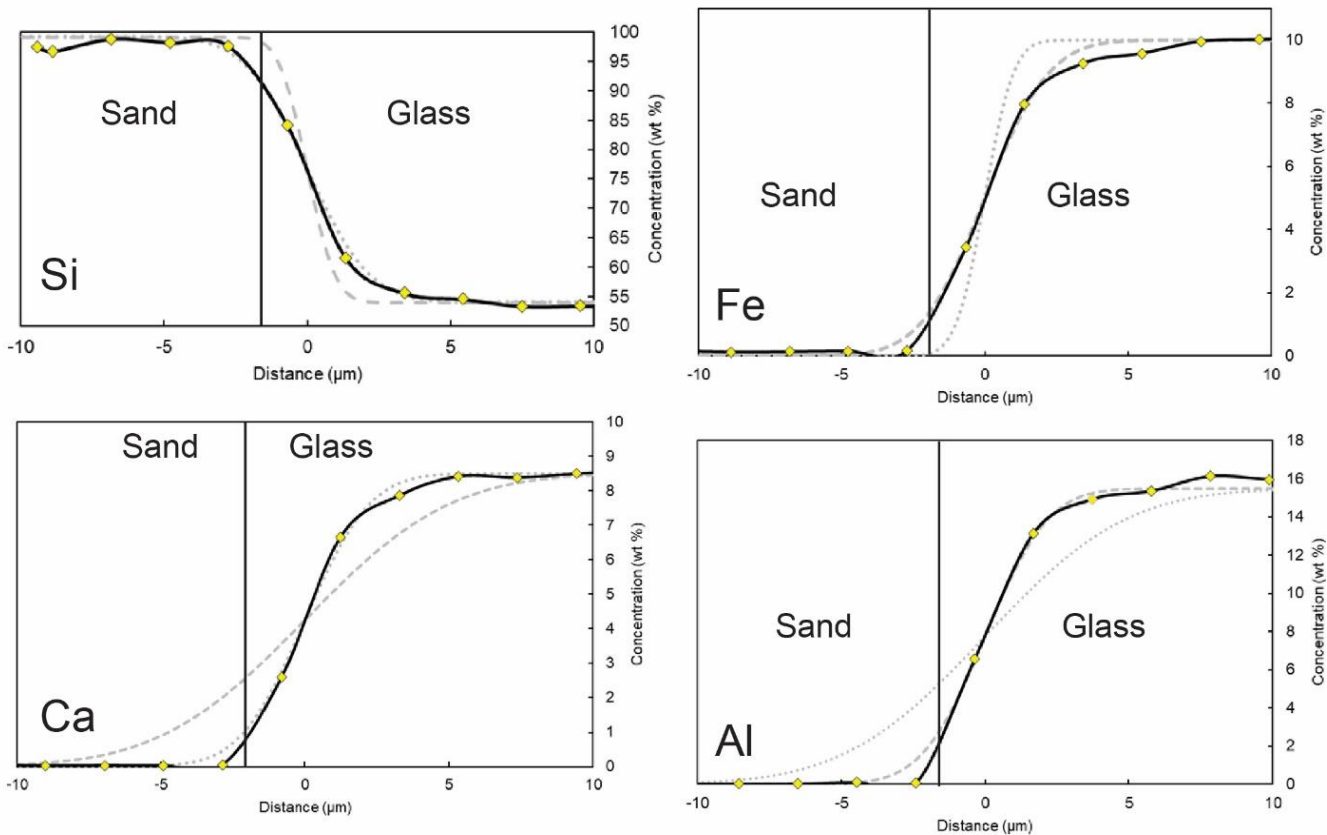


Figure 5. Diffusion modeling results. Modeled diffusion curves were fit to measured concentration gradients to determine diffusive time. Solid lines with diamond points are measured concentration gradients. Grey curves are modeled based on 0.1 sec (dotted) and 0.5 sec (dashed).

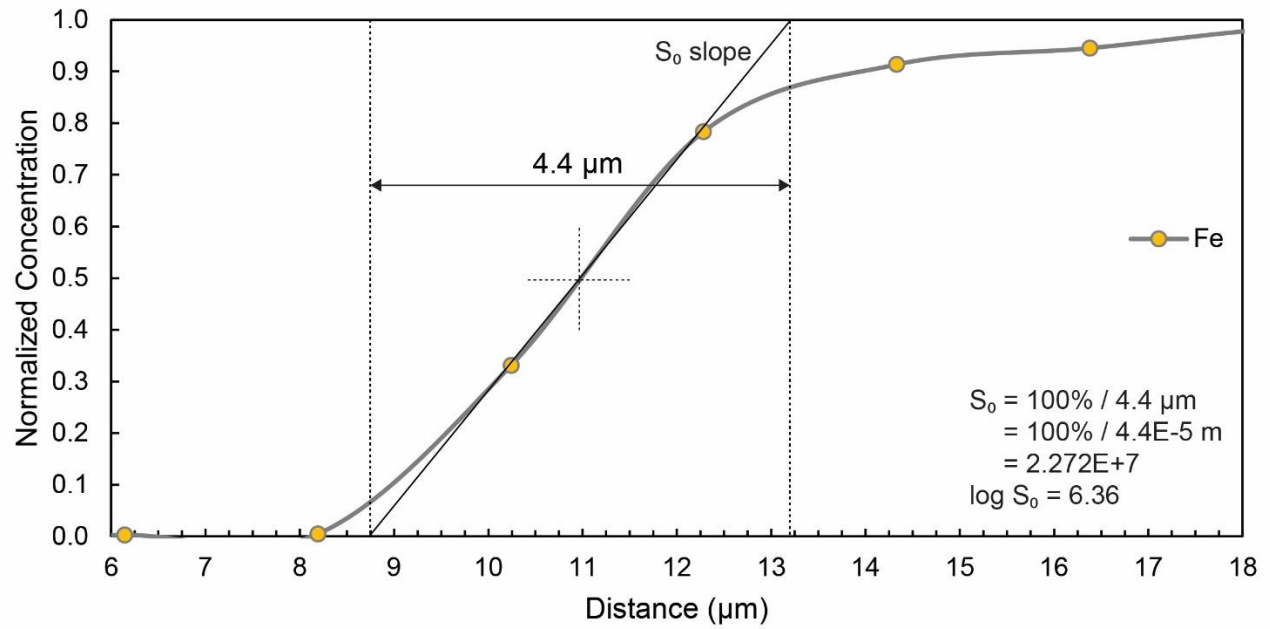


Figure 6. Diffusion profile of Fe across the lava-substrate boundary. Graphically measuring the slope at its midpoint (dotted cross) to obtain S_0 was used to solve for initial lava temperature at the time the lava contacted the substrate at the sample location.

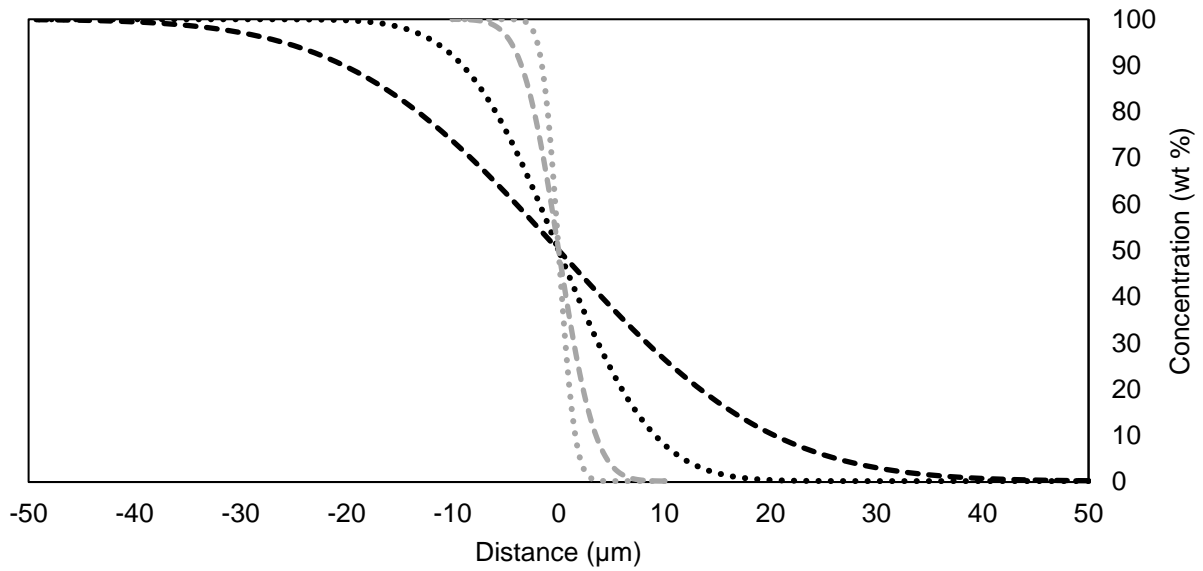


Figure 7. Modeled diffusion profiles of water (black) and carbon dioxide (grey). Diffusion into the lava is represented by starting at the source (100 wt %) and diffusing to measured (< 200 ppm) concentrations. Dotted lines represent 0.1 sec time scales, and dashed lines represent 0.5 second time scales.

Conclusion

Over seventy individual meter-scale lava flows experiments were performed using natural basalt material at natural eruption temperatures. These experiments investigated the production of pāhoehoe breakouts and lava behavior and chemical modification of flows on volatile-rich substrates.

Connecting lava emplacement parameters to a flow's solidified morphology can aid in interpreting ancient flow emplacement conditions. Morphology of lava breakouts are controlled by heat loss, where relatively high viscosity lavas are more likely to generate breakouts than low viscosity breakouts.

Heat transfer from the lava into the substrate can release substrate volatiles as vapor. The liberated volatiles may interact with the lava producing behavior such as surficial bubbling, steam or particle jets at flow margins, and the rapid sliding of lava downslope (termed lava slip). These behaviors are caused by elevated vapor pressure beneath the lava.

Experiments show definitive physical interaction of substrate volatiles with the lava. However, lava-volatile chemical interactions were limited. Despite CO₂ observed in lava-contained bubbles, water and CO₂ concentrations in the lava are well below predicted solubility model values. This suggests that external volatiles are not readily incorporated into active lavas.

The experiments and analyses performed herein apply to studies on ancient and active lava flows. They also serve as a stepping stone to bridge the gap between laboratory studies using analog materials and studies on active flows.

References

- Aster EM, Wallace PJ, Moore LR, et al (2016) Reconstructing CO₂ concentrations in basaltic melt inclusions using Raman analysis of vapor bubbles. *J Volcanol Geotherm Res* 323:148–162. <https://doi.org/10.1016/j.jvolgeores.2016.04.028>
- Baker DR, Freda C, Brooker RA, Scarlato P (2005) Volatile diffusion in silicate melts and its effects on melt inclusions. *Ann Geophys* 48:699–717. <https://doi.org/10.4401/ag-3227>
- Ballard RD, Moore JG (1977) *Photographic Atlas of the Mid-Atlantic Ridge Rift Valley*. Springer-Verlag, New York
- Basaltic Volcanism Study Project (1981) Distribution and morphology of basalt deposits on planets. In: *Basaltic Volcanism on the Terrestrial Planets*. Pergamon Press Inc., New York, pp 702–793
- Belousov A, Behncke B, Belousova M (2011) Generation of pyroclastic flows by explosive interaction of lava flows with ice/water-saturated substrate. *J Volcanol Geotherm Res* 202:60–72. <https://doi.org/10.1016/j.jvolgeores.2011.01.004>
- Belousov A, Belousova M (2017) Dynamics and viscosity of 'a'ā and pāhoehoe lava flows of the 2012-13 eruption of Tolbachik volcano, Kamchatka, Russia. *J Volcanol Seismol* 80:1–23. <https://doi.org/10.1007/s00445-017-1180-2>
- Boreham F, Cashman K, Rust A, Höskuldsson Á (2018) Linking lava flow morphology, water availability and rootless cone formation on the Younger Laxá Lava, NE Iceland. *J Volcanol Geotherm Res* 364:1–19. <https://doi.org/10.1016/j.jvolgeores.2018.08.019>
- Brady JB (1995) Diffusion data for silicate minerals, glasses, and liquids. *American Geophysical*

Union

Carslaw HS, Jaeger JC (1959) *Conduction of Heat in Solids*, 2nd edn. Clarendon Press, Oxford

Cashman K V., Thornber C, Kauahikaua J (2000) Cooling and crystallization of lava in open channels, and the transition of pahoehoe lava to 'a'a. *Bull Volcanol* 62:362–364.

<https://doi.org/10.1007/s004450000090>

Chadwick WW (2003) Quantitative constraints on the growth of submarine lava pillars from a monitoring instrument that was caught in a lava flow. *J Geophys Res* 108:1–14.

<https://doi.org/10.1029/2003jb002422>

Chadwick WW, Clague DA, Embley RW, et al (2013) The 1998 eruption of Axial Seamount: New insights on submarine lava flow emplacement from high-resolution mapping.

Geochemistry, Geophys Geosystems 14:3939–3968. <https://doi.org/10.1002/ggge.20202>

Chen Y, Zhang Y (2008) Olivine dissolution in basaltic melt. *Geochim Cosmochim Acta* 72:4756–4777. <https://doi.org/10.1016/j.gca.2008.07.014>

Cordonnier B, Lev E, Garel F (2016) Benchmarking lava-flow models. *Geol Soc London, Spec Publ* 426:. <https://doi.org/10.1144/SP426.7>

Crank J (1975) *The Mathematics of Diffusion*, Second. Clarendon Press, Oxford

Crown DA, Baloga SM (1999) Pahoehoe toe dimensions, morphology, and branching relationships at Mauna Ulu, Kilauea Volcano, Hawaii. *Bull Volcanol* 61:288–305.

<https://doi.org/10.1007/s004450050298>

Dana JD (1890) *Characteristics of Volcanoes, with Contributions of Facts and Principles, from the Hawaiian Islands*. Dodd, Mead, and Company, New York

- Dietterich HR, Cashman K V., Rust AC, Lev E (2015) Diverting lava flows in the lab. *Nat Geosci* 8:494–496. <https://doi.org/10.1038/ngeo2470>
- Dietterich HR, Diefenbach AK, Soule SA, et al (2021) Lava effusion rate evolution and erupted volume during the 2018 Kīlauea lower East Rift Zone eruption. *Bull Volcanol* 83:. <https://doi.org/10.1007/s00445-021-01443-6>
- Dixon JE, Stolper E, Delaney JR (1988) Infrared spectroscopic measurements of CO₂ and H₂O in Juan de Fuca Ridge basaltic glass. *Earth Planet Sci Lett* 90:87–104. [https://doi.org/10.1016/0012-821X\(88\)90114-8](https://doi.org/10.1016/0012-821X(88)90114-8)
- Dixon JE, Stolper EM, Holloway JR (1995) An experimental study of water and carbon dioxide solubilities in mid-ocean ridge basaltic liquids. Part I: calibration and solubility models. *J Petrol* 3:. <https://doi.org/10.1093/oxfordjournals.petrology.a037268>
- Dobbs E (2013) SketchAndCalc. <https://sketchandcalc.com/>. Accessed 20 Sep 2017
- Edwards B, Karson J, Wysocki R, et al (2013) Insights on lava-ice/snow interactions from large-scale basaltic melt experiments. *Geology* 41:851–854. <https://doi.org/10.1130/G34305.1>
- Edwards B, Magnússon E, Thordarson T, et al (2012) Interactions between lava and snow/ice during the 2010 Fimmvörðuháls eruption, south-central Iceland. *J Geophys Res Solid Earth* 117:1–21. <https://doi.org/10.1029/2011JB008985>
- Fagents SA, Thordarson T (2007) Rootless volcanic cones in Iceland and on Mars. Cambridge University Press, Cambridge
- Farrell J (2019) Viscoelastic Strain, Viscous Rheology, and Behavior of Experimental Lava Flows. Syracuse University

- Farrell J, Karson J, Soldati A, Wysocki R (2018) Multiple-generation folding and non-coaxial strain of lava crusts. *Bull Volcanol* 80:1–17. <https://doi.org/10.1007/s00445-018-1258-5>
- Farrell JA (2020) Mapping the four-dimensional viscosity field of an experimental lava flow. *J Geophys Res Solid Earth* 125:13. <https://doi.org/10.1029/2019JB018815>
- Fine G, Stolper E (1986) Dissolved carbon dioxide in basaltic glasses: concentrations and speciation. *Earth Planet Sci Lett* 76:263–278. [https://doi.org/10.1016/0012-821X\(86\)90078-6](https://doi.org/10.1016/0012-821X(86)90078-6)
- Fine G, Stolper E (1985) The speciation of carbon dioxide in sodium aluminosilicate glasses. *Contrib to Mineral Petrol* 91:105–121. <https://doi.org/10.1007/BF00377759>
- Fink JH, Fletcher RC (1978) Ropy pahoehoe: Surface folding of a viscous fluid. *J Volcanol Geotherm Res* 4:151–170. [https://doi.org/10.1016/0377-0273\(78\)90034-3](https://doi.org/10.1016/0377-0273(78)90034-3)
- Fink JH, Griffiths RW (1990) Radial Spreading of Viscous Gravity Currents With Solidifying Crust. *J Fluid Mech* 221:485–509. <https://doi.org/10.1017/S0022112090003640>
- Fink JH, Griffiths RW (1992) A laboratory analog study of the surface morphology of lava flows extruded from point and line sources. *J Volcanol Geotherm Res* 54:19–32. [https://doi.org/10.1016/0377-0273\(92\)90112-Q](https://doi.org/10.1016/0377-0273(92)90112-Q)
- Furnes H, Banerjee NR, Muehlenbachs K, et al (2004) Early Life Recorded in Archean Pillow Lavas. *Science* (80-) 304:578–581. <https://doi.org/10.1126/science.1095858>
- Gansecki C, Lopaka Lee R, Shea T, et al (2019) The tangled tale of Kīlauea’s 2018 eruption as told by geochemical monitoring. *Science* (80-) 366:. <https://doi.org/10.1126/science.aaz0147>

- Gordeev EI, Murav'Ev YD, Samoilenko SB, et al (2013) The Tolbachik fissure eruption of 2012-2013: Preliminary results. *Dokl Earth Sci* 452:1046–1050.
<https://doi.org/10.1134/S1028334X13100103>
- Greeley R, Fagents SA, Harris RS, et al (1998) Erosion by flowing lava: Field evidence. *J Geophys Res Solid Earth* 103:27325–27345. <https://doi.org/10.1029/97JB03543>
- Gregg T (2017) Patterns and processes: Subaerial lava flow morphologies: A review. *J Volcanol Geotherm Res* 342:3–12. <https://doi.org/10.1016/j.jvolgeores.2017.04.022>
- Gregg T, Keszthelyi L (2004) The emplacement of pahoehoe toes: Field observations and comparison to laboratory simulations. *Bull Volcanol* 66:381–391.
<https://doi.org/10.1007/s00445-003-0319-5>
- Gregg TKP, Chadwick WW (1996) Submarine lava-flow inflation: A model for the formation of lava pillars. *Geology* 24:981–984. [https://doi.org/10.1130/0091-7613\(1996\)024<0981:SLFIAM>2.3.CO](https://doi.org/10.1130/0091-7613(1996)024<0981:SLFIAM>2.3.CO)
- Gregg TKP, Fink JH (2000) A laboratory investigation into the effects of slope on lava flow morphology. *J Volcanol Geotherm Res* 96:145–159. [https://doi.org/10.1016/S0377-0273\(99\)00148-1](https://doi.org/10.1016/S0377-0273(99)00148-1)
- Griffiths RW, Fink JH (1992a) Solidification and morphology of submarine lavas - A dependence on extrusion rate. *J Geophys Res* 97:729–737.
<https://doi.org/10.1029/92JB01594>
- Griffiths RW, Fink JH (1992b) The Morphology of Lava Flows in Planetary Environments: Predictions From Analog Experiments. *J Geophys Res* 97:10

- Hamilton CW, Glaze LS, James MR, Baloga SM (2013) Topographic and stochastic influences on pāhoehoe lava lobe emplacement. *Bull Volcanol* 75:1–16.
<https://doi.org/10.1007/s00445-013-0756-8>
- Harris AJL, Dehn J, Calvari S (2007) Lava effusion rate definition and measurement: A review. *Bull Volcanol* 70:1–22. <https://doi.org/10.1007/s00445-007-0120-y>
- Hoblitt RP, Orr TR, Heliker C, et al (2012) Inflation rates, rifts, and bands in a pahoehoe sheet flow. *Geosphere* 8:179–195. <https://doi.org/10.1130/GES00656.1>
- Hofmann AW, Magaritz M (1977) Diffusion of Ca, Sr, Ba, and Co in a basalt melt: Implications for the geochemistry of the mantle. *J Geophys Res* 82:5432–5440.
<https://doi.org/10.1029/jb082i033p05432>
- Holz M, Soares AP, Soares PC (2008) Preservation of aeolian dunes by pahoehoe lava: An example from the Botucatu Formation (Early Cretaceous) in Mato Grosso do Sul state (Brazil), western margin of the Paraná Basin in South America. *J South Am Earth Sci* 25:398–404. <https://doi.org/10.1016/j.jsames.2007.10.001>
- Hon K, Kauahikaua J, Denlinger R, Mackay K (1994) Emplacement and inflation of pahoehoe sheet flows : Observations and measurements of active lava flows on Kilauea Volcano, Hawaii. *Geol Soc Am Bull* 106:351–370. <https://doi.org/10.1130/0016-7606>
- Hubbert MK, Rubey WW (1959) Role of fluid pressure in mechanics of overthrust faulting: I. Mechanics of fluid-filled porous solids and its application to overthrust faulting. *Bull Geol Soc Am* 70:115–166. [https://doi.org/10.1130/0016-7606\(1959\)70\[115:ROFPIM\]2.0.CO;2](https://doi.org/10.1130/0016-7606(1959)70[115:ROFPIM]2.0.CO;2)
- Jeffreys H (1925) LXXXIV. The flow of water in an inclined channel of rectangular section.

- Philos Mag Ser 6 49:793–807. <https://doi.org/10.1080/14786442508634662>
- Jerram DA, Stollhofen H (2002) Lava-sediment interaction in desert settings; are all peperite-like textures the result of magma-water interaction? *J Volcanol Geotherm Res* 114:231–249. [https://doi.org/10.1016/S0377-0273\(01\)00279-7](https://doi.org/10.1016/S0377-0273(01)00279-7)
- Karson J, Wysocki R (2012) Do-It-Yourself Lava Flows: Science, Art and Education in the Syracuse University Lava Project. *EARTH* 57:38–45
- Kauahikaua J, Cashman K V., Mattox TN, et al (1998) Observations on basaltic lava streams in tubes from Kilauea Volcano, island of Hawai'i. *J Geophys Res Solid Earth* 103:27303–27323. <https://doi.org/10.1029/97JB03576>
- Kennish MJ, Lutz RA (1998) Morphology and distribution of lava flows on mid-ocean ridges: a review. *Earth Sci Rev* 43:63–90. [https://doi.org/10.1016/S0012-8252\(98\)00006-3](https://doi.org/10.1016/S0012-8252(98)00006-3)
- Keszthelyi L, Denlinger R (1996) The initial cooling of pahoehoe flow lobes. *Bull Volcanol* 58:5–18. <https://doi.org/10.1007/s004450050121>
- Lamadrid HM, Moore LR, Moncada D, et al (2017) Reassessment of the Raman CO₂ densimeter. *Chem Geol* 450:210–222. <https://doi.org/10.1016/j.chemgeo.2016.12.034>
- Lavallée Y, Dingwell DB, Johnson JB, et al (2015) Thermal vesiculation during volcanic eruptions. *Nature* 528:544–547. <https://doi.org/10.1038/nature16153>
- Leshner CE, Hervig RL, Tinker D (1996) Self diffusion of network formers (silicon and oxygen) in naturally occurring basaltic liquid. *Geochim Cosmochim Acta* 60:405–413. [https://doi.org/10.1016/0016-7037\(95\)00400-9](https://doi.org/10.1016/0016-7037(95)00400-9)
- Lev E, Spiegelman M, Wysocki RJ, Karson JA (2012) Investigating lava flow rheology using

- video analysis and numerical flow models. *J Volcanol Geotherm Res* 247–248:62–73.
<https://doi.org/10.1016/j.jvolgeores.2012.08.002>
- Lowry RK, Henderson P, Nolan J (1982) Tracer diffusion of some alkali, alkaline-earth and transition element ions in a basaltic and an andesitic melt, and the implications concerning melt structure. *Contrib to Mineral Petrol* 80:254–261. <https://doi.org/10.1007/BF00371355>
- Lube G, Breard ECP, Cronin SJ, Jones J (2015) Synthesizing large-scale pyroclastic flows: Experimental design, scaling, and first results from PELE. *J Geophys Res Solid Earth* 120:1487–1502. <https://doi.org/10.1002/2014JB011666>
- Lube G, Breard ECP, Jones J, et al (2019) Generation of air lubrication within pyroclastic density currents. *Nat Geosci* 12:381–386. <https://doi.org/10.1038/s41561-019-0338-2>
- Macdonald GA (1953) Pahoehoe, aa, and block lava. *Am. J. Sci.* 251:169–191
- Maicher D, White J (2001) The formation of deep-sea Limu o Pele. *Bull Volcanol* 63:482–496.
<https://doi.org/10.1007/s004450100165>
- Malin MC (1980) Lengths of Hawaiian lava flows. *Geology* 8:306–308.
[https://doi.org/10.1130/0091-7613\(1980\)8<306:LOHLF>2.0.CO](https://doi.org/10.1130/0091-7613(1980)8<306:LOHLF>2.0.CO)
- Masson D, Harbitz C, Wynn R, et al (2006) Submarine landslides: processes, triggers and hazard prediction. *Philos Trans R Soc A Math Phys Eng Sci* 364:.
<https://doi.org/https://doi.org/10.1098/rsta.2006.1810>
- Mattox TN, Mangan MT (1997) Littoral hydrovolcanic explosions: a case study of lava-seawater interaction at Kilauea Volcano. *J Volcanol Geotherm Res* 75:1–17.
[https://doi.org/10.1016/S0377-0273\(96\)00048-0](https://doi.org/10.1016/S0377-0273(96)00048-0)

- McClinton JT, White SM (2015) Emplacement of submarine lava fields. *Geochemistry Geophys Geosystems* 16:899–911. <https://doi.org/10.1002/2014GC005632>
- Métrich N, Bertagnini A, Di Muro A (2009) Conditions of magma storage, degassing and ascent at Stromboli: New insights into the volcano plumbing system with inferences on the eruptive dynamics. *J Petrol* 51:603–626. <https://doi.org/10.1093/petrology/egp083>
- Métrich N, Wallace PJ (2008) Volatile abundances in basaltic magmas and their degassing paths tracked by melt inclusions. *Rev Mineral Geochemistry* 69:363–402. <https://doi.org/10.2138/rmg.2008.69.10>
- Mitchell TM, Smith SAF, Anders MH, et al (2015) Catastrophic emplacement of giant landslides aided by thermal decomposition: Heart Mountain, Wyoming. *Earth Planet Sci Lett* 411:199–207. <https://doi.org/10.1016/j.epsl.2014.10.051>
- Mohrig D, Whipple KX, Hondzo M, et al (1998) Hydroplaning of subaqueous debris flows. *Bull Geol Soc Am* 110:387–394. [https://doi.org/10.1130/0016-7606\(1998\)110<0387:HOSDF>2.3.CO](https://doi.org/10.1130/0016-7606(1998)110<0387:HOSDF>2.3.CO)
- Moore JG (2019) Mini-columns and ghost columns in Columbia River lava. *J Volcanol Geotherm Res* 374:242–251. <https://doi.org/10.1016/j.jvolgeores.2019.01.015>
- Moore JG, Phillips RL, Grigg RW, et al (1973) Flow of lava into the sea, 1969-1971, Kilauea volcano, Hawaii. *Bull Geol Soc Am* 84:537–546. [https://doi.org/10.1130/0016-7606\(1973\)84<537:FOLITS>2.0.CO;2](https://doi.org/10.1130/0016-7606(1973)84<537:FOLITS>2.0.CO;2)
- Moore LR, Gazel E, Tuohy R, et al (2015) Bubbles matter: An assessment of the contribution of vapor bubbles to melt inclusion volatile budgets. *Am Mineral* 100:806–823.

<https://doi.org/10.2138/am-2015-5036>

Neal CA, Brantley SR, Antolik L, et al (2019) The 2018 rift eruption and summit collapse of Kilauea Volcano. *Science* (80-) 363:367–374

Newman S, Lowenstern JB (2002) VolatileCalc: a silicate melt-H₂O-CO₂ solution model written in Visual Basic for Excel. *Comput Geosci* 28:597–604. [https://doi.org/10.1016/S0098-3004\(01\)00081-4](https://doi.org/10.1016/S0098-3004(01)00081-4)

Newman S, Stolper E, Stern R (2000) H₂O and CO₂ in magmas from the Mariana arc and back arc systems. *Geochemistry, Geophys Geosystems* 1. <https://doi.org/10.1029/1999GC000027>

Nichols R (1939) Viscosity of lava. *J Geol* 47:290–302

Omega Engineering (2003) ANSI and IEC color codes and limits of error for thermocouples, wire and connectors. <https://www.omega.co.uk/techref/colorcodes.html>

Pedersen GBMM, Höskuldsson A, Dürig T, et al (2016) Lava field evolution and emplacement dynamics of the 2014-2015 basaltic fissure eruption at Holuhraun, Iceland. *J Volcanol Geotherm Res* 340:155–169. <https://doi.org/10.1016/j.jvolgeores.2017.02.027>

Pedersen GBMM, Höskuldsson A, Dürig T, et al (2017) Lava field evolution and emplacement dynamics of the 2014-2015 basaltic fissure eruption at Holuhraun, Iceland. *J Volcanol Geotherm Res* 340:155–169. <https://doi.org/10.1016/j.jvolgeores.2017.02.027>

Perfit MR, Cann JR, Fornari DJ, et al (2003) Interaction of sea water and lava during submarine eruptions at mid-ocean ridges. *Nature* 426:62–65. <https://doi.org/10.1038/nature02032>

Perfit MR, Soule SA (2016) Submarine Lava Types. In: Harff J, Meschede M, Petersen S, Thiede Jö (eds) *Encyclopedia of Marine Geosciences*. Springer Netherlands, Dordrecht, pp

- Peterson DW, Tilling RI (1980) Transition of Basaltic Lava from Pāhoehoe to 'A'ā, Kilauea Volcano, Hawai'i: Field Observations and Key Factors. *J Volcanol Geotherm Res* 7:271–293. [https://doi.org/http://dx.doi.org/10.1016/0377-0273\(80\)90033-5](https://doi.org/http://dx.doi.org/10.1016/0377-0273(80)90033-5)
- Raack J, Conway SJ, Herny C, et al (2017) Water induced sediment levitation enhances downslope transport on Mars. *Nat Commun* 8:1–10. <https://doi.org/10.1038/s41467-017-01213-z>
- Rader E, Vanderkluysen L, Clarke A (2017) The role of unsteady effusion rates on inflation in long-lived lava flow fields. *Earth Planet Sci Lett* 477:73–83. <https://doi.org/10.1016/j.epsl.2017.08.016>
- Rader E, Wysocki R, Heldmann JL (2018) Handmade spatter bombs: Assessing lunar cone-building using clast morphology. In: *Lunar and Planetary Science Conference*. The Woodlands, Texas
- Roche O, Montserrat S, Niño Y, Tamburrino A (2010) Pore fluid pressure and internal kinematics of gravitational laboratory air-particle flows: Insights into the emplacement dynamics of pyroclastic flows. *J Geophys Res Solid Earth* 115:1–18. <https://doi.org/10.1029/2009JB007133>
- Romero JE, Vera F, Polacci M, et al (2018) Tephra from the 3 March 2015 sustained column related to explosive lava fountain activity at Volcán Villarrica (Chile). *Front Earth Sci* 6:1–14. <https://doi.org/10.3389/feart.2018.00098>
- Rowland SK, Walker GPL (1990) Pahoehoe and aa in Hawaii: volumetric flow rate controls the

- lava structure. *Bull Volcanol* 615–628
- Rumpf ME, Lev E, Wysocki R (2018) The influence of topographic roughness on lava flow emplacement. *Bull Volcanol* 80:17
- Sehlke A, Whittington A, Robert B, et al (2014) Pahoehoe to áá transition of Hawaiian lavas: An experimental study. *Bull Volcanol* 76:
- Self S, Keszthelyi L, Thordarson T (1998) The Importance of Pahoehoe. *Annu Rev Earth Plentary Sci* 26:81–110. <https://doi.org/10.1146/annurev.earth.26.1.81>
- Self S, Thordarson T, Keszthelyi L (1997) Emplacement of continental flood basalt lava flows. *Geophys Monogr Ser* 100:381–410. <https://doi.org/10.1029/GM100p0381>
- Shaw AM, Hauri EH, Fischer TP, et al (2008) Hydrogen isotopes in Mariana arc melt inclusions: Implications for subduction dehydration and the deep-Earth water cycle. *Earth Planet Sci Lett* 275:138–145. <https://doi.org/10.1016/j.epsl.2008.08.015>
- Shaw HR, Wright TL, Peck DL, Okamura R (1968) The viscosity of basaltic magma; an analysis of field measurements in Makaopuhi lava lake, Hawaii. *Am. J. Sci.* 266:225–264
- Shreve RL (1968) Leakage and Fluidization in Air-Layer Lubricated Avalanches. *Geol Soc Am Bull* 79:653–658
- Sigurdsson H, Houghton BF, McNutt SR, et al (2000) *Encyclopedia of Volcanoes*, 1st edn. Academic Press, London
- Soldati A, Farrell JA, Sant C, et al (2020) The effect of bubbles on the rheology of basaltic lava flows: Insights from large-scale two-phase experiments. *Earth Planet Sci Lett* 548:1–10. <https://doi.org/10.1016/j.epsl.2020.116504>

- Soule S a., Cashman K V., Kauahikaua JP (2004) Examining flow emplacement through the surface morphology of three rapidly emplaced, solidified lava flows, Kilauea Volcano, Hawai'i. *Bull Volcanol* 66:1–14. <https://doi.org/10.1007/s00445-003-0291-0>
- Soule SA, Cashman K V. (2004) The mechanical properties of solidified polyethylene glycol 600, an analog for lava crust. *J Volcanol Geotherm Res* 129:139–153. [https://doi.org/10.1016/S0377-0273\(03\)00237-3](https://doi.org/10.1016/S0377-0273(03)00237-3)
- Soule SA, Fornari DJ, Perfit MR, et al (2006) Incorporation of seawater into mid-ocean ridge lava flows during emplacement. *Earth Planet Sci Lett* 252:289–307. <https://doi.org/10.1016/j.epsl.2006.09.043>
- Soule SA, Zoeller M, Parcheta C (2021) Submarine lava deltas of the 2018 eruption of Kīlauea volcano. *Bull Volcanol* 83:. <https://doi.org/10.1007/s00445-020-01424-1>
- Stefano CJ, Mukasa SB, Andronikov A, Leeman WP (2011) Water and other volatile systematics of olivine-hosted melt inclusions from the Yellowstone hotspot track. 615–633. <https://doi.org/10.1007/s00410-010-0553-8>
- Stolper E (1982) Water in silicate glasses: an infrared spectroscopic study. *Contrib to Mineral Petrol* 81:1–17. <https://doi.org/https://doi-org.libezproxy2.syr.edu/10.1007/BF00371154>
- Swanson DA (1973) Pahoehoe flows from the 1969-1971 Mauna Ulu eruption, Kilauea volcano, Hawaii. *Bull Geol Soc Am* 84:615–626. <https://doi.org/10.1130/0016-7606>
- The Zen Cart Team and others (2020) FLIR T300: high-temperature thermal imaging infrared camera. http://www.extech-online.com/index.php?main_page=product_info&cPath=89_95&products_id=524

- Thielicke W, Stamhuis EJ (2014) PIVlab – Towards User-friendly, Affordable and Accurate Digital Particle Image Velocimetry in MATLAB. *J Open Res Softw* 2:.
<https://doi.org/10.5334/jors.bl>
- Tribble GW (1991) Underwater observations of active lava flows from Kilauea volcano, Hawaii. *Geology* 19:633–636. [https://doi.org/10.1130/0091-7613\(1991\)019<0633:UOOALF>2.3.CO;2](https://doi.org/10.1130/0091-7613(1991)019<0633:UOOALF>2.3.CO;2)
- Tsang SW, Lindsay JM, Coco G, et al (2019) The heating of substrates beneath basaltic lava flows. *Bull Volcanol* 81:14
- Tucker DS, Scott KM (2009) Structures and facies associated with the flow of subaerial basaltic lava into a deep freshwater lake: The Sulphur Creek lava flow, North Cascades, Washington. *J Volcanol Geotherm Res* 185:311–322.
<https://doi.org/10.1016/j.jvolgeores.2008.11.028>
- U.S. Geological Survey (2022) USGS Multimedia Gallery.
<https://www.usgs.gov/products/multimedia-gallery/images>
- Umino S, Lipman PW, Obata S (2000) Subaqueous lava flow lobes, observed on ROV dives off Hawaii. *Geology* 28:503–506. [https://doi.org/10.1130/0091-7613\(2000\)28<503:SLFLOO>2.0.CO;2](https://doi.org/10.1130/0091-7613(2000)28<503:SLFLOO>2.0.CO;2)
- Van Daele M, Moernaut J, Silversmit G, et al (2014) The 600 yr eruptive history of Villarrica Volcano (Chile) revealed by annually laminated lake sediments. *Bull Geol Soc Am* 126:481–498. <https://doi.org/10.1130/B30798.1>
- Voigt JRC, Hamilton CW, Scheidt SP, et al (2021) Geomorphological characterization of the

- 2014–2015 Holuhraun lava flow-field in Iceland. *J Volcanol Geotherm Res* 419:.
<https://doi.org/10.1016/j.jvolgeores.2021.107278>
- Wafula MD, Zana N, Kasereka M, Hamaguchi H (2008) The Nyiragongo Volcano: A case study for the mitigation of hazards on an African Rift volcano, Virunga Region, Western Rift Valley. *IUGG GeoRisk Com* 1–32
- Waichel BL, Scherer CMS, Frank HT (2008) Basaltic lava flows covering active aeolian dunes in the Paraná Basin in southern Brazil: Features and emplacement aspects. *J Volcanol Geotherm Res* 171:59–72. <https://doi.org/10.1016/j.jvolgeores.2007.11.004>
- Walker G (1973) Lengths of Lava Flows. *Philos Trans R Soc A Math Phys Eng Sci* 274:107–118. <https://doi.org/10.1098/rsta.1948.0007>
- Walker GPL (1995) Plant molds in Hawaiian basalts: was Oahu a desert, and why? *J Geol* 103:85–93. <https://doi.org/10.1086/629724>
- Wallace PJ, Kamenetsky VS, Cervantes P (2015) Melt inclusion CO₂ contents, pressures of olivine crystallization, and the problem of shrinkage bubbles. *Am Mineral* 100:787–794. <https://doi.org/10.2138/am-2015-5029>
- Watson EB, Cherniak DJ (2015) Quantitative cooling histories from stranded diffusion profiles. *Contrib to Mineral Petrol* 169:1–14. <https://doi.org/10.1007/s00410-015-1153-4>
- Waythomas CF, Haney MM, Fee D, et al (2014) The 2013 eruption of Pavlof Volcano, Alaska: a spatter eruption at an ice- and snow-clad volcano. *Bull Volcanol* 76:.
<https://doi.org/10.1007/s00445-014-0862-2>
- Wilson L (1980) Relationships between pressure, volatile content and ejecta velocity in three

types of volcanic explosion. *J Volcanol Geotherm Res* 8:297–313.

[https://doi.org/10.1016/0377-0273\(80\)90110-9](https://doi.org/10.1016/0377-0273(80)90110-9)

Wirth KR, Vervoort JD, Naiman ZJ (1997) The Chengwatana Volcanics, Wisconsin and Minnesota: petrogenesis of the southernmost volcanic rocks exposed in the Midcontinent rift. *Can J Earth Sci* 34:536–548. <https://doi.org/10.1139/e17-043>

Zhang Y (2010) Diffusion in minerals and melts: Theoretical background. *Rev Mineral Geochemistry* 72:5–59. <https://doi.org/10.2138/rmg.2010.72.2>

Zhang Y, Ni H, Chen Y (2010) Diffusion Data in Silicate Melts. *Rev Mineral Geochemistry* 72:311–408. <https://doi.org/10.2138/rmg.2010.72.8>

Zhang Y, Stolper EM (1991) Water diffusion in a basaltic melt. *Nature* 351:306–309. <https://doi.org/10.1038/351306a0>

Biographical Data

Name of Author: Christopher Joseph Sant

Place of Birth: Seattle, WA, USA

Date of Birth: Jan 5, 1983

Educational History:

Master of Science, Geology, 2013, Utah State University, Logan, Utah

Bachelor of Science, Geology, 2009, Brigham Young University – Idaho, Rexburg, Idaho

Awards and Honors:

Chair's Award for outstanding service to the department, 2018, Syracuse University

Faculty Recognition Award, 2014, BYU – Idaho

Significant contribution to IBA competition, 2011, Utah State University

Outstanding student, 2007, BYU – Idaho

Professional Experience:

Satellite Operations Supervisor, 2020-present, Space Dynamics Laboratory, Logan, Utah

Graduate teaching assistant, 2015-2020, Department of Earth and Environmental Sciences,
Syracuse University

Adjunct Faculty, 2012-2014, Department of Geology, Brigham Young University – Idaho

Research assistant, 2010-2012, Department of Geology, Utah State University

Teaching assistant, 2007-2009, Department of Geology, Brigham Young University – Idaho

Publications:

Soldati, A., Farrell, J., **Sant, C.**, Wysocki, R., Karson, J., 2020, *The effect of bubbles on the rheology of basaltic lava flows: Insights from large-scale two-phase experiments*, Earth and Planetary Science Letters, vol. 548, 10 pp.

Lachmar, T., Freeman, T., **Sant, C.**, Batir J., Shervais, J., Evans, J., Walker, J., Blackwell, D., Nielson, D., 2017, *Effect of an 860-m thick, cold, freshwater aquifer on geothermal potential along the axis of the eastern Snake River Plain, Idaho*, Geothermal Energy, vol. 5, 28 pp.

Moore, D., **Sant, C.**, Wood, R., Miller, B., Hansen, S., Shurtliff, R., Grover, S., 2012, *Field Guide to the Eocene Rocks of the Centennial and Henry's Mountains, Idaho & Montana*, Northwest Geology, 41: 83-94.

Sant, C.J., Shervais, J.W., 2013, *Geothermal Alteration of the Basalts of the Snake River Plain, Idaho* (master's thesis). Utah State University. United States.